Subglacial topography and landscape evolution from radio-echo sounding data in the Evans-Rutford Region, southern Antarctic Peninsula.

CARTER, CHARLOTTE,MAY

Subglacial topography and landscape evolution from radio-echo sounding data in the Evans-Rutford Region, southern Antarctic Peninsula.

Charlotte May Carter

MSc by Research

Department of Geography

Durham University

August 2022

Abstract

Knowledge of the subglacial bedrock topography of the Antarctic ice sheet is important for understanding modern and past ice flow as well as the present basal conditions. Inferring landscape evolution from the subglacial geomorphology can also provide insight into ice sheet interactions with other processes such as tectonics. This thesis utilises newly released radio-echo sounding data from the British Antarctic Survey GRADES-IMAGE radar survey to geomorphologically interpret the bed topography in the Evans-Rutford Region of Antarctica. The GRADES-IMAGE survey is a legacy radar survey that has not yet been examined in detail in terms of subglacial bed topography. In the work presented here, a new high-resolution Digital Elevation Model of the region has been generated, and the resulting subglacial landscape was mapped to delineate distinct geomorphological features. Hypsometric (area-elevation) analysis was carried out to characterise the landscape morphology, and a flexural isostatic rebounding model was applied in order to help consider the age and evolution of the pre-glacial landscape. The main finding from analysis of the subglacial features is the identification of ten flat plateau surfaces distributed throughout the study region. These plateaux sit under cold-based ice between deep incised glacial troughs, some of which have potential tectonic controls. Two populations of plateaux have been identified as potentially coherent pre-glacial surfaces. Three hypotheses are presented for the evolution of the regional landscape: passive margin evolution associated with the breakup of the Gondwana supercontinent, or an extensive planation surface that may have been uplifted either in association with the West Antarctic Rift System, or cessation of subduction at the base of the Antarctic Peninsula. Regardless of the process of formation, glacial erosion of the surrounding troughs likely coincided with the inception of the West Antarctic Ice Sheet, with the ice flow and erosion patterns topographically controlled by the regional tectonics.

Table of Contents

List of tables

List of illustrations

List of abbreviations

AP: Antarctic Peninsula

BAS: British Antarctic Survey

BGA: Bellingshausen Gravity Anomaly

CSA: Cubic Spline Approximation

DEM: Digital Elevation Model

EAIS: East Antarctic Ice Sheet

ERR: Evans-Rutford Region

EWM: Ellsworth-Whitmore Mountains

GIS: Geographical Information System

GPS: Global Positioning System

GRADES-IMAGE: Glacial Retreat of Antarctica and Deglaciation of the Earth System / Inverse Modelling of Antarctica and Global Eustasy

IBCSO: International Bathymetric Chart of the Southern Ocean

IDW: Inverse Distance Weighting

IMIS: Institute and Möller Ice Streams

IRH: Internal Reflection Horizon

MBL: Marie Byrd Land

MEaSUREs: Making Earth System data records for Use in Research Environments

MSGL: Mega-Scale Glacial Lineation

PASIN: Polarimetric radar Airborne Science INstrument

RAMP2: Radarsat Antarctic Mapping Project 2

REMA: Reference Elevation Model of Antarctica

RES: Radio-Echo Sounding

TI: Thurston Island

TIN: Triangulated Irregular Network

TAM: TransAntarctic Mountains

TORUS: Targeting ice stream Onset Regions and Under-ice Systems

WAIS: West Antarctic Ice Sheet

WARS: West Antarctic Rift System

Declaration

I confirm that no part of the material presented in this thesis has been previously submitted for a degree in this or any other university. In all cases the work of others, where relevant, has been fully acknowledged.

Statement of Copyright

Acknowledgements

This thesis would not have been possible without the help, support, and collaboration of a number of people, whom I would like to thank here. Firstly, I am extremely grateful to my supervisors Prof. Michael Bentley and Prof. Stewart Jamieson, whose wonderful advice and guidance allowed me to develop so much new knowledge in a field in which I had little experience. Working with them has made my last year in Durham a very enjoyable one. Many thanks are also due to Dr. Guy Paxman, Dr. Tom Jordan, Dr. Neil Ross, Felipe Napoleoni, and Julien Bodart, for their helpful discussions with me around subglacial landscapes and radar data processing. Lastly, I would like to thank my wonderful friends and family, who have given me endless support in following my dreams in academia.

1. Introduction

Subglacial bedrock topography is an important boundary condition influencing ice sheet dynamics across Antarctica, and which can be modified during long periods of glaciation where the ice may also change in terms of thickness and ice flow direction. Underlying this, tectonic controls may help determine patterns of ice flow and landscape evolution (Siegert, 2008). Various types of subglacial landscapes exist across the continent which can influence ice flow. Knowledge of these landscapes is important for determining ice sheet model parameters, which can predict the evolution of the Antarctic ice sheet in response to climatic warming.

1.1. Study Area

This project will provide a high-resolution study of the subglacial topography of a largely neglected region of the West Antarctic Ice Sheet (WAIS) in the southern Antarctic Peninsula, improving upon the gridded datasets provided by Bedmap2 and BedMachine (Fretwell et al., 2013; Morlighem et al., 2020). The Evans-Rutford Region (Figure 1.1) hosts significant outlet glaciers of the WAIS and

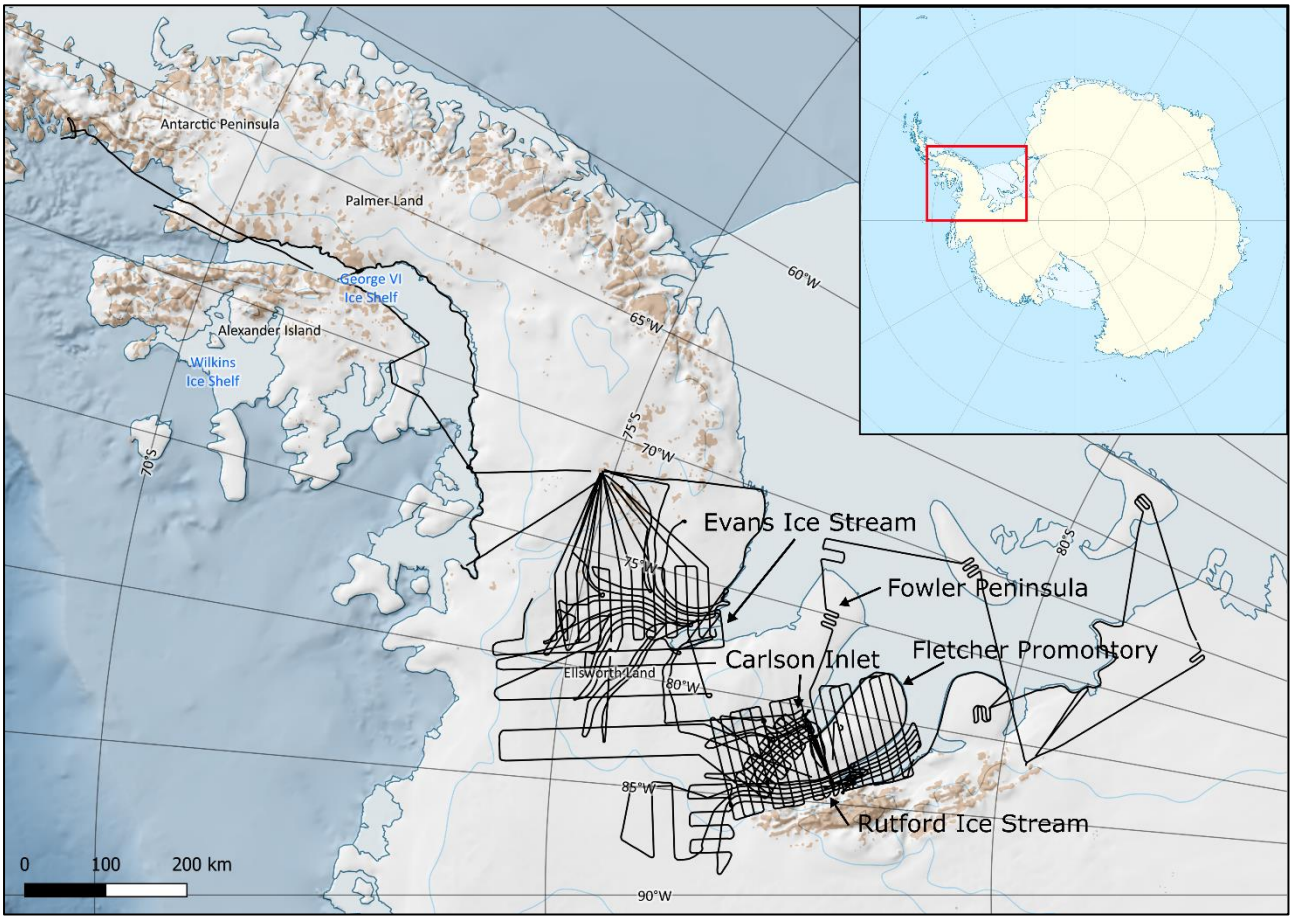

Figure 1.1: Study site map of the Evans-Rutford Region. Black line illustrates the flightlines of the GRADES-IMAGE 2006/7 RES survey carried out by British Antarctic Survey. Detailed basemap sourced from Quantarctica (Matsuoka et al., 2021). Inset map shows location of the study region in relation to the Antarctic continent (red box).

contains some of the highest relief topography in Antarctica, but its subglacial bed and englacial structure have not yet been investigated in detail.

The Evans-Rutford Region (ERR) is located between the base of the Antarctic Peninsula and the Ellsworth Mountains. This area contains two major outlets of the West Antarctic Ice Sheet, namely the Evans and Rutford ice streams, which discharge into the Filchner-Ronne Ice Shelf. The Carlson Inlet contains a stagnated ice stream north of Rutford (King, 2011). Inter-ice stream areas include Fletcher Promontory and Fowler Peninsula, which are higher elevation areas containing slow flowing ice. The 2006/7 GRADES-IMAGE (Glacial Retreat of Antarctica and Deglaciation of the Earth System / Inverse Modelling of Antarctica and Global Eustasy) radio-echo sounding (RES) survey provides high spatial resolution coverage of the ice streams, as well as opportunistic surveys of the ice rises present within the Filchner-Ronne ice shelf. The flightlines of the RES survey and study region are shown in Figure 1.1, and the glaciological setting of the region is evident in Figure 1.2. The ice surface topography illustrated in Figure 1.2a shows that ice has accumulated over the high points of the Fletcher Promontory and Fowler Peninsula, as well as the topography surrounding the Evans ice stream. This alongside the subglacial topography (Figure 1.2b) shows that the Evans and Rutford ice streams are deep troughs cut into the landscape. The region is bounded by two areas of alpine-like topography, at the base of the Antarctic Peninsula to the north and the Ellsworth Mountains to the south. Figure 1.2c demonstrates the ice flow velocity within the region, where the two ice streams show significantly higher velocity, in contrast with the slow-flowing and almost stagnant ice overlying the higher elevation points and within the Carlson Inlet. Ice thickness (Figure 1.2d) is also highest within the ice stream troughs, reaching around 2800m compared to the surrounding higher elevation areas which host less than 1km of ice.

Detailed studies of the subglacial bedrock topography of the whole of the region do not yet exist although there have been smaller scale glaciological investigations into the dynamics of the Rutford ice stream. Previous work on the Evans-Rutford Region has utilised the GRADES-IMAGE radar survey for varying purposes, such as the identification of ‘sticky spots’ and their relationship to radar reflectivity beneath the Evans Ice Stream (Ashmore et al., 2014). The production of a free-air gravity anomaly map for the ERR has inferred moderate but significant crustal thinning of the underlying structure below the Evans Ice Stream, and a potential microplate boundary between the Haag nunataks and southern Antarctic Peninsula (Jones et al., 2002).

Figure 1.2: Glaciology and topography of the study area. Black line illustrates the GRADES-IMAGE RES survey, overlying (a) RAMP2 Digital Elevation Model (200m), (b) Bedmap2 hillshaded bed elevation (1km), (c) MEaSUREs ice flow velocity (450m), (d) Bedmap2 Ice thickness (1km). Created using Quantarctica (Matsuoka et al., 2021).

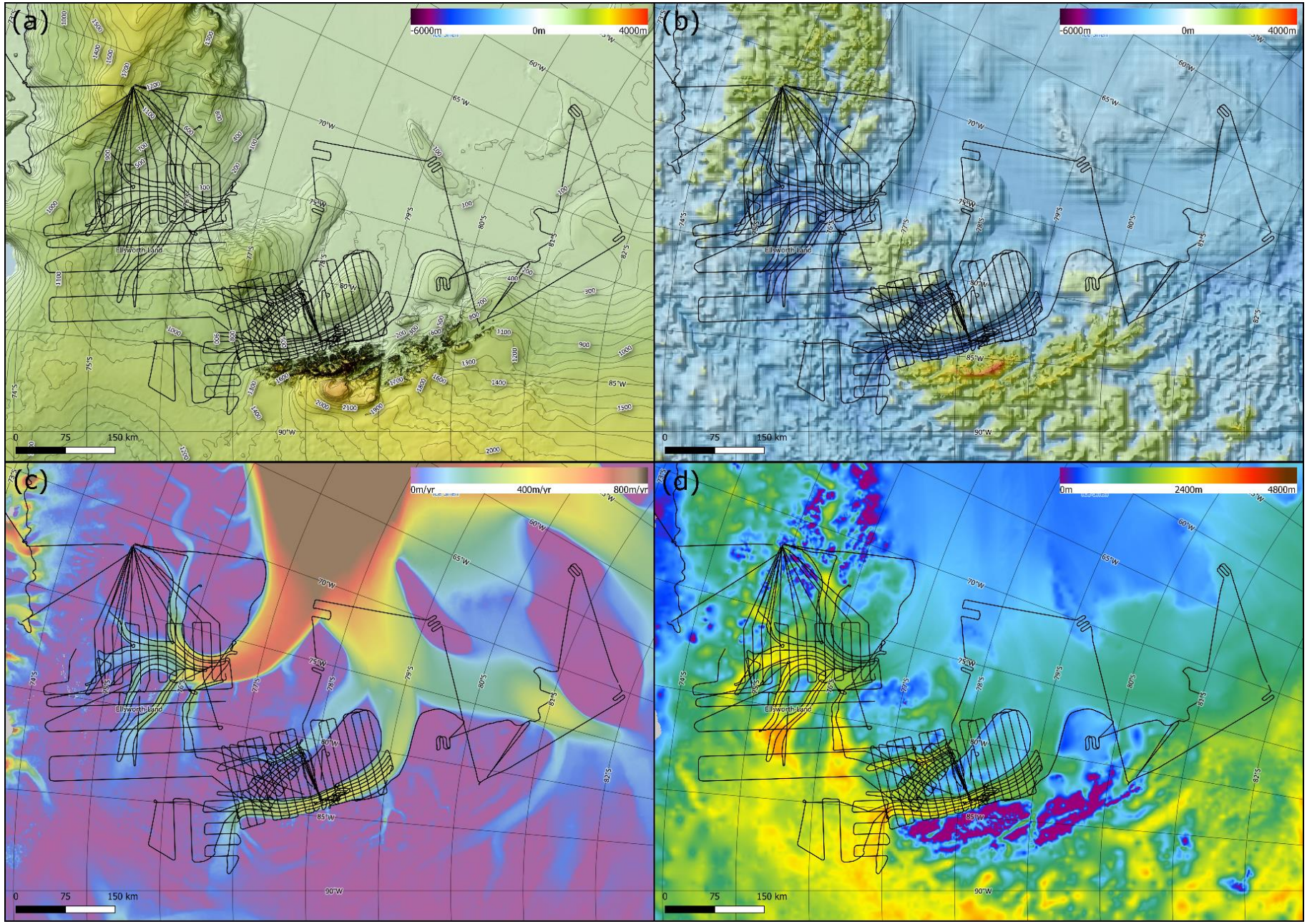
(a)
-6000m
0m
4000m
(b)
-6000m
0m
4000m
(c)
0m/yr
400m/yr
800m/yr
(d)
0m
2400m
4800m
Ellsworth Land
0
75
150 km

Multiple seismic and RES surveys of the basal conditions and subglacial bedforms of the Rutford Ice Stream have been carried out (King et al., 2007; A. M. Smith et al., 2007; Smith and Murray, 2009) in order to understand the local controls on ice flow. High resolution RES surveys of Rutford have identified MSGLs in the ice stream subglacial till (King et al., 2009), establishing Rutford as a region of fast flow within the WAIS.

Carlson Inlet has been interpreted as a stagnant ice stream, based on shallow radar reflection profiling and surface and basal morphology, with ice in the centre having been near-stagnant for between 3.5 to 6.8 kyr (King, 2011). This stagnation has been interpreted to be a result of water piracy, where Carlson Inlet is starved of subglacial water that is currently directed beneath Rutford Ice Stream (Vaughan et al., 2008). This has resulted in Carlson Inlet flowing at speeds 10 to 50 times slower than Rutford, which flows at speeds greater than 350 m a^{-1} (Vaughan et al., 2008).

Aerogeophysical datasets have also produced bed elevation models for the adjacent ice streams of the Weddell Sea sector of the WAIS, namely the Institute, Möller and Foundation ice streams (Jeofry et al., 2018b; Rose et al., 2015). RES data has also revealed a previously unknown subglacial embayment inland of the Institute ice stream grounding zone (Jeofry et al., 2018a), illustrating the need for accurate bed topography measurements in order to fully understand ice sheet processes in this region.

1.2. Aims and Objectives

The aim of this study is to infer the landscape evolution and ice history of the Evans-Rutford Region (ERR) of the southern Antarctic Peninsula using radio echo sounding (RES) data. In order to achieve this aim, the objectives are as follows:

1. Compile available radio echo sounding and other datasets relevant to the ERR.

This study arose from the release of the legacy GRADES-IMAGE 2006/07 RES dataset from British Antarctic Survey, which will be utilised alongside the TORUS and Evans 1994/95 RES datasets (Frémand et al., 2022).

2. Map the subglacial topography of the ERR.

Subglacial topography can be identified through its bright reflection horizon present within a radargram (Figure 1.3) (Corr et al., 2007). From this, the bed will be ‘picked’ to produce a point dataset of the subglacial topography, that will be interpolated to provide improved detail as compared to Bedmap2 or BedMachine.

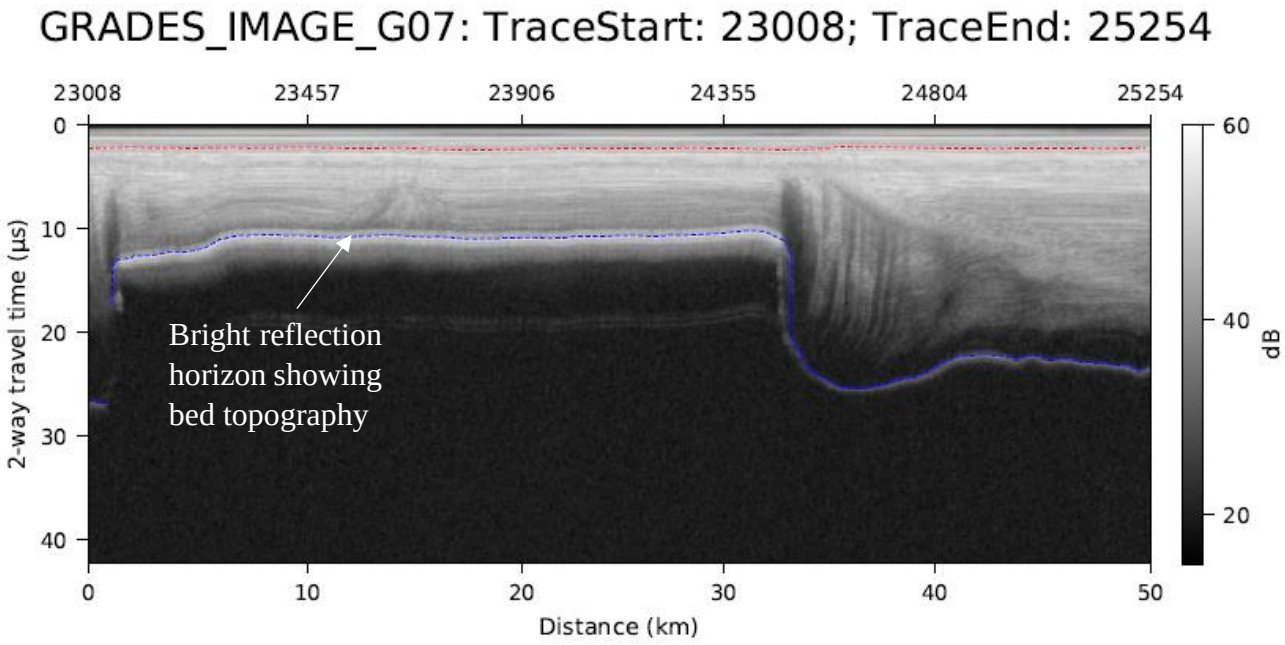

Figure 1.3: Radargram from flightline G07 of the GRADES-IMAGE RES survey. The ice surface (red dashed line) and subglacial bed topography (blue dashed line) have been automatically 'picked' using the brighter reflection horizons.

3. Conduct analysis of bed topography data to identify signatures of different earth surface processes.

The Digital Elevation Model of subglacial topography interpolated from the RES surveys will be analysed in order to classify the landscape of the study region (Jamieson et al., 2005). This initial classification will identify the presence of any highland plateaus or alpine glacial features within the study area. In addition, individual topographic features can be identified, for example, U-shaped troughs typical of intense glacial erosion, V-shaped valleys reflecting past fluvial incision, or undulating sedimentary bed-type topography indicative of ice streaming. This will indicate the potential relict non-glacial surfaces that have been preserved in the landscape (Goodfellow, 2006), in contrast to the overdeepened subglacial troughs that reflect the location of past erosion (Paxman et al., 2017). Moreover, the presence of linear landscape breaks, steep-sided basins, and well-bounded planar surfaces (tilted or otherwise) can be used to infer the presence of geological faults. Hypsometric analysis will also be undertaken to analyse the frequency-distribution of elevations and highlight where there are significant areas of land at particular elevations. The identification of different landscape processes operating in the region will allow the reconstruction of formational processes that have resulted in the present subglacial topography.

4. Infer the geological history and landscape evolution of the ERR from topographic mapping.

GIS software will be used to explore and interpret the landscape patterns evident across the region, and a flexural isostatic rebound model will provide correction for an isostatically adjusted, pre-ice

landscape. The geomorphological analysis of the ERR will then be integrated with the geological and tectonic history, as the geology and basal topography are important boundary conditions governing the dynamics of the overlying ice sheet (Paxman et al., 2019b). From this, the landscape evolution and potential influences of topography on ice flow can be identified for the region.

2. Literature Review

This section reviews the key elements of the tectonic and climate history of Antarctica (Sections 2.1.-2.4.) followed by the key techniques that will be used in this thesis (2.5.-2.7.), and then a short review (2.8.-2.9.) of the key large-scale geomorphological features that might be expected beneath the ice sheet, given the tectonic history of the region.

2.1. Tectonic history of Antarctica

The tectonic history of Antarctica and resulting plate configuration is dominated by the break-up of Gondwana; East Antarctica formed a significant central fragment of the Gondwana super-continent during the Jurassic period (Figure 2.1). From 180 Ma, the supercontinent broke into distinct continental landmasses, leading to the repositioning of Antarctica at southern polar latitudes in the Early Cretaceous (ca. 120 Ma), surrounded by rifted margins (Jamieson and Sugden, 2008; Siegert and Florindo, 2009).

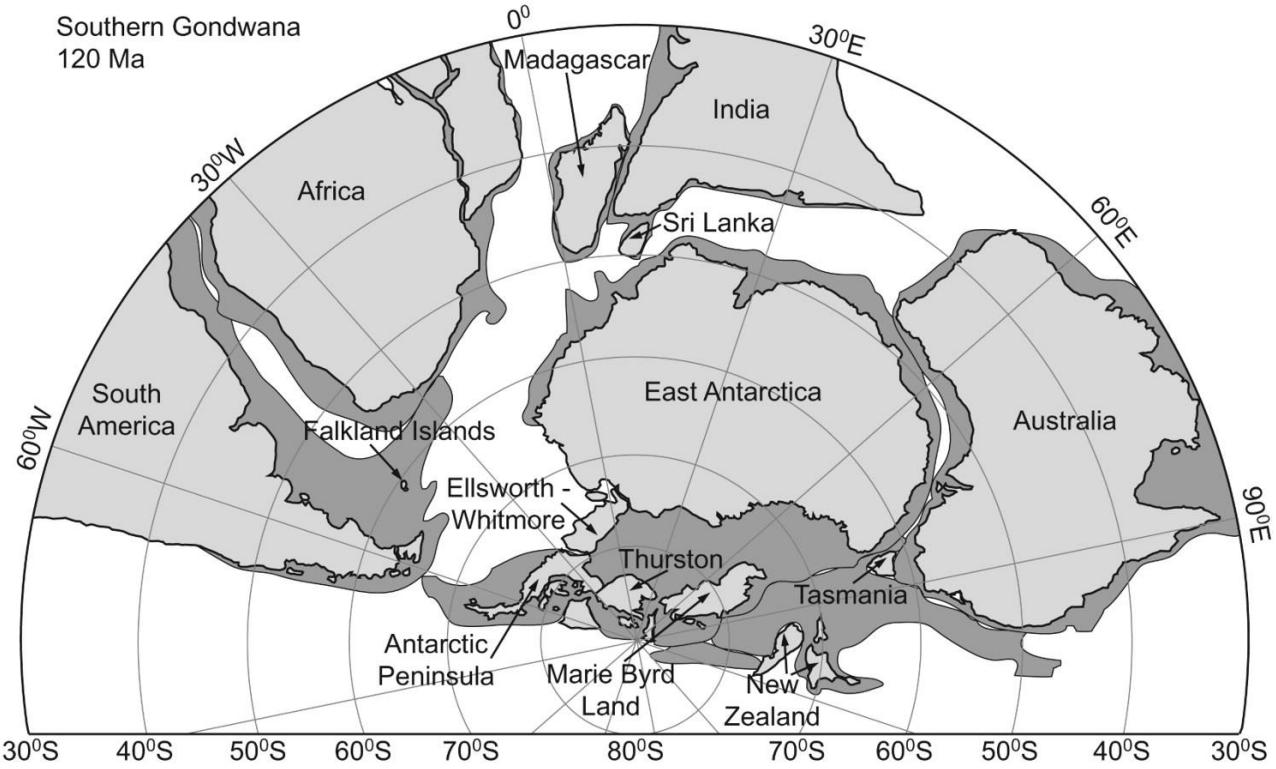

Figure 2.1: Plate configuration of Gondwana at the early stages of breakup ca. 120 Ma (Sugden and Jamieson, 2018).

The breakup of Gondwana began between 160 to 188 Ma, with India and Africa separating first. Tasmania and New Zealand separated from the Ross Sea margins much later, ca. 70 Ma, followed by Australia after 55 Ma. The drift of these continents opened up seaways around Antarctica, changing ocean circulation and productivity (Jamieson & Sugden, 2008). The Antarctic Peninsula (AP) is largely a Mesozoic magmatic arc formed by subduction along the Pacific margin of West Antarctica. The AP was founded on a mid-Palaeozoic basement that was located on the palaeo-Pacific margin of

Gondwana prior to its disintegration in the Middle Jurassic (Storey and Nell, 1988). The West Antarctic Rift System (WARS) extends from North Victoria Land to the base of the AP and demonstrates volcanicity that dates back to ca. 35 Ma. Uplift of the Transantarctic Mountains (TAM), dating from the early Cenozoic, is widely believed to be related to the inception of WARS (Dalziel and Lawver, 2001; Fitzgerald, 1992).

As a result of this tectonic activity associated with Gondwana break-up and subduction, West Antarctica now comprises four microcontinental blocks: the Antarctic Peninsula, Thurston Island, Marie Byrd Land, and the Ellsworth-Whitmore block, which is thought to be associated with extensional rifting (Jamieson and Sugden, 2008). This resulted in three broad physiographic provinces in West Antarctica, illustrated in Figure 2.2 (Jordan et al., 2020). Firstly, the Weddell Sea region, which was furthest from the AP subducting margin but was most impacted by the Jurassic initiation of the Gondwana breakup. Marie Byrd Land and the West Antarctic Rift System developed as a broad continental rift system over the Cretaceous to Cenozoic, reworking a former convergent margin. Finally, the Antarctic Peninsula and Thurston Island preserve an almost complete magmatic arc system.

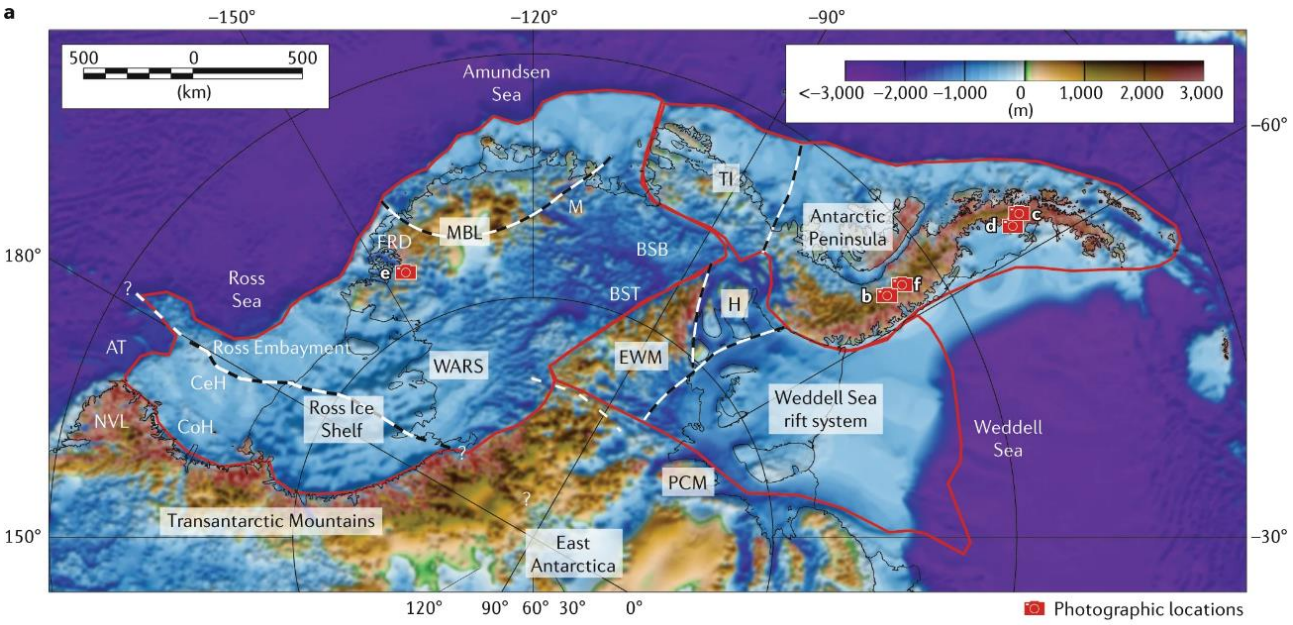

Figure 2.2: Complex West Antarctic subglacial topography from Bedmap2, derived from airborne ice-penetrating radar, with bathymetry beneath the Ross Ice Shelf derived from gravity data. The thick red lines demarcate the three main geotectonic provinces, and the dashed black lines mark sub-provinces. The main provinces include the Weddell Sea sector, which comprises the shallow marine Weddell Sea Rift System and onshore highlands of the Haag Nunataks and Ellsworth–Whitmore Mountains (EWM) block; Marie Byrd Land (MBL) and the West Antarctic rift system (WARS), which are underlain by highly extended crust; and the Antarctic Peninsula and Thurston Island (TI), which expose a well-preserved continental marginal arc (Jordan et al., 2020).

2.2. Tectonic history of the Evans-Rutford Region

The Weddell Sea region is comprised of the shallow marine Weddell Sea Rift System, the onshore highlands of the Haag Nunataks and the Ellsworth-Whitmore Mountains block, and was one of the regions most impacted by the break-up of Gondwana initiated in the Jurassic (Jordan et al., 2020). The majority of the West Antarctic crust developed between 500 to 90 Ma, along an active ocean-continent convergence zone that bordered the ancient Pacific margin of Gondwana (Jordan et al., 2020). During the break-up of Gondwana, the four major crustal units that make up the exposed rocks of West Antarctica, namely the Antarctic Peninsula, Thurston Island, Ellsworth-Whitmore Mountains and Marie Byrd Land, rotated outwards from the convergent Pacific margin of the East Antarctic craton as rigid blocks (Dalziel and Lawver, 2001). The oldest rocks exposed in West Antarctica are the outcrop at the Haag Nunataks, formed in a magmatic arc at 1710 Ma and then deformed at 1060 Ma, with an absence of subsequent deformation suggesting that this has acted as an undeforming microcontinental block from Grenvillian time (Jordan et al., 2020). This movement of crustal blocks during the early stages was thought to involve these as distinct microcontinental fragments (Jordan et al., 2017; Maslanyj and Storey, 1990), driven by a major pulse of large igneous province magmatism by an upwelling mantle plume, triggering the break-up of the Gondwana supercontinent in the Weddell Sea (Jordan et al., 2020).

The Ellsworth-Whitmore Mountains (EWM) block is a large crustal block containing folded 10-km thick Cambrian to Permian sedimentary succession, subsequently deformed by the Permo-Triassic Ellsworth orogeny, and is allochthonous with respect to East Antarctica (Dalziel et al., 1987; Maslanyj and Storey, 1990). Some interpretations suggest that the EWM block was originally located in a position adjacent to both the Antarctic and South African margins, with its rotation into its current position taking place during a complex period of Late Triassic or Early Jurassic crustal shearing during the initial stages of Gondwana break-up (Curtis and Storey, 1996). Most tectonic models suggest that prior to Gondwana break-up, the crustal block was in a pre-rotated orientation, located 1500 km further north, adjacent to the Maud Belt of Southern Africa (Dalziel, 2013). Other models propose a less far travelled model, where the EWM block is located 500 km northeast of its current location and was rifted from East Antarctica by extension and transferred to West Antarctica (Jordan et al., 2017). Whichever initial position is correct, its movement resulted in an extensional rift system (the Weddell Sea Rift System) developing behind the moving block between the Haag-Ellsworth-Whitmore block and East Antarctica. This extensional rifting created major fault systems, with extended and modified crust forming the floors of the Weddell Embayment (Dalziel and Lawver, 2001). The thermal age of the stretched continental crust below the Filchner-Ronne ice shelf has been dated to 230 to 165 Ma, which is in good agreement with the timing of Gondwana break-up and

indicates that later further movement of microplates in this region is unlikely (Jones et al., 2002; Studinger and Miller, 1999). This Weddell Sea Rift System was formed in response to distributed crustal extension within a broad plate boundary region between West and East Antarctica (Jordan et al., 2017), with extension suggested to have been ongoing at ~167 Ma (König and Jokat, 2006). Therefore, the broad assembly of the microcontinental blocks (Haag, EWM, Antarctic Peninsula) in the Evans-Rutford region was likely to have been completed within the Jurassic, with the latest time being approximately 165 Ma, the youngest thermal age of the crust underlying the Filchner-Ronne Ice Shelf. The main geotectonic provinces and sub-provinces in the modern subglacial topography can be seen in Figure 2.2.

Following this assembly, thermochronometry data indicates that the Ellsworth Mountains experienced a huge amount of exhumation during the Early Cretaceous between ca. 145 Ma and 117 Ma, uplifting by 4 km or more, following the initial separation of East and West Gondwana and coinciding with the opening of the Weddell Sea. Subsequent post-Early Cretaceous uplift and denudation has been constrained to a maximum of 3km, however, it has not been distinguished whether this occurred gradually or in a pulse (Fitzgerald and Stump, 1992, 1991).

2.3. Climate and ice sheet history of Antarctica

Over the past 100 Ma or more, the continent of Antarctica shifted from one that is green and tree-covered, to a continent that is encased in ice, holding the largest ice sheet on Earth. This change occurred as a result of tectonic isolation where the Gondwana supercontinent broke up over a period of 170 Ma to 34 Ma, coupled with global climate cooling beginning more than 200 Ma, ending with the opening of the Drake Passage and the establishment of the Antarctic Circumpolar Current (Bell and Seroussi, 2020; DeConto and Pollard, 2003; Livermore et al., 2007). As this tectonic isolation occurred, the concentration of atmospheric CO_2 showed a long-term decline and thus global temperatures were gradually dropping. The Eocene-Oligocene boundary, ca. 34 Ma, marks a point at which there was a marked decline in ocean temperatures (Figure 2.3) (Escutia et al., 2019).

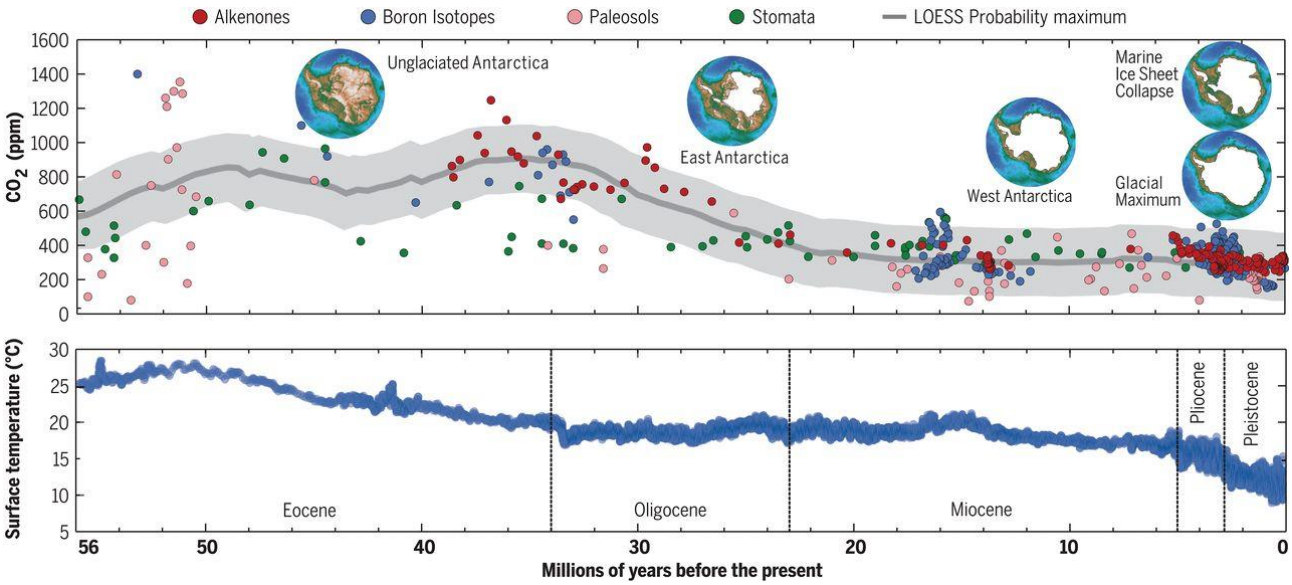

Figure 2.3: Development of Antarctic ice together with global CO_2 and ocean surface temperature (Bell and Seroussi, 2020). Top: Global CO_2. Bottom: Ocean surface temperature.

Little ice is thought to have existed in Antarctica prior to 34 Ma, or the latter half of the Cenozoic, however, after this point the continent was subjected to repeated phases of glaciation (Siegert, 2008). Some observations suggesting the existence of marine-terminating glaciers at the Sabrina Coast have indicated cryospheric evolution of an Antarctic Ice Sheet beginning in the middle Eocene (Gulick et al., 2017). However, the more widely accepted inception of major Antarctic glaciation was in the early Oligocene (ca. 34 Ma) and is represented by a distinct positive anomaly in the marine $\delta^{18}O$ record, accompanied by positive excursions in the biogenic sediment accumulation rates and the mean $\delta^{13}C$ of dissolved inorganic carbon (Zachos and Kump, 2005). At this time, >50 m changes in global mean sea level records were observed, derived from Pacific benthic foraminiferal $\delta^{18}O$ and Mg/Ca records (Miller et al., 2020), implying large fluctuations in Antarctic ice sheet volume. The declining Cenozoic atmospheric CO_2 and Southern Ocean cooling as a result of the opening of ocean gateways led to the formation of small, highly dynamic ice caps on high Antarctic plateaux at the Eocene-Oligocene transition (Colleoni et al., 2022; DeConto and Pollard, 2003). However, a continental-scale Antarctic Ice Sheet with frequent calving at the coastline was not formed until ca. 32.8 Ma, coincident with the earliest time at which atmospheric CO_2 fell below approximately 600ppm (Colleoni et al., 2022; Galeotti et al., 2016). The threshold of atmospheric CO_2 for the onset of large-scale Antarctic glaciation remains uncertain, with values in numerical climate and ice sheet simulations varying between 560 to 900ppm (Colleoni et al., 2022).

Coupled ice sheet-general circulation models have depicted growth of a large East Antarctic Ice Sheet at the Eocene-Oligocene boundary, with very limited ice in West Antarctica (Wilson and Luyendyk, 2009). Within 400 kyr of ice sheet inception, the climate system settled into a more moderate but stable 'glacial' state (Zachos and Kump, 2005). The small dynamic ice masses in East Antarctica

expanded rapidly through the early Miocene, coalescing to form a continental-scale ice sheet. The middle Miocene and Pliocene was a time of significant ice sheet expansion in concert with orbital variations, with the ice masses evolving into a major and persistent ice sheet undergoing repeated phases of glaciation (DeConto & Pollard, 2003; Siegert, 2008).

2.4. Inception and instability of the West Antarctic Ice Sheet

The West Antarctic Ice Sheet (WAIS) formed in concert with the continental-scale expansion of the East Antarctic Ice Sheet (EAIS); reconstructions of the palaeo-topography for the late Eocene have shown that much of West Antarctica lay above sea level after accounting for glacial erosion and thermal subsidence, meaning that it was capable of supporting terrestrially-grounded ice (Wilson et al., 2013). Initially, the WAIS was comprised of isolated ice caps centred over islands and continental blocks during the Oligocene through to the early Miocene, which then coalesced into an ice sheet which advanced onto the continental shelf multiple times throughout the late Miocene and Pleistocene (Anderson and Shipp, 2001). However, it is now classed as a marine ice sheet as most of it is grounded below sea level. The ice is underlain by rifted sedimentary basins, marine sediments deposited by glacial processes, crystalline bedrock, and active volcanic terrains (Jordan et al., 2020; Tinto et al., 2019). This meant the WAIS required substantial cooling to form a large ice sheet, resulting in extensive ice forming much later than the EAIS and not fully forming until 14 Ma (Bell and Seroussi, 2020). Tectonic movement also contributed to the inception of the WAIS as the uplift of Marie Byrd Land established elevated terrain on which the ice sheet could form. Uplift to current elevations, which peak at ~2700 m in the centre of Marie Byrd Land, were likely driven by buoyant mantle effects since ca. 34 Ma (Jordan et al., 2020). The Ellsworth Subglacial Highlands also represent a major seeding centre of the WAIS, with the landscape being covered and eroded by small dynamic ice fields similar to those of the present-day Antarctic Peninsula (Ross et al., 2014).

As a Marine Ice Sheet, the WAIS is subject to the Marine Ice Sheet instability and so is potentially vulnerable to rapid retreat. During past warm periods, the West Antarctic Ice Sheet retreated beyond its current extent, and experienced complete collapse in some instances (Naish et al., 2009). Over the past 5 Ma, modelled variations in ice sheet extent range from full glacial extents with grounding lines near the continental shelf break, intermediate states similar to the modern configuration, and brief but dramatic retreats which left only small, isolated ice caps (Pollard and Deconto, 2009). Therefore, the WAIS is of concern in a warming climate, as a collapse of the marine ice sheet in West Antarctica, forced by atmospheric or ocean warming, would produce a contribution to sea level rise of more than 3 m (Joughin and Alley, 2011).

2.5. Radio-echo sounding data

Airborne radio-echo sounding (RES) is a powerful geophysical approach used for characterisation of the subsurface conditions of ice masses at local to global scales. It has been used in glaciology to observe ice thickness, basal topography and englacial layers for over five decades (Schroeder et al., 2020). RES is based on the transmission and detection of electromagnetic waves at frequencies between 1 to 1000 MHz, where the radar signal propagation is controlled by relative electrical permittivity and electrical conductivity. This may be considered in terms of signal velocity, attenuation and resolution, which are widely used to investigate the internal and basal properties of ice masses (Plewes and Hubbard, 2001). Changes in the dielectric contrast can result from density variation, permittivity variations from changes in crystal fabric, or aerosols from volcanic eruptions, which produce internal reflection horizons (IRHs) imaged by the radar (Corr et al., 2007). This layering within ice sheets provides isochrones over distances of up to hundreds of kilometres, allowing the correlation of stratigraphic and palaeoclimatic records between ice cores (Dowdeswell and Evans, 2004).

The vast majority of RES surveys have been motivated by locating the reflection of the bed topography, in order to map the basal topography and estimate the total volume and sea-level potential of the major ice sheets (Schroeder et al., 2020). Construction of Digital Elevation Models of the glacier surface and bed from ice thickness and subglacial topography data derived from radar surveys may then be used to support the numerical modelling of glacier dynamics, as well as determining ice thickness and volume changes (Plewes and Hubbard, 2001). RES can provide information on past WAIS behaviour by directly measuring subglacial elevations and quantifying glacial landscapes that may have been influenced by former ice sheet configurations, which is critical for evaluating the present risk of regions susceptible to change (Ross et al., 2012).

2.6. Hypsometric analysis of topography

Hypsometric analysis is the study of the distribution of ground surface area, or horizontal cross-sectional area, of a landmass with respect to elevation (Strahler, 1952). Absolute hypsometric curves display the frequency-distribution of elevations and are often used to characterise landscape morphology (Brocklehurst and Whipple, 2004). For example, the hypsometric curves of the northern, central and southern Andes have strikingly different but regionally consistent shapes, illustrating latitudinal variations suggesting that fluvial tectonic, and glacial processes, respectively dominate the morphology of the mountain range in these different zones (Montgomery et al., 2001). The hypsometric curve can also indicate the relative degree of glacial modification in a drainage basin, as the transition from non-glaciated to glaciated conditions with the formation of cirque glaciers tends

to skew the frequency-distribution to higher elevations (Brocklehurst and Whipple, 2004). Geomorphic signatures of some glaciated landscapes have also illustrated local hypsometric maximums which relate to low relief landscapes formed primarily in response to glacial erosion, and the compensating isostatic uplift of unglaciated hillslopes initially found below the snowline (Pedersen et al., 2010). Therefore, the hypsometry of glaciated regions can be used to infer how rates of glacial erosion compare with tectonic uplift rates, although many other factors can exert a major influence (Brocklehurst and Whipple, 2004). In terms of landscape evolution underneath a continental ice sheet, hypsometry of the buried landscape can be used alongside analysis of relief and slopes to identify whether topography has been selectively eroded or smoothed. In a landscape dominated by glacial erosion, the density of individual peaks is higher when compared to one where topography is submerged beneath an ice sheet (Jamieson et al., 2014).

2.7. The role of flexural isostasy in landscape development

The lithosphere undergoes an isostatic adjustment when a load is added or removed from the crust, for example, post-glacial uplift, or crustal unloading by denudation (Summerfield, 1991). The loading of ice on the crust has a profound effect on the underlying mantle and crust, where regions that were loaded are subject to subsidence, whilst regions adjacent to the ice experience uplift (Watts, 2001). If the isostatic compensation is local, the isostatic uplift reduces the rate at which a land surface is lowered by denudation. However, as the lithosphere has a finite strength, local compensation cannot occur at a small scale, therefore even fairly local changes in load result in *regional* isostatic adjustments over a greater area; this adjustment is known as flexural isostasy (Summerfield, 1991). An example of this would be a plateau summit increasing in elevation as a result of erosional unloading, as erosion occurs on either side of the plateau either in deep valleys or at the foot of a bounding escarpment; however, the magnitude of these effects depend on the flexural rigidity of the lithosphere. In the context of Antarctica, an example of flexural isostatic uplift can be seen to provide an explanation for the emergence of the Shackleton Range as a coherent block from beneath the East Antarctic Ice Sheet at 2.5 Ma, as a result of ongoing glacial erosion of the adjacent troughs (Paxman et al., 2017).

2.8. Modern topography of Antarctica

The pattern of glacial landscape evolution in Antarctica has been controlled by the size of its overlying ice mass, the orientation of flow, and its basal temperature (Jamieson et al., 2014). As well as this, the behaviour of the Antarctic ice sheet has been influenced by the pre-existing crustal structure established over the course of Antarctica's geological history, in addition to the geomorphic processes that act to modify the subglacial landscape since ice sheet inception (Paxman et al., 2020).

Reconstructions of Antarctica's topography at the Eocene-Oligocene climate transition have demonstrated significant upland areas in the Ross Sea, Marie Byrd Land, and Weddell Sea sectors, and much shallower East Antarctic coastal troughs (Wilson et al., 2011). The land area situated above sea level was ~25% larger than present at the Eocene-Oligocene boundary; incision of East Antarctic deep subglacial marginal troughs occurred predominantly in the Oligocene and early Miocene, in contrast to West Antarctica where erosion and sedimentation rates only accelerated after major WAIS formation in the mid-Miocene (Paxman et al., 2019c). However, some parts of East Antarctica have not changed much as they have been protected under non-erosive, cold-based ice since 34 Ma (Wilson et al., 2011). Prior to 33.7 Ma, the only glacial erosion occurred in the highest elevation coastal and interior highlands which were eroded by local, warm-based alpine glaciers. Through to 14 Ma, the continent supported a significant range of erosion configurations depending on the scale of cyclical margin advance and retreat, after which point, alpine glacial erosion was largely limited to coastal mountain ranges and the Antarctic Peninsula (Jamieson et al., 2014).

The evolution of Antarctic subglacial topography has occurred as a result of different stages of continental glaciation and their associated erosional processes. Much of the lowland interior can be seen to resemble landscapes of areal scouring which are typical of the Laurentian and Scandinavian shields, whereas selective linear erosion near the continental margins has overdeepened pre-existing river valleys (Jamieson et al., 2010). Morphometric analysis of the continent has shown the presence of alpine landscapes both along the coastlines and isolated in the interior of East Antarctica, which are for the majority surrounded by zones of selective linear erosion (Jamieson et al., 2014). The distribution and dominance of this erosional process illustrates the importance of pre-glacial topography in steering ice flow during all phases of ice growth, and the impact of continental-scale ice sheet flow that is consistent in pattern (Jamieson et al., 2014).

The most novel, high-resolution description of Antarctic bed topography is BedMachine, which uses a combination of radio echo-sounding and a mass conservation algorithm (in areas with less radar coverage) to map the subglacial topography (Morlighem et al., 2020). The results have revealed previously unknown basal features with major implications for glacier response to climate change, as compared to the previous Bedmap2 topographic map, based only on a compilation of RES data (Fretwell et al., 2013). Understanding changes in glacier flow and projecting ice sheet evolution is limited by uncertainty and lack of small-scale detail in bed topography, therefore requiring detailed and accurate subglacial topography maps. Both Bedmap2 and BedMachine are limited by their interpolation approaches, and so further high-resolution maps of basal topography in key regions are still required.

2.9. Geomorphological expression of large-scale tectonic processes

Plateaux or low-relief surfaces can be formed close to sea-level by long-term wave erosion to form a coastal strandflat, or by long-term coastal scarp retreat. These mechanisms require long-term stability in base level, which is usually sea level, for them to form. This means plateau formation tends to be associated with periods of very low uplift. Periods of uplift can cause an eroded low-relief surface to move to a higher elevation, and a new surface form at, or close to, base level. Troughs can be eroded by rivers or by glaciers, but if a trough is fluvially eroded, then it is unlikely to erode below contemporary sea level. Alpine landscapes form where ice cover is fairly restricted, through processes associated with ice caps or ice fields. These tend to be temperate (warm-based) causing erosion beneath small cirque and valley glaciers, as there are seasonal fluctuations in temperatures above and below zero to promote frost-weathering.

2.9.1. Landscape and geomorphology of rifted margins

The most prominent landforms that would accompany the continental breakup of Gondwana are high elevation passive margins and their associated major escarpments (Cockburn et al., 2000). These rifted margins are initially uplifted as a result of thermal buoyancy and crustal flexure in response to denudation near the coast and deposition offshore. This uplift leads to erosion promoted by high local relief and the establishment of a lower base level along the new continental margin. They are subjected to fluvial processes and evolve into a seaward-facing escarpment formed at the drainage divide (Jamieson and Sugden, 2008). Denudation rates eventually decrease, as a result of the eventual adjustment to the base levels created at the time of continental rifting and breakup (Cockburn et al., 2000). Evidence of this landscape evolution can be seen between southwestern Africa (e.g. Namibia) and southern South America, which demonstrate patterns of denudation from low elevation coastal plains and escarpment summits that are compatible with the presence of high topography along newly-created continental margins and the establishment of a new, lower base level. Interconnecting rift and horst structures also developed between the two landmasses during the initial rift phase (Brown et al., 2000). Passive margin evolution has also been observed in the Dronning Maud Land region of Antarctica, which demonstrates a coastal plain backed on its inland margin by an escarpment and mountain crest, where the interior flank also slopes down to a lowland plain (Sugden and Jamieson, 2018).

2.9.2. Geomorphological evidence of erosional surfaces beneath the Antarctic Ice Sheet

Erosional surfaces can record key intervals in the evolution of a continental landscape, often equating to periods of relative base level stability. The preservation (and thus detection) of pre-glacial landscape remnants beneath the Antarctic ice sheet is most likely where the direction of ice flow

under a selective erosion regime remains constant, as the cold base of an overlying ice sheet can remain unchanged despite having evolved through 58 glacial cycles during the last 13 Ma (Jamieson et al., 2014).

Radio-echo sounding evidence for preserved pre-glacial flat surfaces has been identified across multiple regions of Antarctica, specifically in the Wilkes Subglacial Basin (Paxman et al., 2018), the Weddell Sea Embayment (Rose et al., 2015), the Ross Embayment (Wilson and Luyendyk, 2006), and Marie Byrd Land (LeMasurier and Landis, 1996). Common features of these surfaces are that they are laterally continuous over 10-100 km scales and demonstrate a flat and level (low-angle) nature with low relief. Interpretations of the formational processes of these surfaces have involved marine erosion or wave action into the basement in the absence of glacial ice (Wilson and Luyendyk, 2006), or in front of a retreating escarpment following the Gondwana break-up (Paxman et al., 2018). Prolonged fluvial erosion down to a peneplain has also been proposed, the processes of which may have interplayed with marine planation (LeMasurier and Landis, 1996; Rose et al., 2015). In either case, the erosional surfaces represent prolonged intervals of erosional levelling that must have taken place in a relatively stable tectonic environment.

2.10. Research Questions

In the context of the key large-scale geomorphological features that might be expected beneath the ice sheet, given the tectonic history of the region, this study will therefore answer the following research questions:

1. What is the subglacial topography of the Evans-Rutford Region?
2. What formational processes are recorded in the geomorphology of the subglacial topography of the ERR?
3. What is the relationship between subglacial topography, its underlying geological structure, and ice flow, for example through topographic steering?

3. Methodology

This section outlines the radio-echo sounding datasets used within this study, as well as the instrumentation and processing used for data collection. The process of interpolating a Digital Elevation Model (DEM) in a GIS software is discussed, along with the subsequent geomorphological mapping and large-scale morphometric analysis from the resultant DEM. The use of a flexural isostatic rebounding model applied to the DEM to produce a model of the pre-glacial landscape is also explained.

3.1. Survey data

During the 2006/07 austral summer, the GRADES-IMAGE survey collected approximately 27,550 km of airborne radio-echo sounding data over 100 hours of surveying (Corr, 2021). The survey was flown over the Antarctic Peninsula, Ellsworth Mountains, and Filchner-Ronne Ice Shelf, with particular focus on the Evans and Rutford ice streams (Figure 1.1). The survey aircraft was equipped with dual-frequency carrier-phase GPS for navigation with absolute GPS positional accuracy of 0.1 m, wing-tip magnetometers, a radar altimeter for surface mapping and the bistatic Polarimetric radar Airborne Science Instrument (PASIN) system (Corr et al., 2007; Vaughan et al., 2006).

3.1.1. Instrumentation and Processing

The instrumentation and initial processing of the RES data are outlined in Corr (2021), the key aspects of which are summarised here. The PASIN radar system was operating with a centre frequency of 150 MHz and using 2 interleaved pulses: a 4 μs, 10 MHz bandwidth linear deep-sounding chirp, and a 0.1 μs unmodulated shallow-sounding pulse. Along-track data was collected at a post-processing trace spacing of 20 m and vertical resolution of 8.4 m. No gravimetric survey was conducted. Compression of the chirp data, best used to assess the bed and englacial features in deep ice conditions, was applied using a Blackman window to minimise sidelobe levels, and then processed using a coherent averaging filter along a moving window of length 15. An incoherent averaging filter along a moving window length of 25 was used to process the pulse data, using a combination of the upper and lower channels, which enabled assessment of the internal structure and bed in shallow ice conditions. The bed reflector was automatically picked on the chirp data, using a semi-automatic picker in the PROMAX software package. Surface elevation was derived from the radar altimeter for ground clearance less than 750m, and from the PASIN system for higher altitudes. Longitude, Latitude and Height are all referred to the WGS1984 ellipsoid.

Raw SEGY files were imported into ReflexW and plotted on a natural log scale to visualise and enhance weaker radar reflections (Winter et al., 2015). After visual inspection of the radargrams to assess the quality of the semi-automatic picker, areas of erroneous bed reflection picks were

corrected, which applied to approximately 10% of total line length. Sources of error within the picked bed reflections can arise from surface clutter returns masking the echoes of the ice-bedrock transition at depth, or diffracted hyperbolae cause by an unfocused return of the energy, meaning that the ice-bed interface becomes unclear and difficult to identify in some radar lines (Hélière et al., 2007; Napoleoni et al., 2020). Picked travel time was converted to depth using a radar wave velocity through ice of 168 m/μs (Corr et al., 2007), and a constant firn correction of 10 m was applied (Ross et al., 2012).

An artefact in the radargrams that can result from airborne radio-echo sounding is the upwarping of the edges of flat surfaces, as the aircraft is flown at a constant elevation, causing changes in ice thickness to appear as an upwarping. However, the conversion of the bed reflection picks to a point dataset of bed elevation values is not impacted by this effect, as profiles of flat surfaces taken from this data do not indicate upwarping. Key areas of uncertainty in generation of DEMs from radio-echo sounding data can arise in precise determination of bed reflection depths, from the range precision of the radar system, applying a constant firn correction, and variations in the electromagnetic wave propagation in ice (Cavitte et al., 2016). The manual repicking of bed elevation picks also introduced areas of absent picks, where the bed reflection was determined to not be strong enough to accurately identify the bed.

To increase the spatial coverage and point density of the bed elevation picks within the region of study, bed picks from the TORUS (Targeting ice stream Onset Regions and Under-ice Systems) and Evans 1994/95 radio-echo sounding surveys were utilised in addition to those derived from the GRADES-IMAGE survey. The TORUS survey collected 9500 km of line data over the Rutford ice stream drainage basin during the 2001/02 austral summer. Similar to the GRADES-IMAGE survey, the BAS PASIN radar depth sounding system was used for airborne radio-echo sounding, using a 4 μs linear frequency modulated pulse in addition to a standard short 2 μs pulse (Corr and Smith, 2020). 11,500 km of RES line data was collected during the Evans 1994/95 RES survey (Corr, 2020), with the ice thickness data being obtained using a BAS-built RES system (Corr and Popple, 1994). This survey was oriented perpendicular to the strike of both the Bouguer anomaly field and the major sub-ice topographical features (Doake et al., 1983; McGibbon and Smith, 1991).

Exposed bedrock datapoints were also derived from the Reference Elevation Model of Antarctica (REMA) (Howat et al., 2019), to provide a reference for the elevation of above-ice bedrock features such as nunataks present within the study region. The data were extracted from REMA using the bedrock mask derived from automated analysis of Landsat8 imagery (Burton-Johnson et al., 2016). These combined datasets created a bed elevation point dataset covering 48,550 km of line data spanning from the base of the Antarctic Peninsula to the Ellsworth Mountains (Figure 3.1).

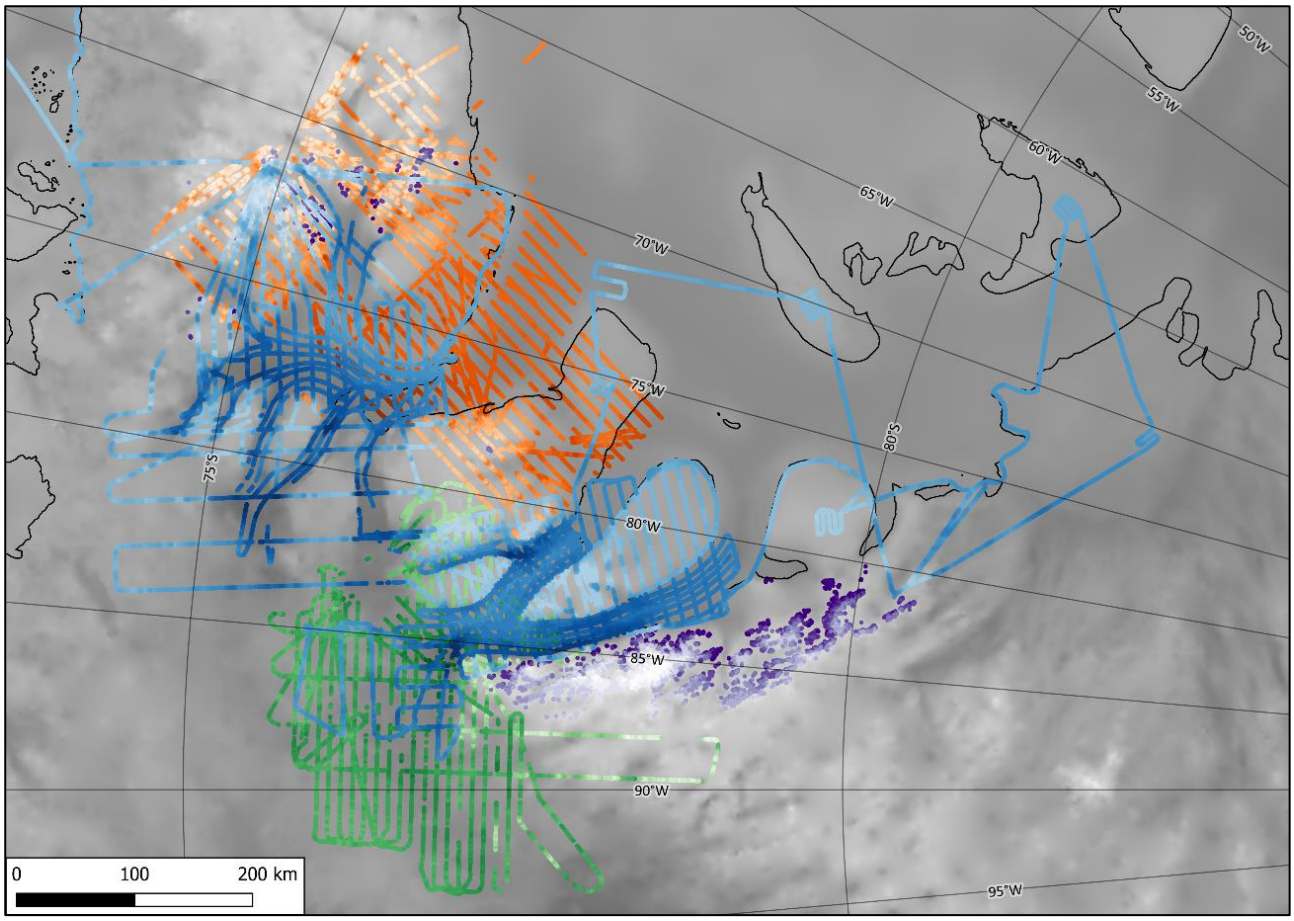

Figure 3.1: All survey datapoints used to interpolate the Digital Elevation Model: blue = GRADES-IMAGE, green = TORUS, purple = REMA exposed bedrock, orange = Evans 1994/95. Higher to lower elevation shown as light to dark colour gradients. Overlain on BedMachine subglacial topography map.

3.2. Generation of Digital Elevation Models

Interpolation of similar bed elevation datasets derived from radio-echo sounding surveys have utilised a range of algorithms, namely, natural neighbour (Ross et al., 2012; Young et al., 2011), kriging (Aitken et al., 2014; Rippin et al., 2004), and minimum curvature gridding (Bianchi et al., 2003). Methods utilising tension spline algorithms have produced realistic DEMs of similar subglacial bedrock topography (Napoleoni et al., 2020; Paxman et al., 2019b, 2018). Such methods are used with irregularly distributed data confined to discrete transects in order to create a grid of the inferred subglacial bed topography (Young et al., 2011).

Given the range of previous approaches to Digital Elevation Model (DEM) interpolation, we tested a variety of interpolation algorithms in order to produce a 500 m resolution DEM of the region. These included bicubic B-splining, Triangulated Irregular Network (TIN), and Inverse Distance Weighting (IDW), all of which were tested using ranges for their associated parameters. These methods produced topographies that were unrealistic in that they contained multiple artefacts within the DEMs; common artefacts included erroneously high and low spots of elevation and stepped and boxy hillslopes where

sharp edges of terrain were expected from the survey data. A detailed analysis of these different approaches and their limitations has been provided in Appendix 1, for full reference.

After exploring the various approaches, a continuous bivariate cubic spline algorithm in QGIS, known as cubic spline approximation, was chosen. It was more successful at interpolating the bed elevation points as it produced a DEM which filled in the gaps in a way that was not only smooth between the survey lines but captured the sudden changes in topography that were evident in the radargrams, without producing clear outliers/artefacts. Pre-processing of the bed elevation data involved rasterising the full point dataset into 100 m and 500 m cells and converting the raster back to a point dataset where each point contained the average value of points that lay within the cell. This was carried out in order to avoid anti-aliasing, as without this process, the splining algorithm was often trying to fit to too many points within a closely localised area. This included survey points that had slightly different elevations at flightline crossover points, therefore producing spikes in elevation. As a result of effectively averaging points within a certain grid cell, the anti-aliasing artefacts were removed. Points were masked to remove those that did not pertain to grounded ice, using the BedMachine grounded ice mask (Morlighem, 2020). Details of the parameter testing can be seen in Table 3.1 below.

Table 3.1: Table showing the parameters tested for interpolation using cubic spline approximation: min. points = minimal number of points locally involved in spline calculation, max. points = maximal number of points locally involved in spline calculation, points per square = average number of points per cell (increased if point distribution is strongly non-uniform), tolerance = relative tolerance multiple in fitting spline coefficients (i.e. higher value = higher degree of locally fitted spline). Notes describe the issues evident within the Digital Elevation Models produced.

Output name	**Cell size (m)**	**Min. points**	**Max. points**	**Points per Square**	**Tolerance**	**Notes**
Using survey_all_ rasterised_100m_points						
CSA_survey1	2000	3	20	150	40	
CSA_survey2	2000	3	20	100	40	
CSA_survey3	2000	3	20	40	40	
CSA_survey4	2000	3	20	40	40	Removed REMA points around area with major artefact
CSA_survey5	500	3	20	40	40	
CSA_survey6	2000	3	20	40	40	Using survey_all_points_merged
Using survey_masked_ 500m_points						
CSA_survey7	2000	3	20	40	40	Blurred + squared topography
CSA_survey8	500	3	20	40	40	Blurred + squared topography, more high and low artefacts
Using survey_masked_ 100m_points						
CSA_survey9	500	3	20	40	40	Some squared topography and artefacts
CSA_survey10	500	3	20	100	40	Big artefacts
CSA_survey11	500	3	20	20	40	Some squared topography and artefacts
Using survey_all_ grounded_masked						

CSA_survey12	500	3	20	40	40	Artefacts in certain points on either side of flightlines
Using survey_masked_ 100m_points						
CSA_survey13	500	3	20	40	80	Couple of artefacts - but would be excluded by 2km buffer
Using survey_all_ grounded_masked						
CSA_survey14	500	3	20	40	60	Multiple artefacts
CSA_survey15	500	3	20	40	20	Squared off topography but minimal artefacts
CSA_survey16	500	3	20	40	30	Squared topography and artefacts
CSA_survey17	500	3	40	40	20	Squared topography, high points on edges of plateaus
CSA_survey18	500	3	60	40	20	Similar to 17 - squared topography
Using survey_masked_ 100m_points						
CSA_survey19	500	3	20	40	20	Blurry squared topography and artefacts
CSA_survey20	2000	3	20	40	20	Squared topography around plateau edges
CSA_survey21	2000	3	20	20	40	Artefacts and spiky edges
CSA_survey22	2000	3	20	60	40	Strong artefacts, squared topography
CSA_survey23	2000	3	20	50	40	Some squared topography, artefacts on flightlines
CSA_survey24	2000	3	20	30	40	Artefacts in certain points on either side of flightlines
CSA_survey25	2000	3	20	30	30	Removes some artefacts, but one major
CSA_survey26	2000	3	20	30	25	Removes some high point artefacts but still one major
CSA_survey27	2000	3	20	30	20	Plateau edges more blurry
CSA_survey28	2000	3	20	30	20	Removed some strange points around major artefact
CSA_survey29	1000	3	20	30	20	Major artefact gone, but still some artefacts along flightlines around plateaus
CSA_survey30	500	3	20	30	20	Major artefact gone, but still some artefacts along flightlines around plateaus
Using survey_masked_ 500m_points						
CSA_survey31	2000	3	20	30	20	Blocky/square topography
CSA_survey32						resampled CSA_survey28
Using survey_all_ grounded_masked						
CSA_survey33	500	3	20	30	20	Final DEM

Key issues that arose whilst testing the interpolation method included DEMs with blurred and square-like topography, as well as significant artefacts represented as extreme topographic highs or lows within the landscape (Figure 3.2).

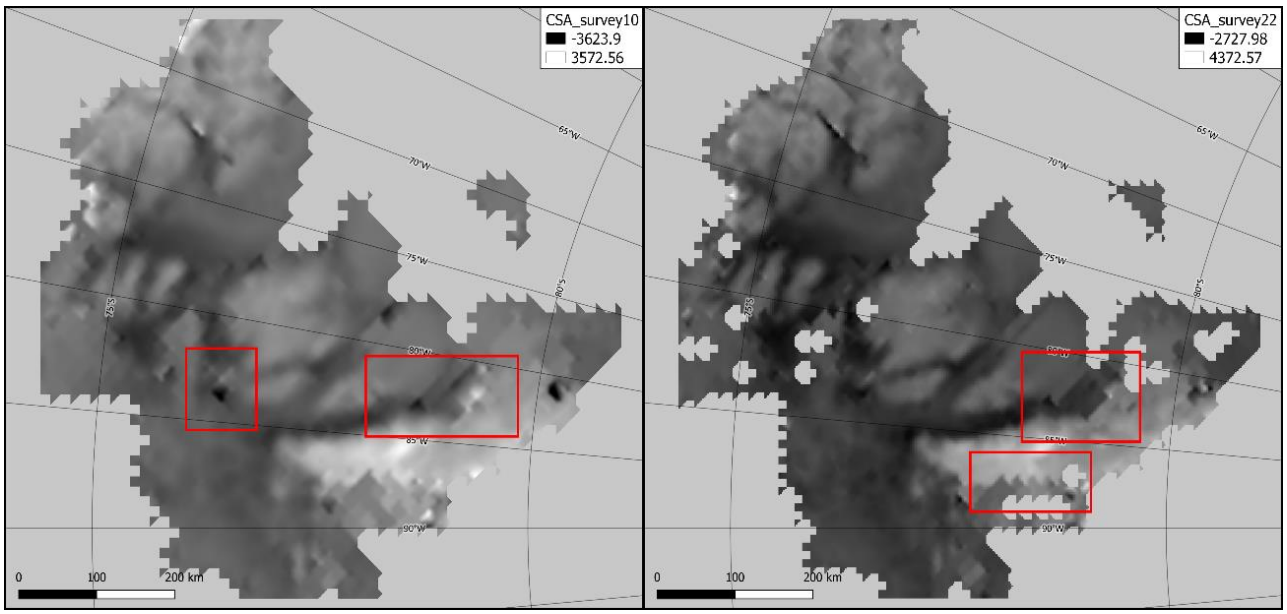

Figure 3.2: Interpolation issues (shown in red boxes) produced in early versions of the Digital Elevation Model. Significant artefacts are evident in CSA_survey10, creating topographic rises and lows. Squared and blurry topography is demonstrated in CSA_survey22.

The removal of some anomalous REMA exposed bedrock topography points resolved some of these artefacts, where checking against satellite imagery showed that no exposed bedrock was present at sites where the automated mask derived from Landsat8 imagery (Burton-Johnson et al., 2016) suggested bedrock. The resulting final DEM of the subglacial landscape is shown in Figure 3.3, using parameters of 30 points per square and a tolerance of 20, and interpolated at a 500 m resolution. These parameters produced the Digital Elevation Model with the least evident artefacts, as well as troughs that showed profiles that were the most accurate when compared to the survey data.

All survey datapoints were used, as the trough slopes produced by an averaged point dataset (as used in CSA_survey30) did not resolve the steep topography accurately and produced shallower trough walls as compared to the radargrams (Figure 3.4). The DEM was refined by masking the grid to remove interpolated values >2 km from the nearest measured datapoint, in order to reduce artefacts appearing far from the survey flightlines that were not topographically logical. The BedMachine grounded ice mask was also used again to remove all grid cells outside of the grounding line (Morlighem, 2020), as the radar data only gives an accurate bed reflection where the ice is grounded. The characteristics and landscape shown in the final DEM are discussed in detail in the results.

3.3. Assessment of Digital Elevation Model

To assess the accuracy of the interpolated DEM, it was compared to the BedMachine modelled subglacial topography (Morlighem et al., 2020). BedMachine uses interpolation but, crucially, also

uses ice surface velocities and mass conservation, as well as streamline diffusion to provide further constraints on subglacial topography.

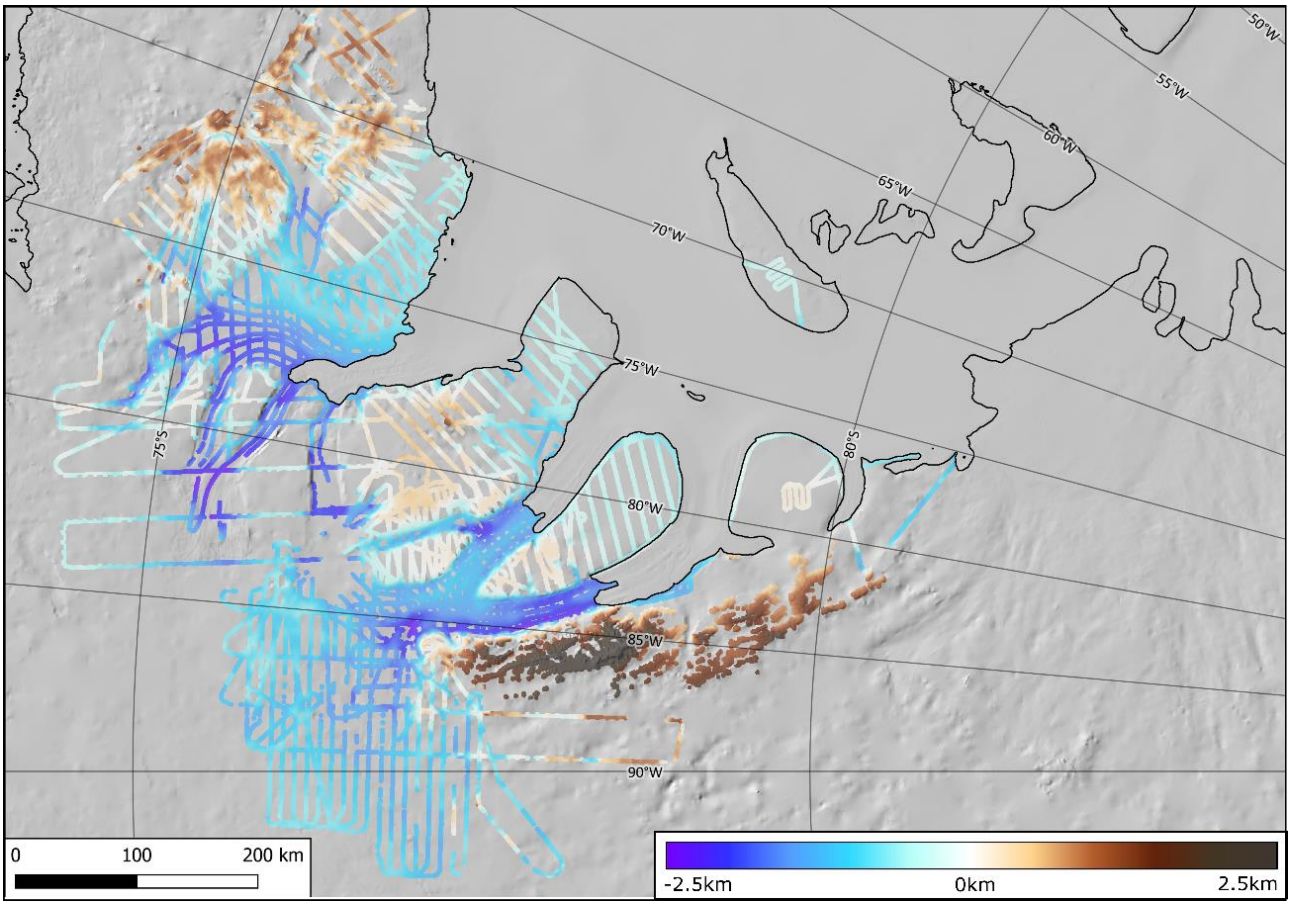

Figure 3.3: Final interpolated DEM overlain on hillshaded BedMachine subglacial topography map. Black line delineates grounding lines.

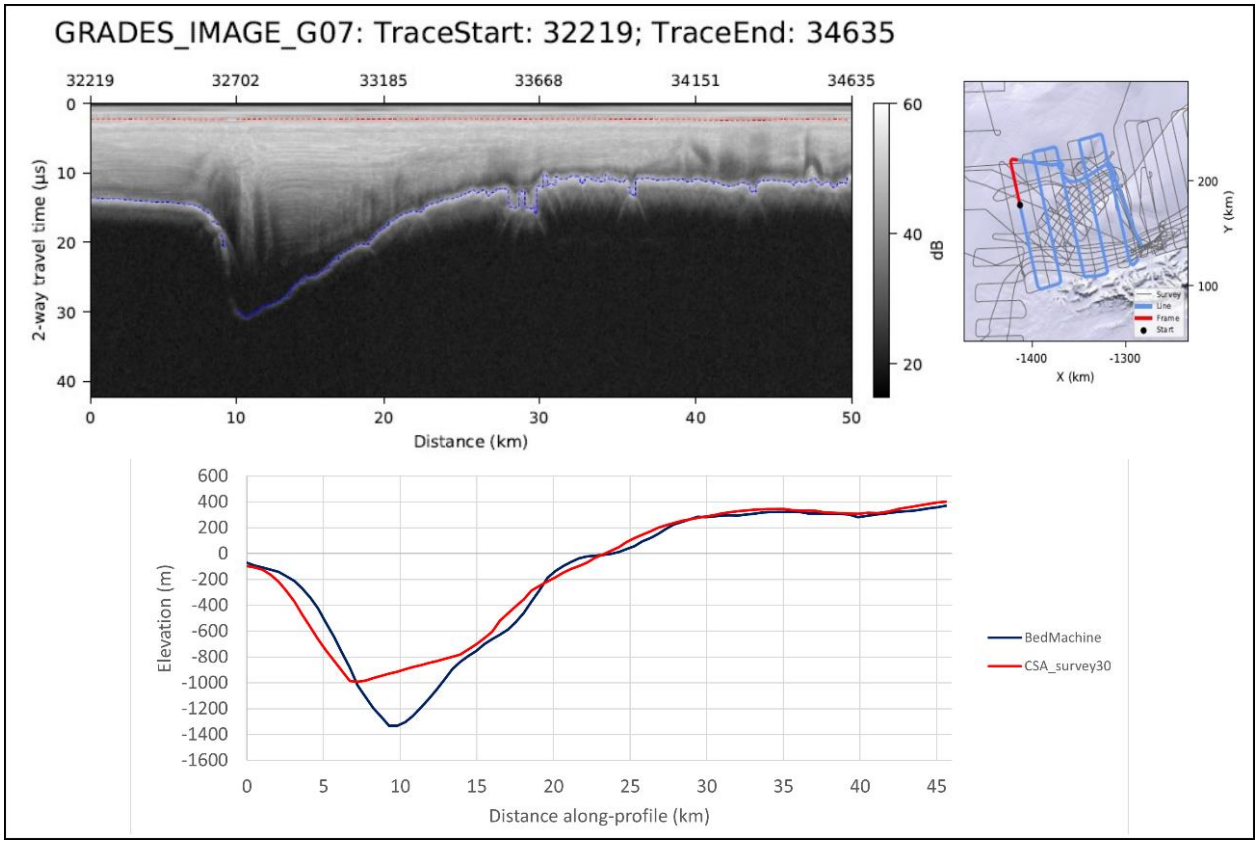

Figure 3.4: Comparison of GRADES-IMAGE G07 radargram and interpolated Digital Elevation Model profiles. The CSA_survey30 DEM (red profile) was interpolated using averaged point values and produced much shallower trough sides compared to BedMachine (blue profile) and the G07 radargram.

3.4. Geomorphological landscape mapping

In order to identify specific modes of landscape evolution, different types of feature or landform were mapped across the study area. These included troughs, plateaux, possible faults and channels. Areas of different geomorphologies within the study region were delineated using polylines and polygons in QGIS, using the interpolated DEM as well as the BedMachine bed topography data to fill data gaps (Morlighem, 2020). This was supplemented by the GRADES-IMAGE radargrams (Corr, 2021), which provided clear profiles of the subglacial topography where interpolation may have been lacking.

Plateau surfaces were defined as nearly flat surfaces separated from surrounding lower elevations by at least one steep side (Wilson and Luyendyk, 2006), and were mapped to the edges where sharp slope breaks were evident on profile lines. A series of radially-oriented channels within the plateau surface on Fletcher Promontory were also evident and mapped as individual features. In contrast, alpine topography was delineated as areas of sharp peaks and ridges, and deep, closely spaced troughs (Jamieson et al., 2014). Alpine topography shows high relief, and very few areas of low-gradient topography.

Troughs surrounding the plateaus and containing ice streams were separated into different morphological types. Firstly, the widest troughs with more gently sloping trough walls were U-shaped in terms of their cross-profiles. These wide troughs contained less sharp slope breaks in comparison to the other trough features. Fault-bounded troughs were identified where linear, steeply sloping trough walls with excavation at the base were evident. Two thalwegs close to the slope breaks and a central topographic were a common feature in such troughs, giving the floor a W-shaped profile, similar to those identified in the George VI Sound as being tectonically controlled (Smith et al., 2007). Potential faults were mapped aligned with the fault-bounded troughs. Asymmetric V-shaped troughs were commonly situated between plateaus, with their profile lines showing V-shaped cross-sections with steep slopes and clear thalwegs. The thalwegs were mapped using profile lines across each channel to find the deepest section. Depths of the V-shaped asymmetric troughs were calculated using the DEM elevation data, with average width being calculated from 10 profiles across the length of the channel.

The geomorphological mapping from an interpolated Digital Elevation Model may have areas of uncertainty where the interpolation produced artefacts between flightlines. The DEM was also

masked to remove interpolated values >2 km from the flightlines, meaning that landscape interpretation also relied on BedMachine to visualise a full representation of the landscape. When using the radargrams to visualise the landforms, the flightlines were not always oriented in a way that provides the clearest representation of the landform, such as flightlines running obliquely to channel or trough features.

3.4.1. Hypsometric analysis

Linking a landscape to its genesis and evolution requires characterisation of its topography and identification of different landscape types through hypsometric analysis (Jamieson et al., 2014). This method allows the characterisation of landscape morphology through the study of the distribution of ground surface area of a landmass with respect to elevation (Brocklehurst and Whipple, 2004; Strahler, 1952). The hypsometry of glaciated regions can be used to infer how rates of glacial erosion compare with tectonic uplift rates, although many other factors can exert a major influence on the landscape (Brocklehurst and Whipple, 2004). Hypsometric curves were calculated for the interpolated DEMs, in order to analyse the frequency-distribution of elevations and highlight where there are significant areas of land at particular elevations.

The hypsometric curve calculated from the DEM may have a potential bias introduced due to non-uniform survey grids and the consequent higher density of sampling in some areas of the landscape compared to others. For example, if original surveys were focussed on ice stream troughs, there would likely be a bias towards lower elevations in the hypsometry.

3.4.2. Rebounding of landscape

In order to provide insight into the age and genesis of the landscape, a flexural isostatic correction rebound grid (Paxman et al., 2021) was applied to the DEM in order to produce a model of rebounded elevations as they might have looked if we were to assume that they were formed before the region was covered by an ice sheet. The model uses contemporary ice thickness and lithospheric effective elastic thickness to calculate the fully re-equilibrated flexural isostatic response of the bedrock topography to the complete removal of the modern ice sheet load (Paxman et al., 2022). This resulting rebounded DEM was then subject to hypsometric analysis to enable comparison against the non-rebounded DEM. Whilst the model doesn't account for the full complexity associated with vertical movements as a consequence of glacio-tectonic interactions, a general indication of pre-glacial elevations is produced (Rose et al., 2015).

4. Results

The Digital Elevation Model interpolated from the GRADES-IMAGE, TORUS and Evans 1994/95 RES surveys has produced a clear representation of the subglacial bedrock landscape within the Evans-Rutford Region (Figure 4.1). Key features of this landscape have been mapped and classified into distinct geomorphological features in Figure 4.2, using the Digital Elevation Model alongside BedMachine subglacial topography data. These include deeply incised troughs containing current and past ice flow, namely, the Evans and Rutford ice streams, and Carlson and Talutis Inlets. These troughs demonstrate abrupt linear margins, and in some cases W-shaped cross-profiles. Wider and more gently sloping cross-profiles are demonstrated in the trough containing the main outlet of the Evans ice stream, which flows into the Filchner-Ronne ice shelf. Flat plateaux located at similar elevations are also evident across the region, with each plateau segment generally bounded by steeply sloping trough walls. Alpine topography is prevalent at the base of the Antarctic Peninsula, with sharp peaks and troughs surrounding the tributaries of the Evans ice stream, as well as the alpine topography of the Ellsworth Mountains at the southern boundary of the study region. The following sections provide more detailed descriptions of these key features, as this mapping will form the basis of interpreting the potential formational processes that have resulted in the present subglacial landscape.

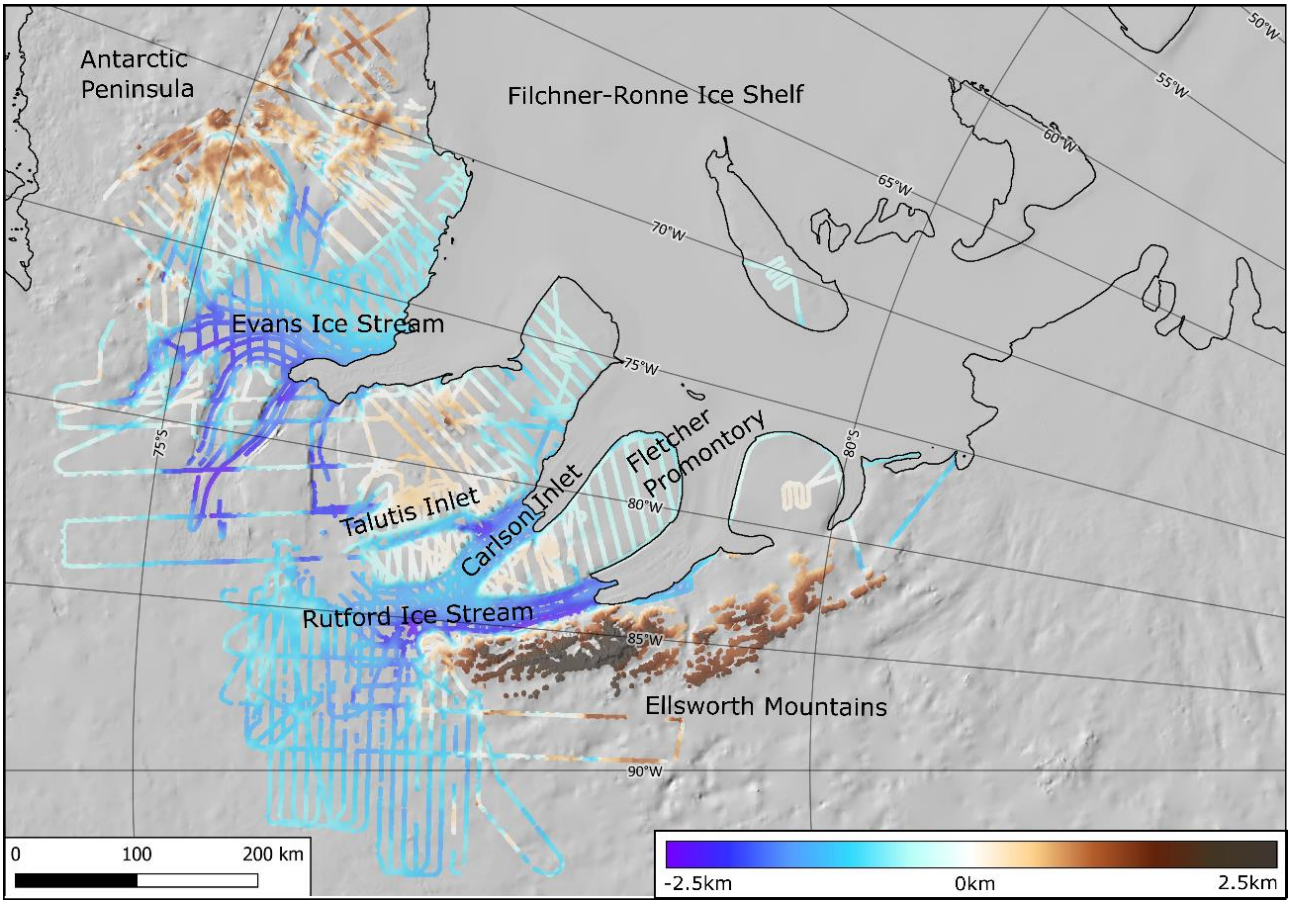

Figure 4.1: Digital Elevation Model of the Evans-Rutford Region, overlain on hillshaded BedMachine subglacial topography. The black line delineates the grounding lines.

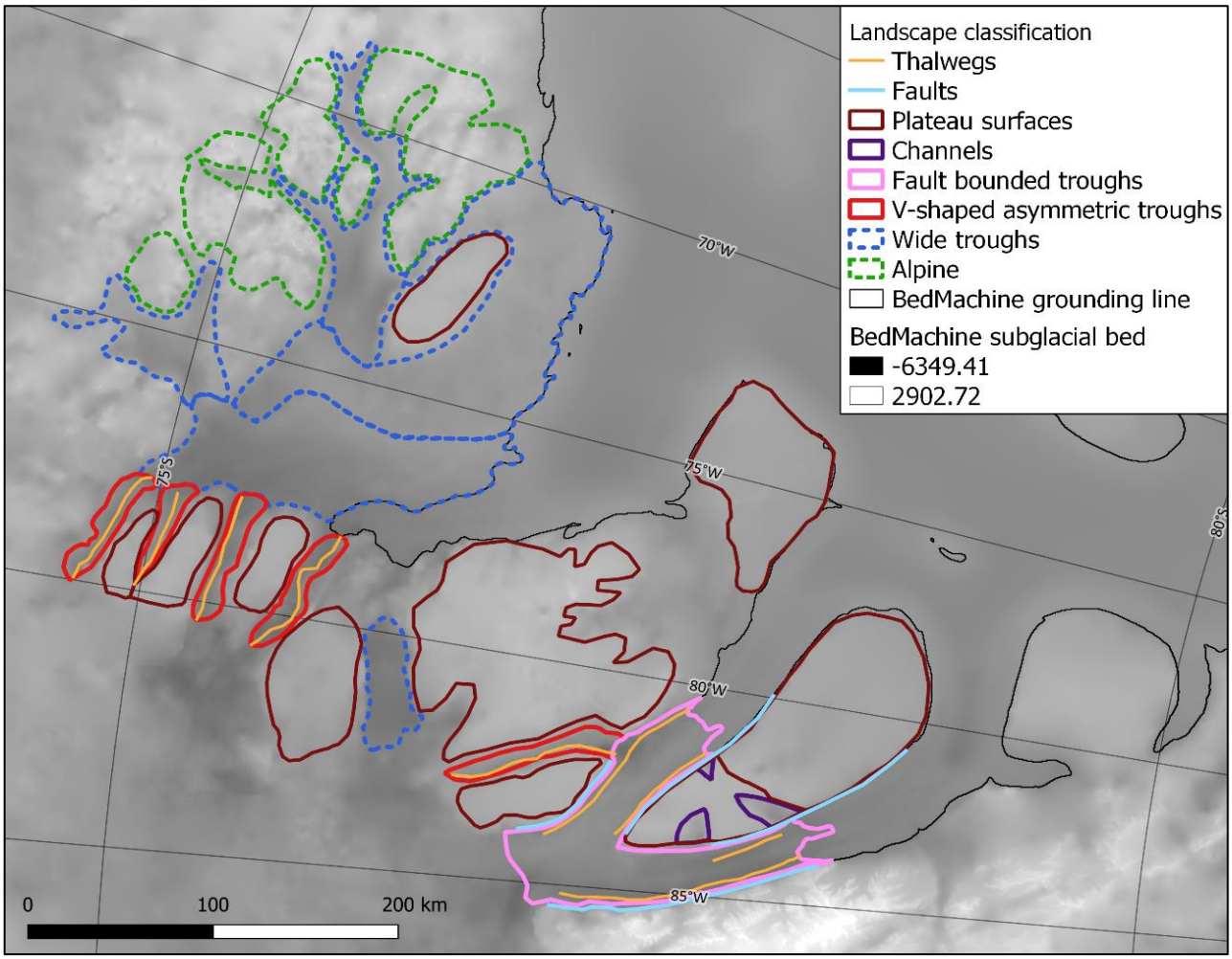

Figure 4.2: Landscape classification of the Evans-Rutford Region, displayed over BedMachine subglacial topography map. Dashed lines indicate lower levels of certainty around the extent of the morphological classification.

4.1. Landscape classification

4.1.1. Plateaux

Plateaux were identified as landscape elements where there are continuous, low-relief, low-angle surfaces that extend over significant areas, and are often continuous across intervening depressions. Flat plateau surfaces are dispersed across the region, with 10 individual plateaux having been delineated (Figure 4.3), the majority being located in the central parts of the study area between the Antarctic Peninsula and the Ellsworth Mountains. The area of each plateau ranges from 650 to 11032 km^2, as evident in Table 4.1. Mean elevations lie for the majority below sea level, with the lowest being plateau 4 at an average of -475.78 m, however plateaux 5 and 6 have mean elevations at 125.82 m and 164.69 m above sea level respectively. Groups of highly similar mean elevations are also evident; plateaux 7 and 9 reside at -61.95 m and -60.13 m respectively (and are located close to one another in the south-western part of the study area), as well as plateaux 4 and 8 at -475.78 m and -

455.60 m. The plateaux which are closest in terms of location, plateaux 1, 2 and 3, sit at mean elevations within a range of less than 50 m. Mean slopes across the plateaux are all <5 °. Mean current velocity of the ice overlying the plateau ranges between 7.32 m yr^{-1} to 22.82 m yr^{-1}, and mean ice thicknesses range between 654.2 m to 1252.4 m. Two potential plateau surfaces are also indicated by opportunistic radar data where the GRADES-IMAGE RES survey was extended to include single flight line coverage over the Filchner Ronne Ice Shelf: an ice rise under the Filchner-Ronne ice shelf, and a circular feature south of the Fletcher Promontory (Figure 4.3). These demonstrate low-relief surfaces at broadly similar elevations to the identified plateaux.

The majority of these plateaux have extremely flat surfaces as evident on the directly overflown radargrams, for example, plateau 1, 2 and 3 (Figure 4.4). In contrast, plateau 6 contains more variable topography, as it contains a topographic peak to its eastern side, as well as some shallow peaks and troughs across its surface. The margins of plateau 6 are also more crenelated in comparison to the more linear margins visible in the other plateaux.

Plateau ID	**Area (km^2)**	**Mean elevation (m)**	**Mean slope (°)**	**Mean ice velocity (m yr^{-1})**	**Mean ice thickness (m)**
1	649.736	-237.24	2.96	11.53	1037.2
2	1332.895	-196.61	3.97	14.40	849.4
3	1122.865	-199.35	3.84	22.82	685.4
4	3248.881	-475.78	0.97	10.26	1252.4
5	1832.457	125.82	1.83	7.32	654.2
6	11031.96	164.69	2.55	11.43	786.2
7	1619.115	-61.95	1.47	10.46	917.6
8	5079.483	-455.60	0.65	11.39	785
9	2562.495	-60.13	4.58	12.31	596.1
10	7612.398	-342.16	1.42	12.43	799.3

Table 4.1: Zonal statistics calculated for each individual plateau. ID numbers are shown in Figure 4.3.

Figure 4.3: Plateau surfaces and troughs evident in the Evans-Rutford Region. Plateaux are delineated using black lines, with V-shaped asymmetric troughs in red, fault-bounded troughs in brown and thalwegs shown in yellow. Each plateau is referred to by identification numbers 1 through 10 as shown above. The geomorphological mapping is overlain on the Digital Elevation Model and BedMachine subglacial topography map, with grounding lines illustrated with thin black lines.

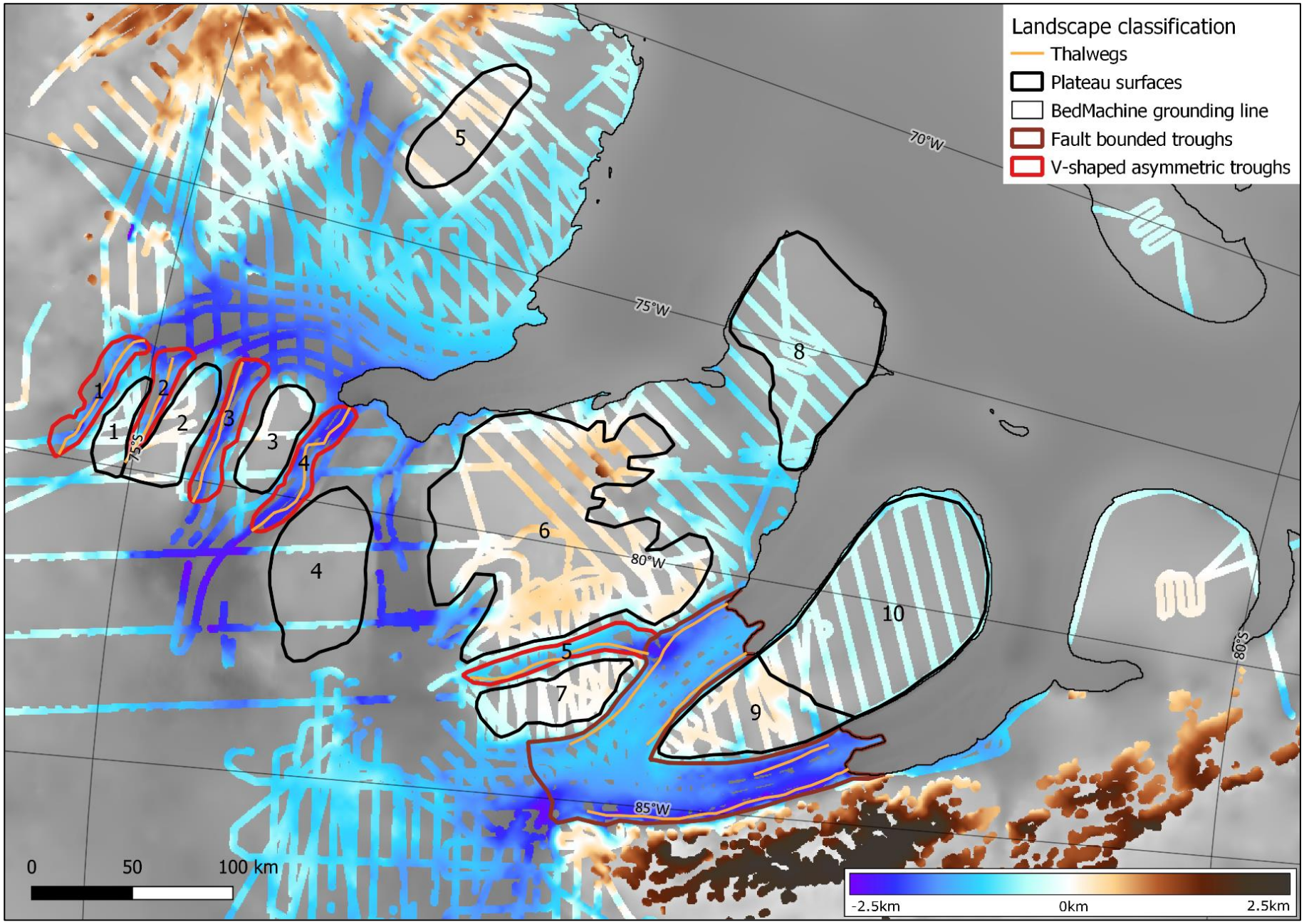
Landscape classification
Thalwegs
Plateau surfaces
BedMachine grounding line
Fault bounded troughs
V-shaped asymmetric troughs
70°W
75°W
80°W
85°W
75°S
80°S
1
2
3
4
5
6
7
8
9
10
0
50
100 km
-2.5km
0km
2.5km

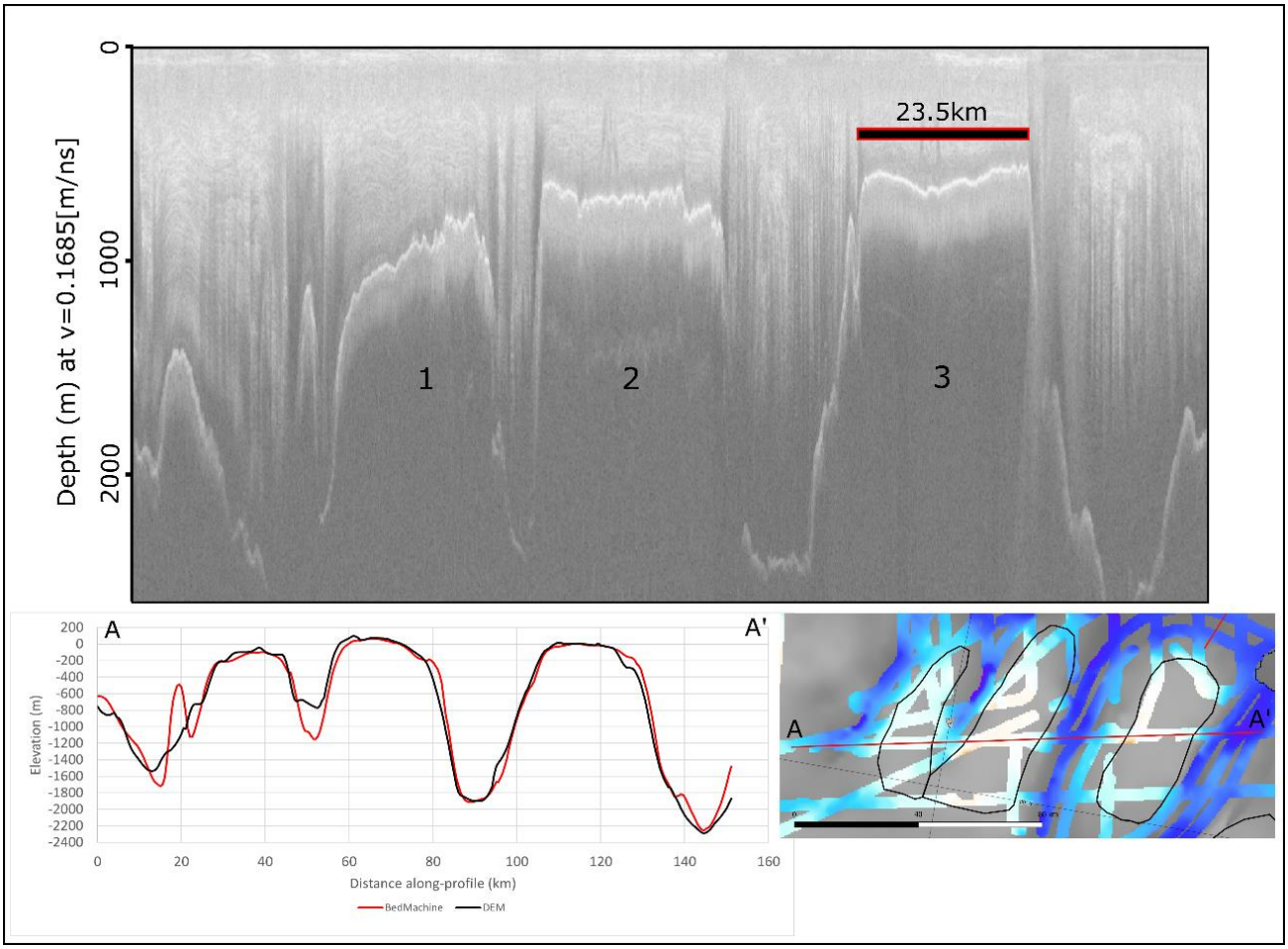

Figure 4.4: Radargram illustrating plateau surfaces 1, 2 and 3. Interpolated profiles from DEM (black line) and BedMachine (red line).

The subglacial topography of the Fletcher Promontory consists of two plateaux, 9 and 10, which appear at two different elevations, separated by a step or scarp. A west-east long profile across the promontory (Figure 4.5a), shows the lower surface (10) sitting at an elevation of approx. -400 m, with the higher surface (9) lying at approx. 200 m, a difference in elevation of 600 m. A characteristic that differentiates plateau 9 from the others in the region is that three valleys radiate from its centre, with two connecting to the Rutford ice stream on the southwest margin and one connecting to Carlson Inlet on the northeast margin. Cross profiles indicate that they range from approx. 8 to 14 km wide at their widest points, reaching approximately 1 km in depth, and are V-shaped. Surface velocities show that the larger of the southwestern V-shaped channels contains marginally faster flowing ice than the surrounding plateau, at a speed of ~30 m yr^{-1}. The ice flow velocity is evident immediately upstream of the grounding line of Rutford ice stream (Figure 4.5b).

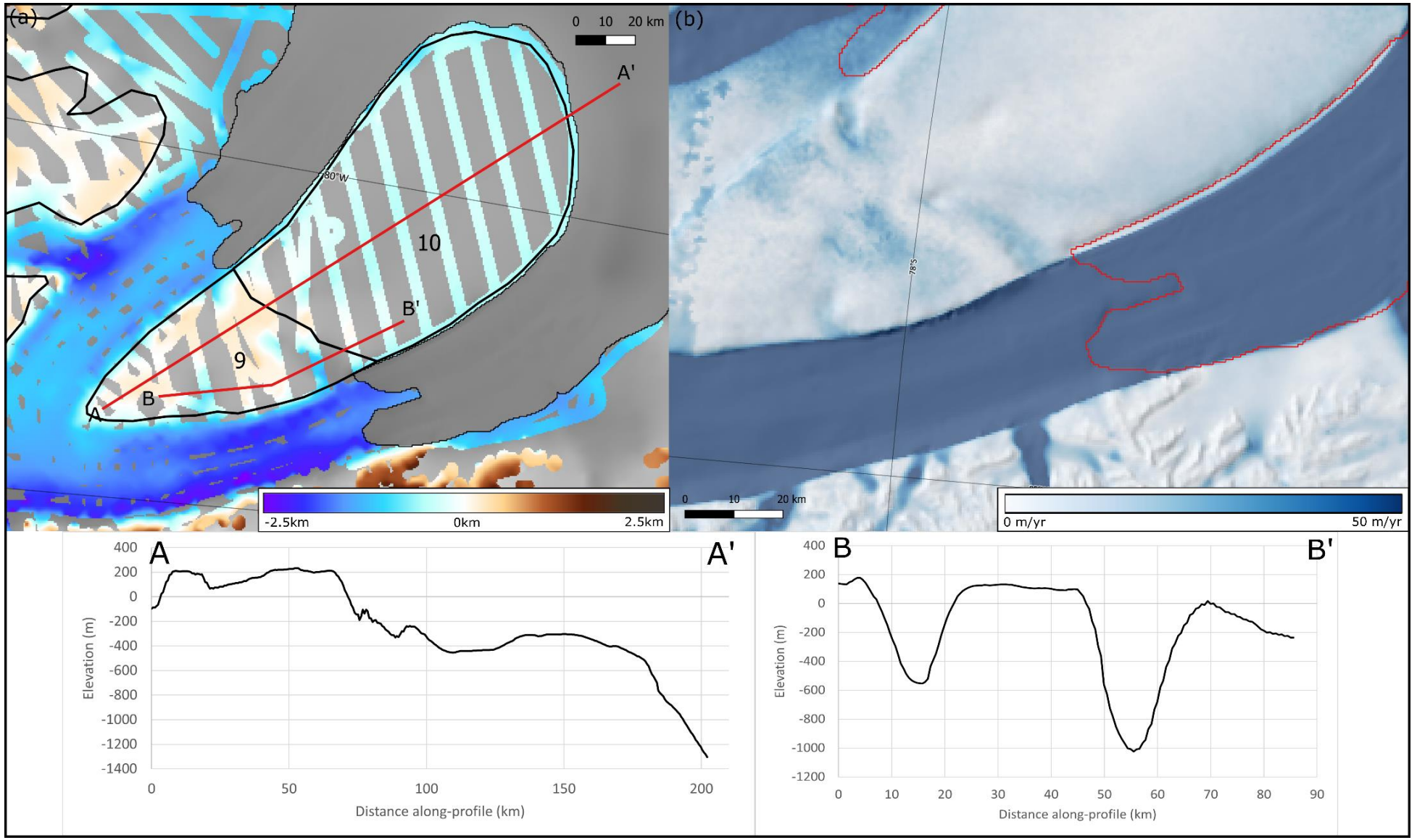

Figure 4.5: (a) Profile lines illustrating the features of plateaus 9 and 10 on the Fletcher Promontory. Interpolated profiles from BedMachine (black line). (b) Flow velocity overlying hillshaded BedMachine subglacial topography. Red line illustrates the grounding line.

4.1.2. Troughs

Troughs are identified as linear valley features, mostly U-shaped but some are V- or W-shaped with abrupt, steep margins. In Figure 4.2, multiple classifications of troughs throughout the Evans-Rutford Region have been mapped, as there are three distinct morphologies present. These troughs surround all the identified plateau surfaces, some of which are at present inhabited by fast-flowing ice, reaching a maximum of 641 m yr^{-1} in the mapped wide troughs containing Evans ice stream, whereas some appear to contain slow-flowing ice, for example reaching as low as 0.2 m yr^{-1} in Carlson Inlet. Troughs indicative of fault bounding contain the Rutford ice stream and Carlson Inlet, surrounding the Fletcher Promontory (Figure 4.6). The cross-profiles of these troughs demonstrate a W shape, as the subglacial bed is deeper directly adjacent to the base of the trough walls and borders a raised central ridge, similar to those identified as tectonically-controlled in the George VI Sound (Smith et al., 2007). The trough walls are linear and reach a maximum of ~46 °, despite appearing near-vertical in the associated radargrams. Asymmetry can be seen in the Carlson Inlet, where the grid north side of the trough reaches elevations of ~2300 m below sea level. It appears to be deeper compared to the grid south which sits at an elevation of ~1500 m below sea level, demonstrating an elevation difference of approx. 800 m across the trough. At the intersection of Talutis and Carlson Inlets, the northern margin of Carlson appears significantly deeper where Talutis, which currently demonstrates relatively slow ice flow, joins it.

V-shaped asymmetric troughs are present between plateaux, with one containing the Talutis Inlet (Figure 4.6). The thalwegs of these troughs often tend to be located along one side, with a steeper trougher wall closer to the line of the thalweg. The widths of these troughs average between 10.16 km to 12.1 km across, with maximum relief ranging between 1398 m to 2424 m (Table 4.2).

Valley ID	**Average width (km)**	**Maximum relief (m)**
1	11.995	1598
2	10.47	1800
3	12.105	1389
4	11.983	1434
5	10.156	2424

Table 4.2: Average width for each channel was calculated as a mean of 10 cross-profiles downvalley. Maximum relief was calculated using the highest and lowest elevations within the valley polygons. Valley IDs can be found in Figure 4.6.

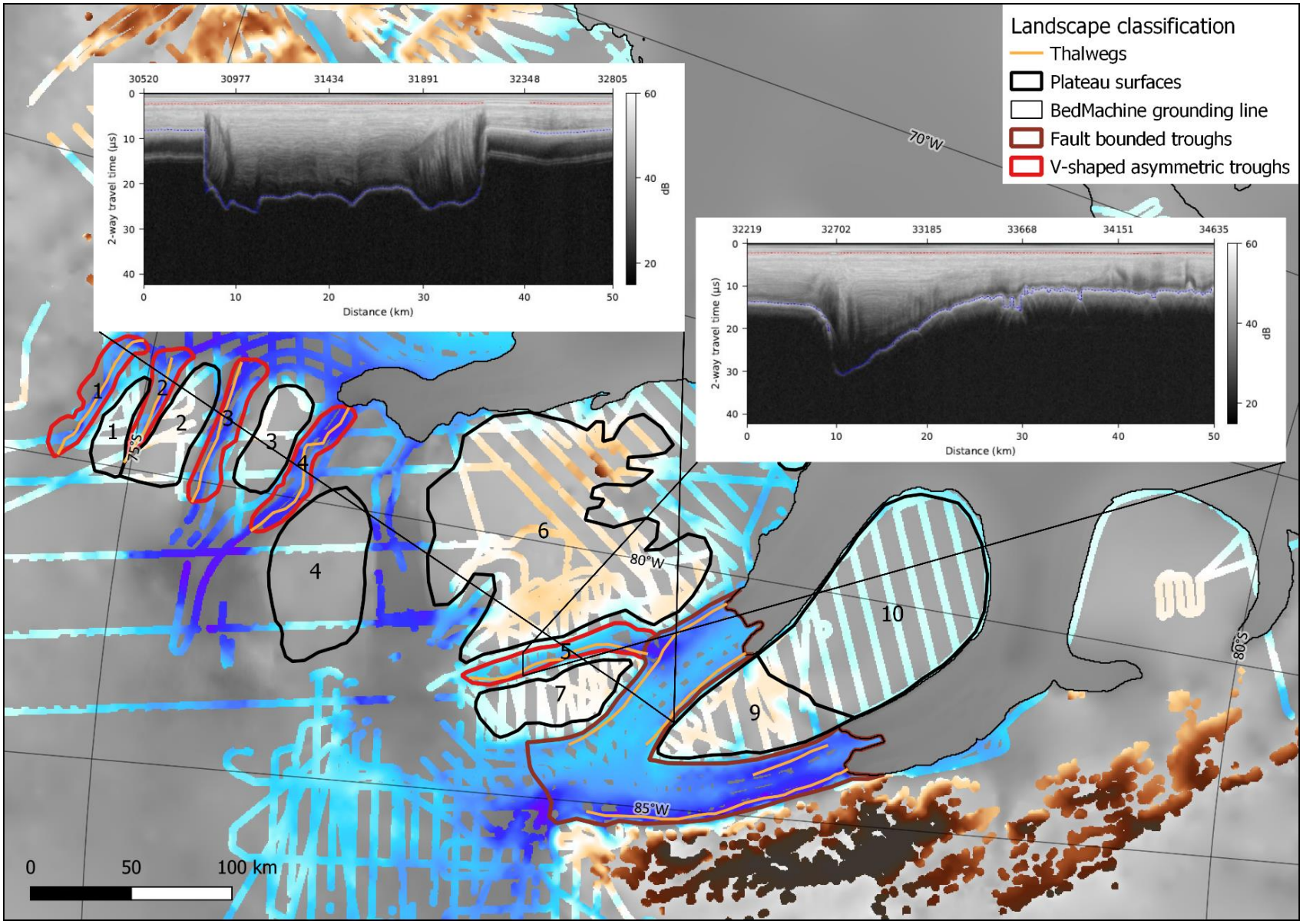

Figure 4.6: Troughs and plateaux mapped in the Evans-Rutford Region. Radargrams illustrate the cross-profiles of the V-shaped asymmetric and fault-bounded troughs in Carlson and Talutis Inlet.

Wider, more gently sloping cross-profiles are evident in the trough containing the main outlet of the Evans ice stream, with the long profile parallel to ice flow demonstrating a retrograde bed (Figure 4.7). A central topographic ridge runs in the direction of ice flow, dividing the trough, illustrated by Figures 4.7b and 4.7c. The grid north side appears shallower than the grid south side, sitting at mean elevations of -700.28 m and -1370.5 m below sea level respectively. Multiple narrower troughs contain tributaries feeding into the central outlet of Evans.

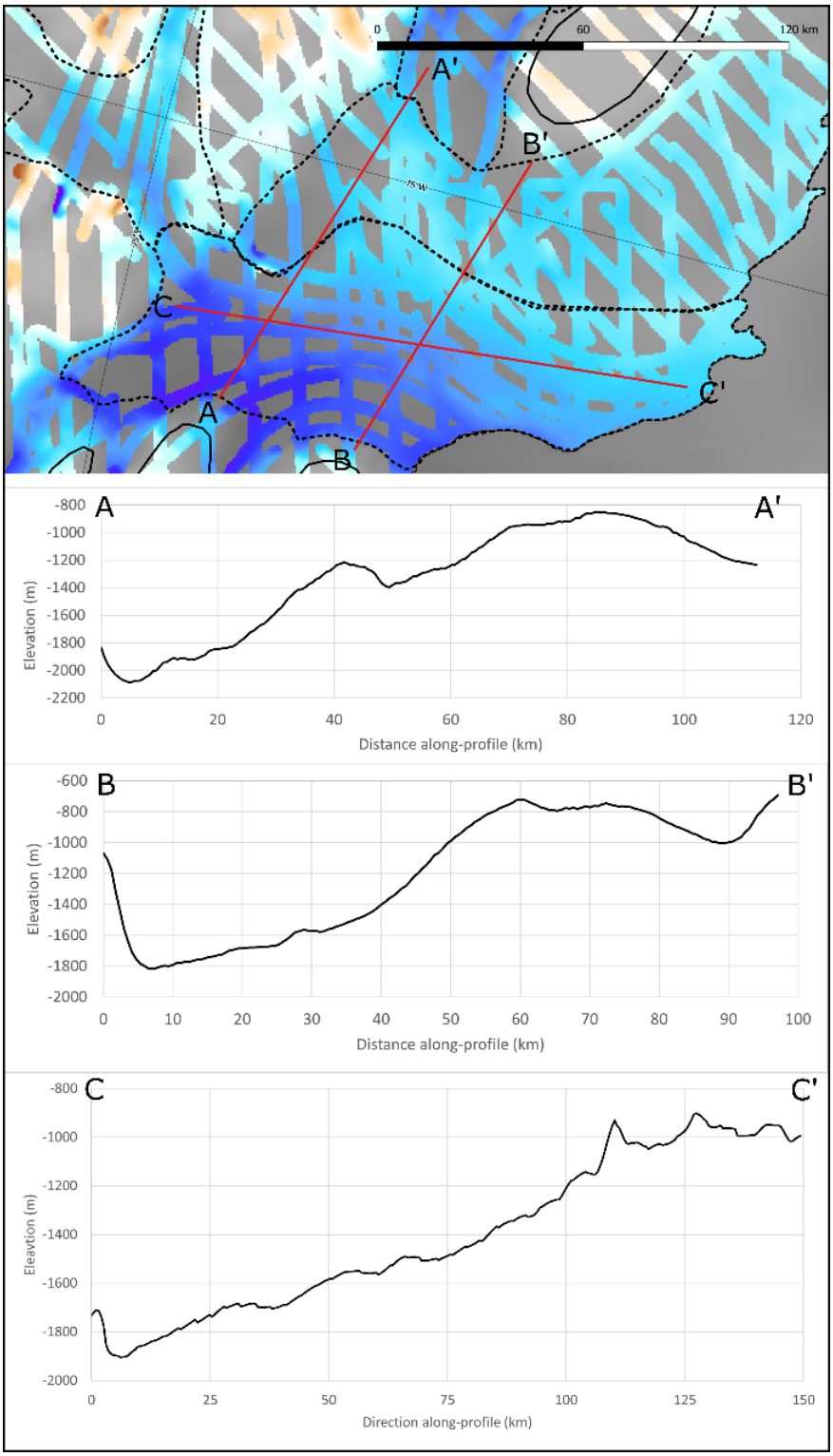

Figure 4.7: Cross-profiles of the Evans Ice Stream to illustrate its subglacial topography. Profiles A-A' and B-B' run perpendicular to ice flow, and profile C-C' runs parallel to ice flow direction.

4.1.3. Alpine topography

Low wavelength, rough topography with sharp peaks and troughs is evident at the base of the Antarctic Peninsula, surrounding the tributaries of Evans ice stream (Figure 4.2). Figure 4.8 demonstrates a radargram exemplifying this region, which contains major valleys that range from 9100 m to 15,350 m in width, as well as numerous smaller valleys. The peaks within the mapped regions of alpine topography reach a maximum elevation of 1651 m above sea level, with the relief between peaks and troughs reaching up to 2148 m. Cross-profiles of the valleys often demonstrate U-shaped troughs between sharp peaks.

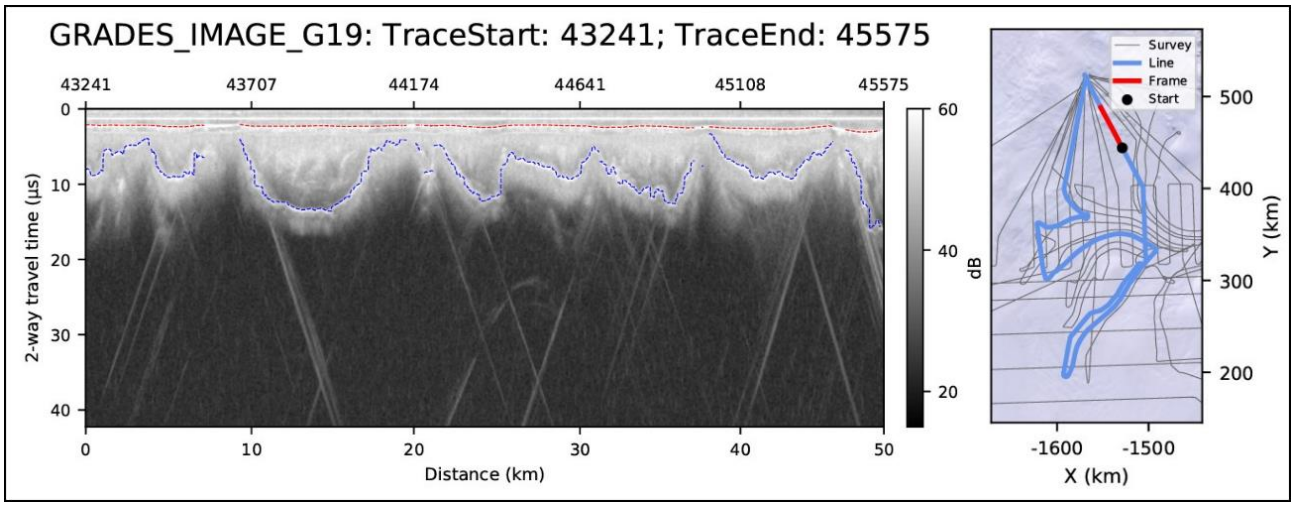

Figure 4.8: Radargram exemplifying the alpine topography situated at the base of the Antarctic Peninsula.

4.2. Hypsometry

The hypsometric curve derived from the Digital Elevation Model can be seen in Figure 4.9b. The curve demonstrates three significant peaks with other minor inflection points. The elevations within the uppermost peak range between -28 m to 471 m, with the peak sitting at 171 m above sea level. The middle peak ranges from -528 m to -28 m, peaking at -328 m. The lowest significant peak reaches a maximum at -728 m and has a range of elevations between -1028 m and -528 m below sea level. In terms of percentage of the total area of the DEM, the lowest peak comprises 24 %, the middle peak makes up 17 %, and the highest peak in area-elevation contains 16 %, totalling 57 % of the landscape interpolated by the DEM. Figure 4.9c illustrates the hypsometric curve divided into these significant peaks, which has been used to classify the elevations of the DEM (Figure 4.9a). This classification highlights two sets of plateau surfaces, illustrated in white and light blue, and which manifest as the two highest elevation significant peaks in the hypsometric curve. The higher elevation plateau population (light blue) sits between -50 m below and 500 m above sea level, whilst the lower elevation plateau population sits at -550 m to -50 m below sea level. The lowest elevation hypsometric peak is associated with the east side of Evans ice stream, and the onset zone of Rutford ice stream. The lowest

elevations within the DEM can be attributed to the deeper west side of Evans and its tributaries, as well as the troughs containing Rutford ice stream, Carlson Inlet, and Talutis Inlet.

4.3. Flexural Isostatic Rebounding

A flexural isostatic rebounding model (Paxman et al., 2022) was applied to the DEM, in order to determine the pre-glaciation landscape by adjusting elevations to account for ice loading. This allows for an understanding of the elevations at which the plateaux surfaces may have sat if they were to have existed prior to the onset of glaciation in Antarctica.

The hypsometric curve of the rebounded DEM (Figure 4.10b) only demonstrates two significant peaks in area-elevation, in contrast to the three peaks in the present-day subglacial topography. The higher of the peaks ranges between 182 m and 582 m, with the peak lying at 382 m above modern sea level. The lower peak in elevation sits reaches a maximum at -217 m below modern sea level, ranging between -417 m and -17 m. The rebounded DEM, classified according to the peaks evident in the hypsometric curve (Figures 4.10a and 4.10c), also clearly illustrates the two populations of plateaux that were evident in the present-day DEM, shown in yellow and light blue. The lower population (yellow) now resides between 0 m and -450 m below modern sea level, whereas the higher population of plateaux (light blue) sits between 150 m to 600 m above modern sea level. The majority of the plateaux have remained in the same population as the non-rebounded hypsometry, although Plateau 1 has rebounded to a higher elevation and is now included within the higher population. The troughs containing the Evans and Rutford ice streams continue to make up the majority of the lowest elevations, with the deepest elevations evident in Rutford at approx. -2600 m at its deepest point, at the convergence of Carlson and Talutis Inlet at a depth of -1950 m, and the western side of Evans ice stream, which reaches depths of -2000 m, even when isostatically rebounded.

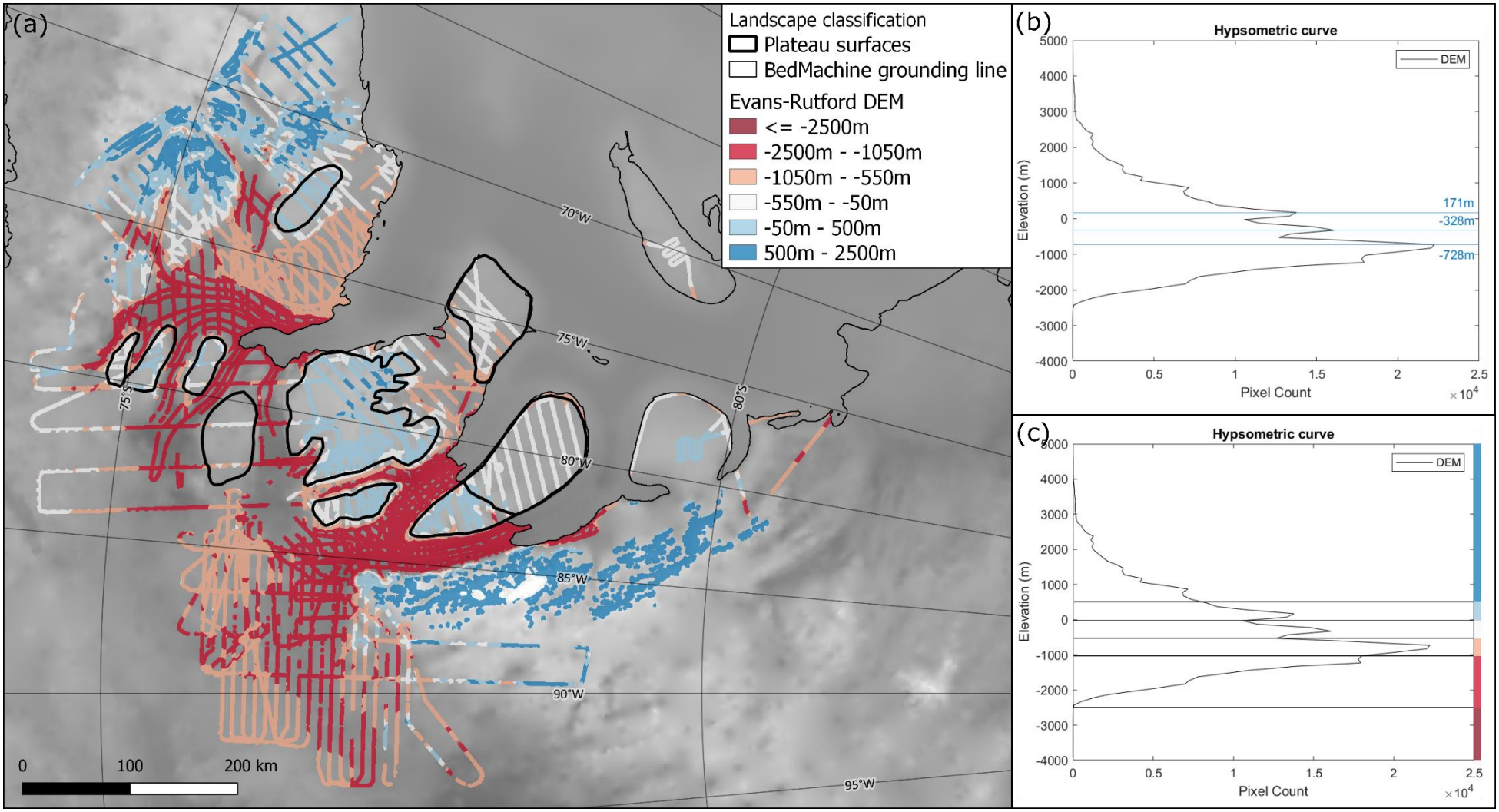

Figure 4.9: (a) Digital Elevation Model displayed in categorised symbology relating to hypsometric peaks. Plateau surfaces are outlined in black. Displayed over BedMachine subglacial topography map. (b) Hypsometric curve derived from the Digital Elevation Model with significant peak values marked. (c) Hypsometric curve classified according to significant peaks (coloured bars on right elevation scale correspond to colours in panel (a)).

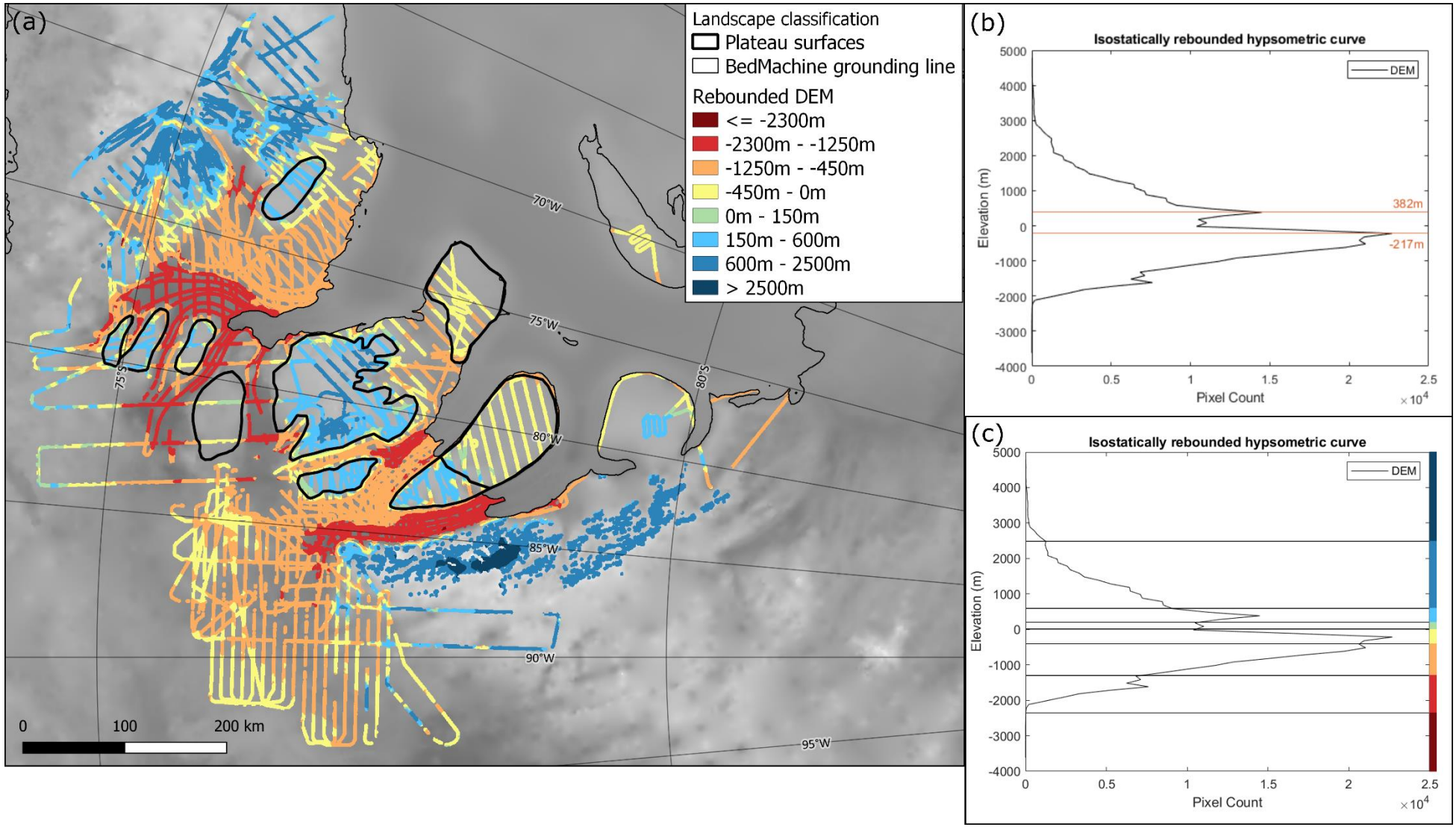

Figure 4.10: (a) Isostatically rebounded Digital Elevation Model displayed in categorised symbology relating to hypsometric peaks. Plateau surfaces are outlined in black. Displayed over BedMachine subglacial topography map. (b) Hypsometric curve derived from the isostatically rebounded Digital Elevation Model with significant peak values marked. (c) Hypsometric curve classified according to significant peaks (coloured bars on right elevation scale correspond to colours in panel (a)).

4.4. Comparison of Digital Elevation Model and BedMachine

Pixel differences between the new interpolated DEM and BedMachine are illustrated in Figure 4.11a, where positive values indicate that BedMachine has produced higher elevation values, and negative values indicate lower elevation values in the BedMachine DEM. The raster histogram derived from the pixel difference raster (Figure 4.11b) is centred around zero, indicating a lack of bias towards higher or lower elevations within the DEM. The hypsometric curve produced from both rasters also follows a very similar pattern (Figure 4.11c).

However, key areas of difference are evident, particularly in the fast-flowing inland tributaries and alpine topography of Evans ice stream. Figure 4.12 illustrates that the tributaries have been interpolated using a mass conservation method in BedMachine, whereas the slow-moving sectors including bed topography downstream and between the Evans tributaries has been calculated using streamline diffusion (Morlighem et al., 2020).

In addition, comparison of the terrain profile along the edge of the Rutford ice stream shows a deep trough present in BedMachine that is not present to the same depths on the GRADES-IMAGE survey radargrams (Figure 4.13). This may have been produced by the change in the interpolation method from streamline diffusion to IBCSO/Bedmap2, occurring where the ice shelf meets grounded ice. Significant areas of difference can also be seen in sections of the TORUS survey, grid south of the Ellsworth Mountains. However, the interpolated DEM for the majority matches the bed topography of BedMachine, particularly in areas of slow-moving ice where streamline diffusion has been used.

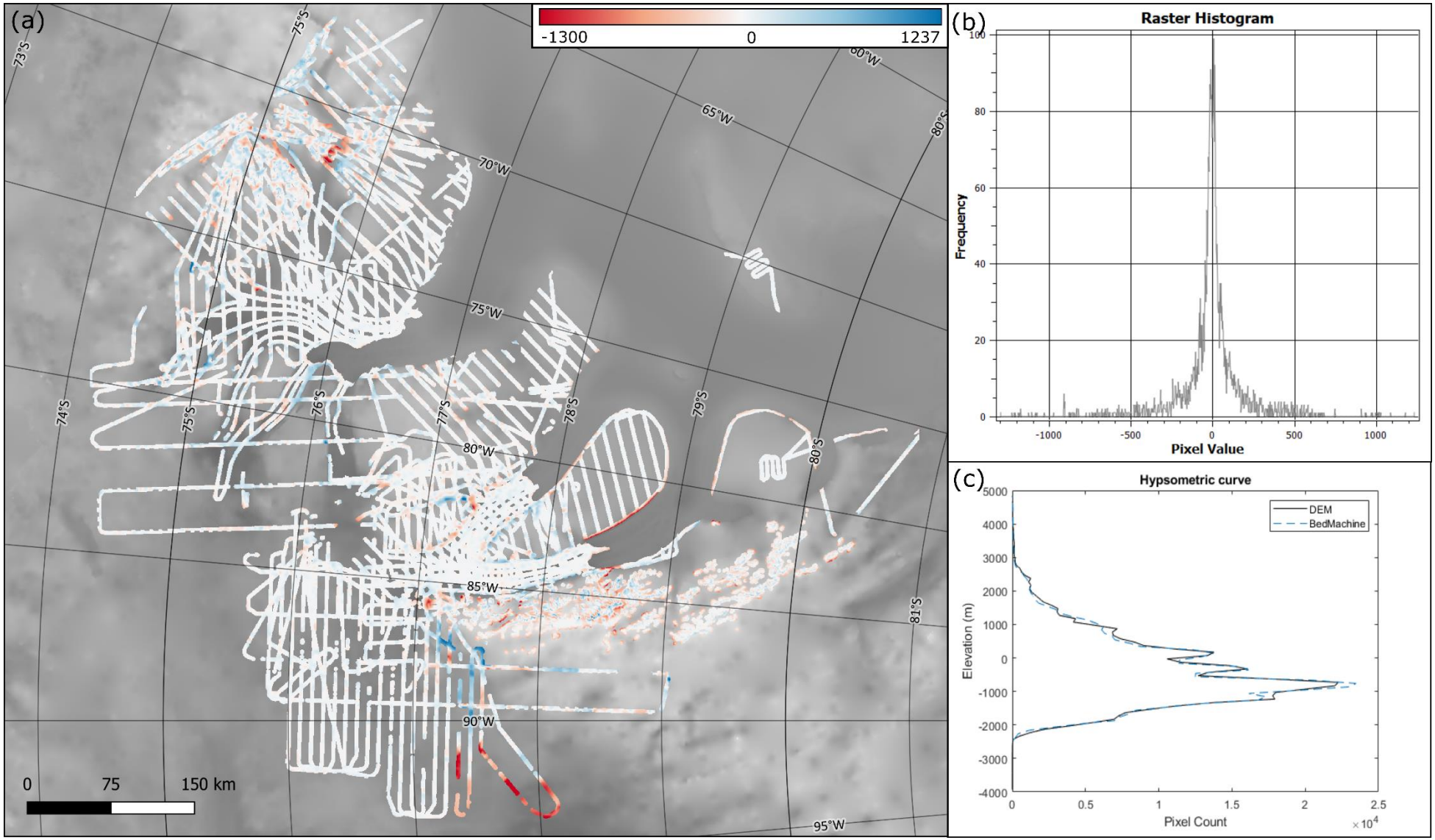

Figure 4.11: (a) Raster of pixel difference between interpolated DEM and BedMachine, where positive values indicate that BedMachine has interpolated a higher elevation value, and negative values indicate a lower elevation value. (b) Histogram of pixel values illustrating the concentration of values around 0, indicating a lack of bias. (c) Hypsometric curves of the interpolated DEM and BedMachine, producing very similar curves.

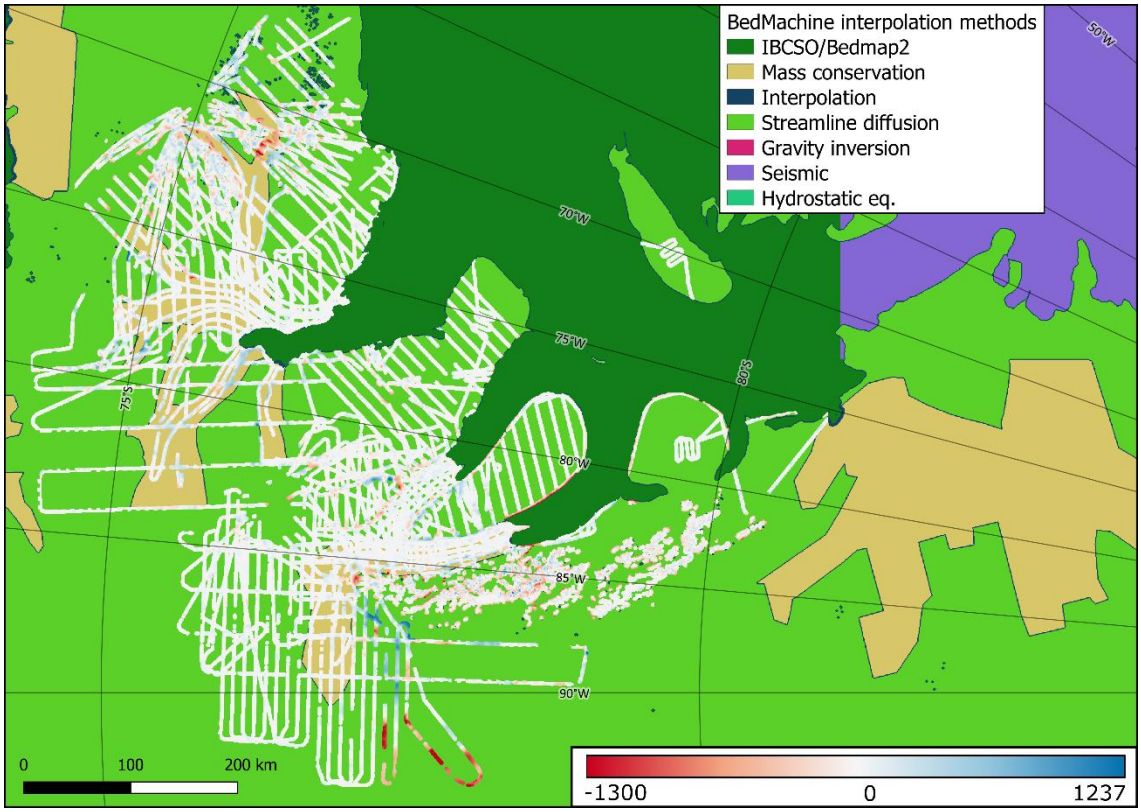

Figure 4.12: Raster of pixel difference between interpolated DEM and BedMachine overlain on map of BedMachine interpolation methods used within the study area.

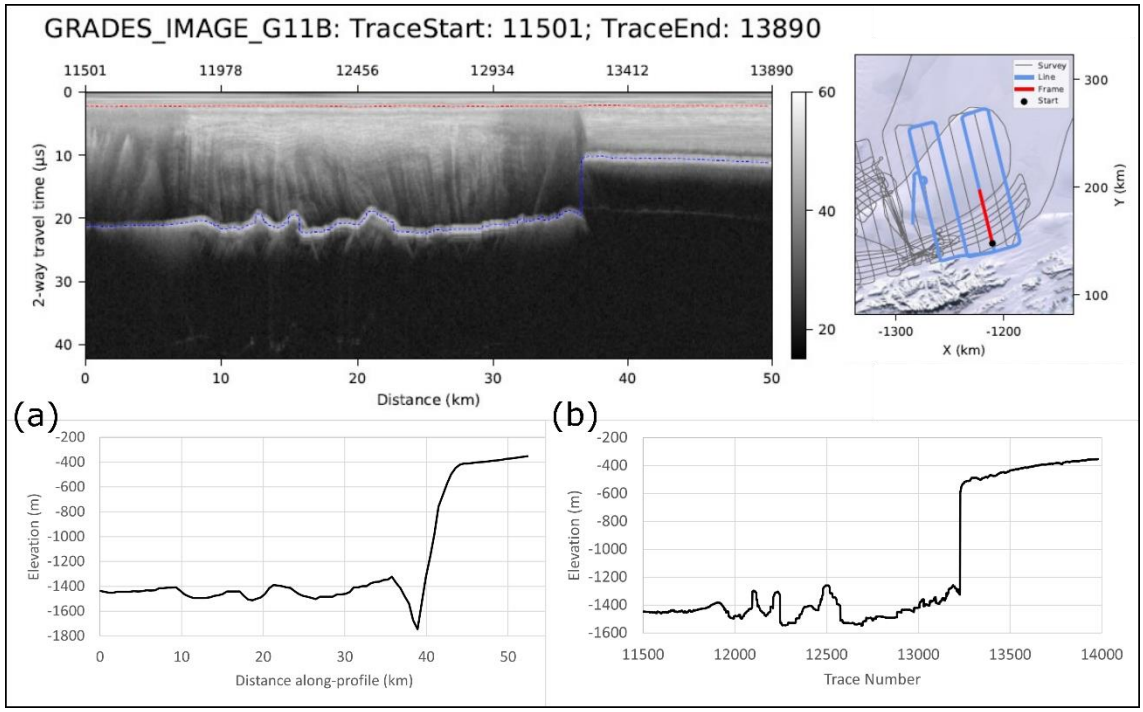

Figure 4.13: Comparison of BedMachine interpolated profile (a) and GRADES-IMAGE G11B radargram bed elevation picks (b). A 400m depth trough is present at the edge of the Fletcher Promontory within the BedMachine bed topography DEM, which is not visible reaching the same depth within the direct data measurements of the radargram.

5. Discussion

The geomorphology of the Evans-Rutford Region illustrates a complex landscape of flat plateaux, troughs, and alpine landscapes. A number of different processes and geological events could potentially have formed these features, however, without direct sampling it can be difficult to elucidate potential formational processes. Here, I will identify a set of three hypotheses for the overarching regional landscape evolution and ages of the features will be proposed. Interpretation of the geomorphological classification across the landscape will be discussed, including the possible regionally coherent surfaces suggested by the plateaux extending beyond the study area, incised by fault-bounded glacially eroded troughs. The subsequent implications for ice dynamics in this region of the West Antarctic Ice Sheet will then be explored.

5.1. Interpretation of landscape elements

5.1.1. Plateau surfaces

The Digital Elevation Model interpolated from the radio-echo sounding data, alongside its derived hypsometric curve (Figure 4.9) clearly demonstrate two populations of flat surfaces extending across the region, suggesting regionally coherent surfaces. The significant peaks in area-elevation evident in the hypsometry are highlighted in the classified symbology, further supporting that these surfaces were once continuous across this area of Antarctica. The plateaux can be identified as pre-glacial landscape remnants lying at similar elevations over a large area, and are separated by sharp boundaries, for example trough walls (Jamieson et al., 2014). Similar extensive flat bedrock surfaces have been identified using radar data elsewhere in Antarctica including in the Wilkes Subglacial Basin (Paxman et al., 2018), the Weddell Sea Embayment (Rose et al., 2015), the Ross Embayment (Wilson and Luyendyk, 2006), and Marie Byrd Land (LeMasurier and Landis, 1996), features which have a similar geomorphology to those in the Evans-Rutford Region and in some cases are also separated by linear troughs. These have remarkably constant elevation, steep edges, gentle slopes, and little topographic variation, features which are consistent with the majority of the plateaux identified in the Evans-Rutford Region. Plateaus 1, 2 and 3 particularly exhibit these features, shown in Figure 4.4, where the mean elevations of the three plateaux surfaces sit within a range of 50 m. The hypsometric peaks within which the plateaux are contained are both relatively narrow, and reach a peak in area at 171 m for the higher elevation plateaux and -328 m for the lower surface. The plateaux are laterally continuous over 100s of kilometres and their relatively smooth surfaces suggest that they have been preserved beneath non-erosive cold-based ice, as evident in

the low ice velocities overlying the areas containing the plateaux (Figure 1.2c, Table 4.2), whilst incision via glacial erosion has been concentrated in the adjacent troughs of the Rutford and Evans ice streams.

Although these plateaux sit within fairly narrow elevation ranges that indicate a laterally continuous surface, there are topographical variations within some of the surfaces that might affect the mean elevation values or inclusion within the hypsometric peaks. Firstly, Plateau 6 contains an evident peak in topography towards its east side, which can be identified as the outcropping basement of the Haag Nunataks. This outcrop exposure identifies the underlying geology as Precambrian basement, which may occur beneath the ice cover throughout this topographically elevated block and has remained at a high crustal level for the past 1000 Ma (Dalziel et al., 1987; Garrett et al., 1987; Maslanyj and Storey, 1990). A separate microplate has been postulated here, defined by a distinct area of high amplitude and high frequency magnetic anomalies (Jones et al., 2002).

Plateau 9, the higher surface of the Fletcher Promontory, also includes V-shaped radial channels which reach a depth of up to 1.2km. The origin of these channels is subject to debate; the erosion required to produce the depth of the troughs would be difficult to achieve fluvially because the deepest floors of the isostatically rebounded channels lies below modern and palaeo sea level. However, this may be an inherited fluvial pattern, that has been subsequently incised by radially flowing ice that has formed as a very low elevation ice cap with glaciers overdeepening existing topography to below sea level. At present, the ice within the channels exhibits a flow velocity of approximately 30m yr^{-1}, shown in Figure 4.5.

The two populations of plateaux suggest incision of one surface into another, particularly when looking at the Fletcher Promontory, or Plateau 9 and 10. The stepped surface of Fletcher Promontory shows a 600 m change in elevation (Figure 4.5), with the two distinct surfaces being contained within the two different populations of flat plateaux. The more seaward plateaux, namely Plateau 8 and 10, make up the lower potential surface (illustrated in white in Figure 4.9) including the plateau underneath the Filcher-Ronne ice rise which sits within the same hypsometric peak. The higher elevation surface consists of Plateau 1-3, 5-7, and 9, demonstrated on the DEM (Figure 4.9) as the light blue surface, and resides landward of the lower surface. Plateau 4 lies within the hypsometric peak of the lower surface; however, it is located landward of some of the higher surfaces to the north of the Fowler Peninsula and Fletcher Promontory.

5.1.2. Regional extent of plateau surfaces

The identification of similar potential pre-glacial, extensive erosion surfaces preserved beneath upstream of the Institute and Möller ice streams (Figure 5.1) (Rose et al., 2015), indicate that the surfaces may extend across microplate boundaries, suggesting a timing of formation that was after their convergence. The geometry of the Evans-Rutford Region is comparable to the gently sloping, low relief topographic

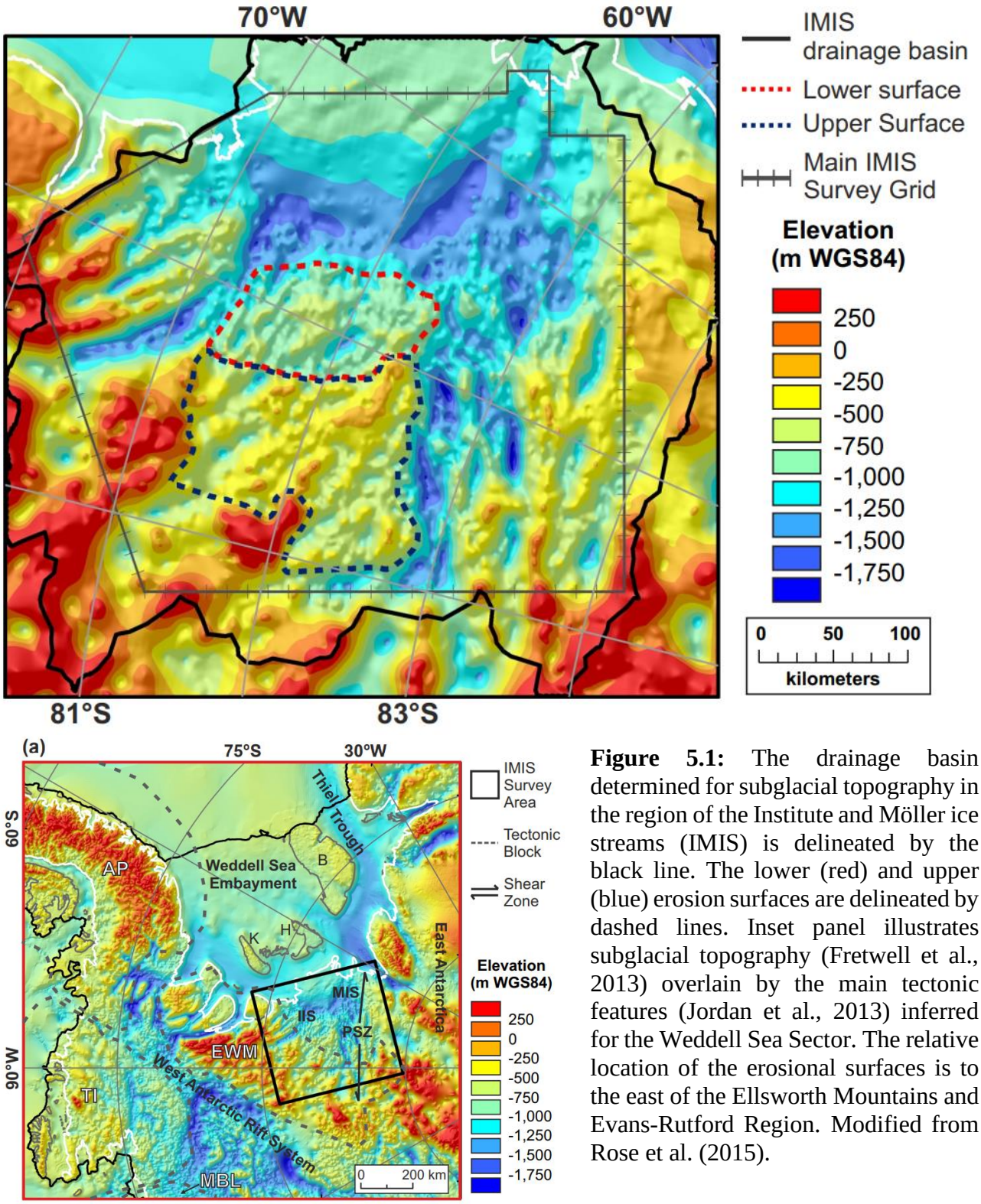

Figure 5.1: The drainage basin determined for subglacial topography in the region of the Institute and Möller ice streams (IMIS) is delineated by the black line. The lower (red) and upper (blue) erosion surfaces are delineated by dashed lines. Inset panel illustrates subglacial topography (Fretwell et al., 2013) overlain by the main tectonic features (Jordan et al., 2013) inferred for the Weddell Sea Sector. The relative location of the erosional surfaces is to the east of the Ellsworth Mountains and Evans-Rutford Region. Modified from Rose et al. (2015).

block, which comprises two surfaces separated by a distinct break in slope. Under present day ice cover, the elevation is predominantly below sea level, and rises when isostatically rebounded, but with the mean elevation remaining below sea level. Marine and fluvial peneplain erosion models have been presented for the formation of these surfaces (Rose et al., 2015).

The Institute and Möller erosional surfaces are also made up of a lower seaward surface and a higher landward surface with hypsometric peaks at 900 m and 400 m below sea level, a similar elevation difference to the Evans-Rutford surfaces, potentially supporting the hypothesis of an extensive erosional surface that extends around the Weddell Sea Embayment.

5.1.3. Troughs

Deep glacial troughs have been incised between the plateau surfaces by glacial erosion, the depths of which can only be achieved by the expansion of a large ice sheet and repeated cycles of glacial erosion. This pattern of low relief plateaux cut by deep glacial troughs is distinctive of regions affected by selective linear erosion (Sugden and John, 1976) where glacial troughs are eroded into a pre-existing surface. Three categories of troughs are evident across the region, each with distinct morphological differences in the cross-profiles.

The morphology of the troughs containing Rutford Ice Stream and Carlson Inlet demonstrates a W-shaped cross-profile, with near-vertical trough walls and a topographic ridge running centrally down-trough, aligned with the trough axis. The troughs are also very linear and have abrupt changes in slope where they meet the plateau surfaces. The features of these troughs can be characterised as representing a fault-bounded trough, similar to those found in the George VI Sound where two lateral troughs are separated by a central ridge (Smith et al., 2007). These linear bedrock depressions bounded by steep escarpments are indicative of faults (Garrett et al., 1987). Similar deep subglacial troughs have been described in the Shackleton Range, where the fast-flowing glaciers reflect the trend of, and have exploited, the subglacial fault systems (Paxman et al., 2017).

Primarily, the troughs have been identified as a structural feature or tectonic valley, the topography of which has been subsequently modified by glacial activity (Smith et al., 2007). Glaciation is likely to have exploited the underlying weakness in the faulted bedrock, leading to the W-shaped morphology where erosion has been concentrated at the base of the trough walls (faults) (Figure 5.2). The ridge running along the bed of the Rutford Ice Stream follows current ice flow direction, as well as similar but lower ridges running parallel to ice flow in Carlson Inlet, suggesting an erosional or depositional feature which is associated with ice stream flow (Vaughan et al., 2008). The coincidence of these features in both

troughs suggests a common origin. The nature of the faulted plateau segments may suggest a block-faulted landscape, which can be produced by extension in rifted basins.

The development of these troughs has resulted from selective linear erosion, as the large-scale tectonic structure has caused ice to be topographically steered along the faultline (Jamieson et al., 2014). This has left the intervening plateaux unmodified, as the erosion has been concentrated in a series of troughs which over time have developed beneath the ice sheet (Sugden and John, 1976). There is also an overdeepening at the intersection of the two conduits at the convergence of Carlson and Talutis Inlet, which is consistent with the geomorphology of fjord landscapes (Holtedahl, 1967).

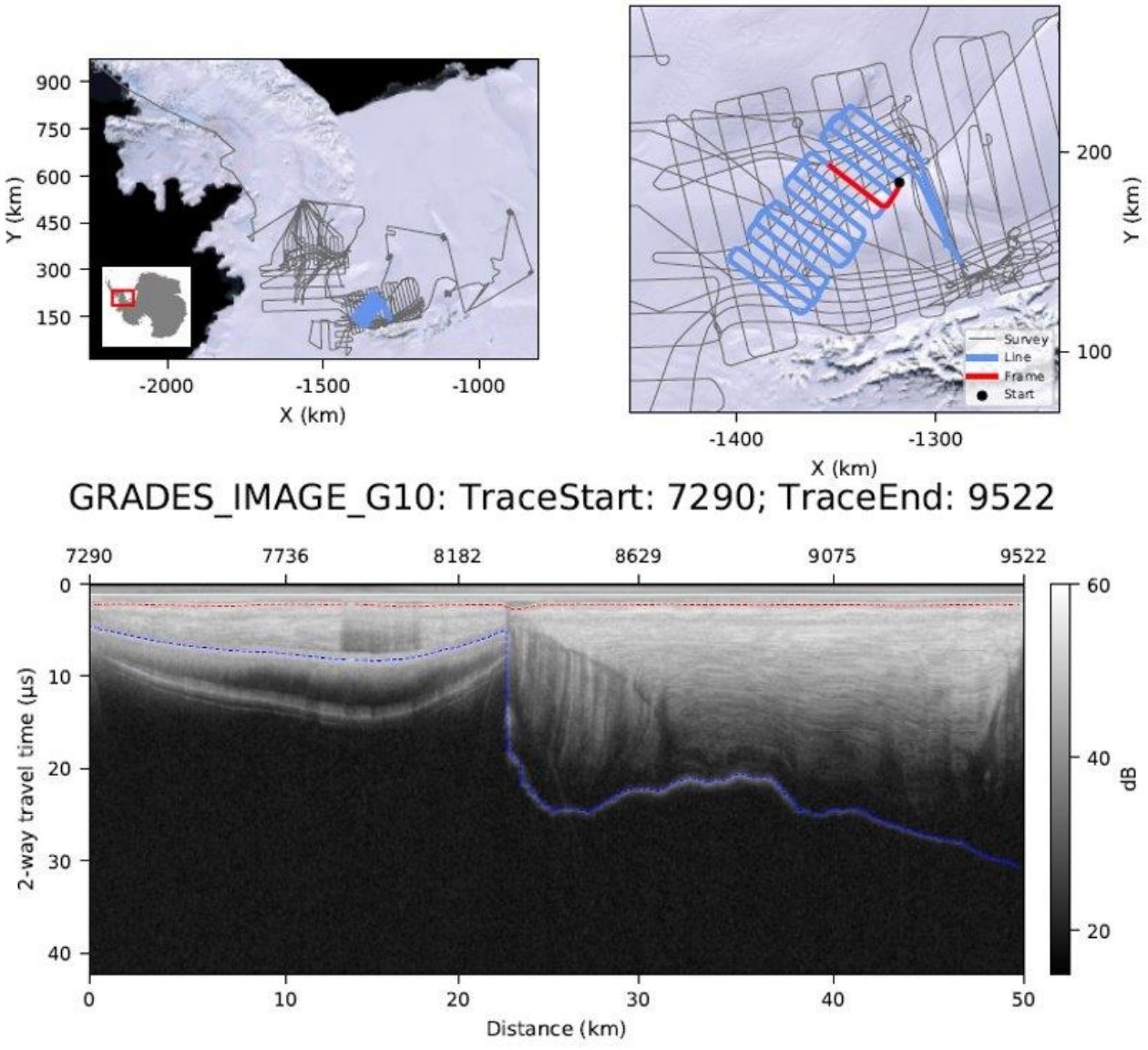

Figure 5.2: Radargram illustrating excavation at the base of a trough wall. Location of radargram in lower panel is shown by red highlight in upper right panel.

A second category of troughs are those incised between the northernmost plateaux, as well as the Talutis Inlet, and have an asymmetric V-shaped morphology (Troughs 1-5, Figure 4.6). The thalwegs of each tend to be located along one side, with one trough wall often being much steeper than the other (Figure 4.6). In form, these resemble half-graben structures, and may be related to areas where faulting has been concentrated on one side of a trough in extensional tectonic environments.

A third category is the very broad trough of the Evans Ice Stream, which is much wider than the other troughs. A central topographic ridge running in the direction of ice flow divides the trough, (Figure 4.7), with the grid north side appearing shallower than the grid south side, with a difference in mean elevation of 670 m. The valleys surrounding the Evans Ice Stream act as tributaries feeding the main ice trunk, flowing from the alpine topography at the base of the Antarctic Peninsula. The wide valley has been said to be of tectonic origin, with the ice surface topography showing the valley changing orientation several time, which may be the product of a segmented rift (Jones et al., 2002).

5.1.4. Alpine topography

The low wavelength, rough topography, sharp ridges, and steep troughs bordering the study region to the north (Antarctic Peninsula) and south (Ellsworth Mountains) are indicative of alpine topography, as they demonstrate a dendritic network of troughs reminiscent of former stream networks exploited by ice (Sugden and John, 1976). The density of individual peaks is higher in these areas which are dominated by glacial erosion, in comparison to the areas where the topography is submerged beneath the ice sheet (Jamieson et al., 2014). It is notable that the alpine topography occurs in regions where elevations are highest, especially the Ellsworth Mountains, which are the highest range in Antarctica.

5.1.5. Flexural isostatic rebounding

The isostatic rebounding of the Digital Elevation Model (Figure 4.10) reinforces the interpretation of two pre-glaciation laterally continuous surfaces, as even after rebounding the hypsometry still illustrates two significant peaks in area-elevation which represent the plateau surfaces. After flexural rebound Plateau 1 is now part of the hypsometric peak for the higher elevation surface, whereas in the modern DEM, it occurred within the lower hypsometric peak. The range of the hypsometric peaks within which the plateaux reside has narrowed to 450m, with the higher elevation population sitting between 150 m to 600 m above modern sea level, compared to the lower elevation surfaces residing between 0 m and 450 m below.

However, the model of flexural isostatic rebounding may not take into account all other processes that may have affected the elevation of these plateau surfaces through uplift or subsidence. Processes leading to uplift of the surfaces include incision of the glacial troughs into the surrounding landscape, with relatively little erosion occurring on the plateau surface; the flexural isostatic response would have acted upon the plateaux to raise their elevation even as intervening erosion occurred (Summerfield, 1991). The extent of this effect would also be dependent upon the relative rigidity of the lithosphere: within this region of West Antarctica, there is a low effective elastic thickness value, resulting in shorter wavelength variability in isostatic uplift (Paxman et al., 2022). Flexural uplift may also be contributed to by resultant unloading of the footwall by the hanging wall in troughs that are subject to fault bounding, as demonstrated in the Shackleton Range (Paxman et al., 2017). The resultant effect of these processes would lead to surfaces now being at higher elevations than without the processes. In other words, the pre-glaciation elevation of the plateau surfaces was likely lower previously, meaning that the higher population of plateau may have resided at around palaeo-sea level before ice loading at the inception of the Antarctic Ice Sheet.

Two possible processes that may have caused post-formation subsidence of the surfaces include long-term thermal subsidence after any rifting processes, and long-term sediment loading in the Weddell Sea to the north and east. A process which is not well constrained, but which can cause uplift or subsidence, is the effect of dynamic topography (Austermann et al., 2015). The potential net effects of all of these uplift and subsidence processes in the landscape evolution of the region is discussed further below.

5.2. Regional landscape evolution

The overarching landscape seen in the DEMs spanning this study region indicates two pre-glacial surfaces, one of which has potentially been cut into the other, leaving a prominent escarpment between, as demonstrated in Figure 4.5. Following the formation of these laterally continuous surfaces, the troughs were incised between the plateaux and were likely to be tectonically controlled. This has led to the topographic steering of ice through these deeply eroded conduits. This region of West Antarctica has been suggested to contain horst and graben structures (Figure 5.3) within the subglacial topography between the Antarctic Peninsula and Ellsworth Mountains (Doake et al., 1983; Jones et al., 2002), with the faults bounding the horst indicated by steep topographic scarps (Garrett et al., 1987). This type of topography often consists of unpaired normal faults creating half-grabens, or fault-angle depressions, generating basins in which sediments can accumulate (Burbank and Anderson, 2001). Such horst-graben and half-graben structures are visible on radargrams across the area (Figure 4.6, Figure 5.2). The

exploitation of these structural faults by glacial erosion has resulted in the deep subglacial troughs seen in the modern topography, leaving the plateaux surfaces relatively unmodified where they have been preserved by slow-flowing, non-erosive ice. Whilst the geometrically flat bedrock surfaces are likely to have formed during periods of stable base level, the timing of the geological events that formed these are currently not known.

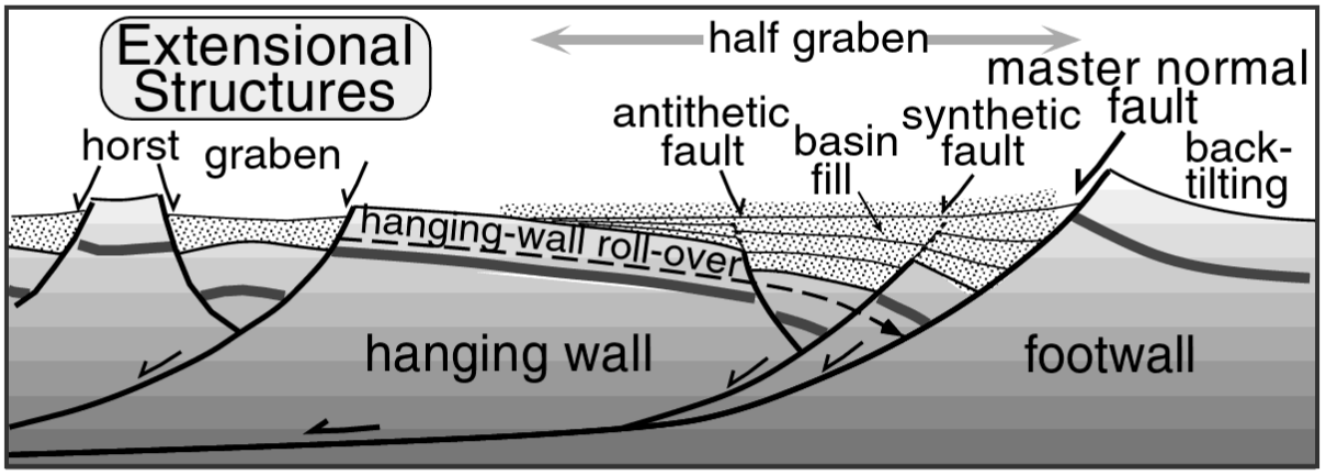

Figure 5.3: Schematic of cross-section of normal faults in an extensional regime (Burbank and Anderson, 2001). The master fault delineates footwall and hanging-wall blocks. A broad half-graben is cut by synthetic and antithetic faults.

The relative age of some of the events that formed the landscape can be discerned by the relationships of the different landscape elements. Firstly, the faults must pre-date the plateau surfaces as the surfaces are not displaced across the faults. Secondly, the lower surface post-dates the higher surface into which it is eroded. Thirdly, the troughs must post-date the surfaces, and imply a period of ice-sheet scale glaciation that covered the area. The relative age of the alpine glaciation to other elements is not clear as no cross-cutting relationships are observed: they are not seen to cut, nor are cut by the surfaces. If they pre-date the surfaces, it implies that the alpine glaciation left the surfaces unmodified which might be possible given their low elevation compared to the alpine areas. If they post-date the surfaces, they may be associated with expansion of ice that went on to form the ice sheet cutting the troughs.

Given this sequence of events and what is known about the geological evolution of the region three potential hypotheses for the initial formation of the plateau surfaces are presented. The implication of the geological evolution of the region (see Section 2.4) for landscape evolution is that the main crustal blocks of the study region were assembled together by 165 Ma, just prior to the late Jurassic. Following this, exhumation of the Ellsworth Mountains occurred between ca. 145 to 117 Ma, constrained by thermochronometry data, resulting in ~4 km of uplift. This provides a maximum age for when the plateau

surfaces that extend across the multiple blocks may have started to be eroded, as this would require a stable base level to occur.

5.2.1. Hypothesis 1: Passive margin evolution

The first potential mechanism for the formation of the plateau surfaces is through passive margin evolution, where the upper surface forms through the initial updoming and erosion associated with the continental break-up of Gondwana, with subsequent post-rifting scarp retreat forming the lower surface. The most prominent landforms resulting from continental break-up are high elevation passive margins and their associated major escarpments. For example, the central Namibian margin demonstrates similar topographic elements of a well-defined major escarpment with a relief of 1000 m, separating a gentle inclined coastal plain from an interior plateau (Cockburn et al., 2000). An Antarctic analogy can also be drawn to the McMurdo Dry Valleys Mountain block, which contains two escarpments with relief over 1000 m. As a result of initial lithospheric extension and rifting, fluvial denudation to a new sea level has removed ~4 km of material from the coast, accompanied by isostatic uplift and faulting (Sugden and Jamieson, 2018). This has left a coastal plain 100 km wide, backed on the inland margin by an escarpment (Figure 5.4). Similar formational processes could have created the geomorphology seen in the Evans-Rutford Region, as there is a lower, seaward surface, backed by a landward higher elevation surface, with a relief of at least 600 m between them as shown on the Fletcher Promontory (Figure 4.5).

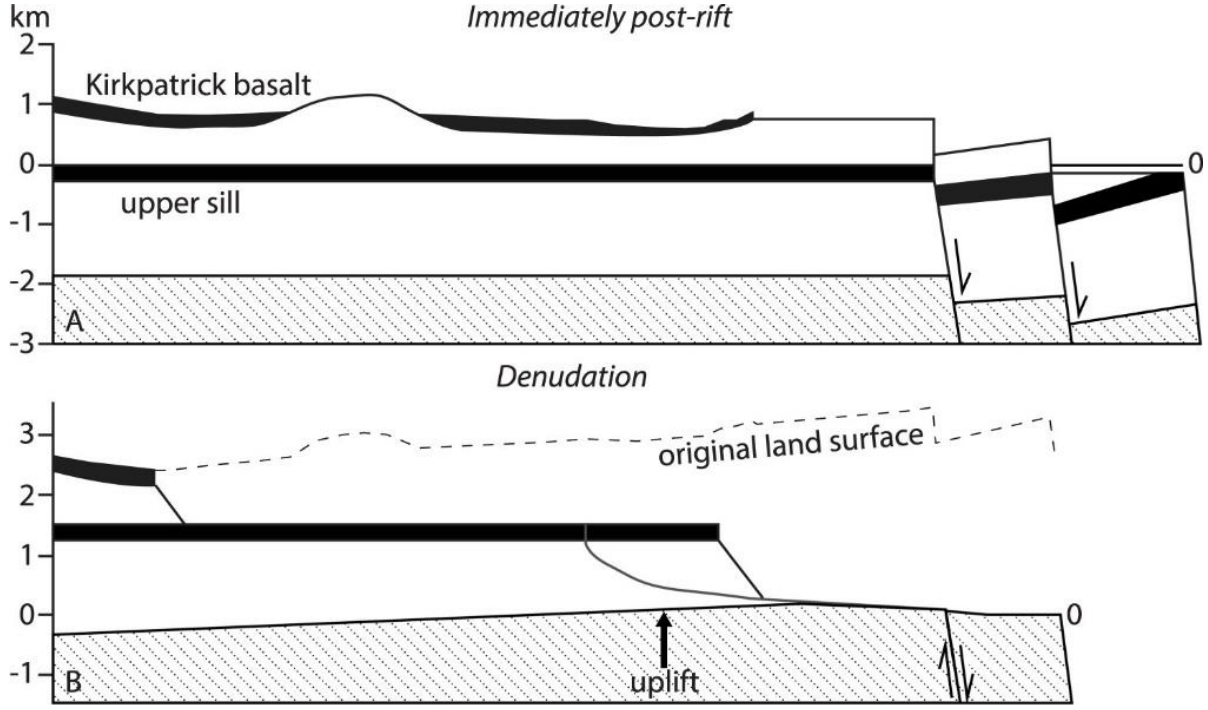

Figure 5.4: Schematic evolution of the Dry Valleys. (A) Initial lithospheric extension and rifting. (B) Fluvial denudation to the new sea level removes ~4 km from the coast and is accompanied by isostatic uplift and faulting. Modified from Sugden and Jamieson (2018).

Passive margin retreat on a similar spatial scale over 100s of kilometres, as well as a similar timescale of movement post-Gondwana break-up, can be seen in the continental rifting between South America and Africa, which began during the late Jurassic (Brown et al., 2000). A complex mosaic of interconnecting rift and horst structures developed in the initial rift phase, following a prolonged period of extensional and strike-slip motion between several microplates. This break-up of Gondwana and continental rifting resulted in newly created continental margins, leading to the presence of high topography along them and the establishment of a new, lower base level for substantial denudation which is reflected in the fission track data (Brown et al., 2000).

However, the isostatically rebounded lower surface in the study region sits below sea level, which would indicate other processes that have led to subsidence of this and the upper surface, as original erosion would have occurred to create the surface at sea level. Potential mechanisms for creating this subsidence include prolonged regional subsidence that will have occurred after the uplift resulting from the main magmatic event in the region at ~180Ma. This would have been due to physical thinning of the crust caused by extension in the Weddell Sea Rift System, followed by long-term thermal relaxation.

A second potential mechanism for subsidence is sediment loading in the Weddell Sea over million-year timescales, where the erosion of troughs and subsequent glacial sediment loading would cause subsidence. Sedimentation prior to the Oligocene was dominated by current-controlled sediment transport and deposition in isolated basins that evolved after the break-up of Gondwana, such as the Weddell Sea, leading to a post-34 Ma sediment volume of 3.04 $x10^6$ km^3 (Hochmuth et al., 2020). Pre-glacial Cenozoic deposition in the Weddell Sea was controlled by tectonic evolution and sea-floor spreading history interacting with the terrigenous sediment supply, resulting in thicknesses of up to 5 km (Huang et al., 2014). However, sediment loading offshore has the potential to lead to bedrock subsidence offshore and uplift onshore, causing a flexural response, as seen in the Wilkes Subglacial Basin (Paxman et al., 2019a).

Dynamic topography is another process by which subsidence may have taken place, as evolving viscous stress and buoyancy associated with mantle convection flow can drive vertical deflections of the crust (Austermann et al., 2015). These buoyancy variations can alter the bedrock elevation of sea-level markers subsequent to their formation across million-year timescales (Austermann et al., 2017), meaning that subsidence of the plateau surfaces may have occurred due to flow within the Earth's convective mantle. It also may be that the region has been subject to other tectonic events may have resulted in subsidence, as there is sparse and somewhat contradictory evidence that the Evans Ice Stream was affected by

extensional events in the Mesozoic and Cenozoic (Studinger and Miller, 1999), however, these are not well constrained.

5.2.2. Hypothesis 2: West Antarctic Rift System

The second potential hypothesis by which the plateau surfaces may have formed is through the planation of an extensive surface throughout the region, which has then been uplifted in association with the West Antarctic Rift System (WARS) to allow subsequent incision of a second lower elevation surface. These processes would have to have occurred after the Jurassic assembly of the microplates and exhumation of the Ellsworth Mountains, with sea level remaining stable in order to allow for the prolonged erosion and planation that would result in an erosional surface of this nature.

Marine planation forming erosional surfaces has been seen in the Ross Embayment, creating plateaux and terraces sitting 350 m to 100 m below sea level, separated by bedrock troughs occupied by West Antarctic ice streams (Wilson and Luyendyk, 2006). Their flat and level nature, with similar elevation over large distances, indicates features that would be expected to result from wave erosion in the absence of coastal ice. These plateaux are wave cut platforms, similar to uplifted strand flats seen fringing Norwegian coastlines. In contrast, a model of fluvial peneplain erosion has been proposed for bedrock surfaces in the Institute and Möller catchments of the Weddell Sea, during or after the rifting and break-up of Gondwanaland around ~180 Ma (Rose et al., 2015). In response to the downward shift in base level caused by the rifting of Gondwanaland (Beaumont et al., 2000), fluvial systems incised into the landscape, resulting in the formation of broad, extensive coastal surfaces backed by erosional escarpments.

Similar low-relief erosion surfaces have been found to occur in West Antarctica and New Zealand, representing prolonged intervals of erosional levelling in a stable tectonic environment (LeMasurier and Landis, 1996). The low relief and regional extent of these surfaces in West Antarctica are compatible with prolonged fluvial erosion, marine planation, or a combination of both, with the New Zealand surface being found to consist of a composite of features produced by fluvial erosion, followed by wave planation. The levelling of these erosional surfaces was nearing completion by ca. 75 Ma, having begun around 85 Ma when New Zealand began to break away from West Antarctica. The data from these surfaces does not support a continuous low-relief landscape pre-breakup (LeMasurier and Landis, 1996), however, they can provide a clear comparison for the surfaces found in the Evans-Rutford Region and could allow for speculation that these surfaces extend into the study region. Erosion surfaces in western

Marie Byrd Land have also been identified, which formed around ca. 70-60 Ma corresponding with slow cooling following activity in the West Antarctic Rift System (Zundel et al., 2019).

Rock uplift in the Ellsworth-Whitmore Mountain (EWM) block in the Early Cretaceous may have been caused by early rifting in the WARS between EWM and Marie Byrd Land (MBL) (Figure 5.5) (Fitzgerald, 2002). The West Antarctic Rift System saw further activity in the Cenozoic and ongoing fracturing, volcanic activity, and bordering uplift associated with development of the rift combined to modify the subglacial topography of the West Antarctic Ice Sheet (Dalziel and Lawver, 2001). This may

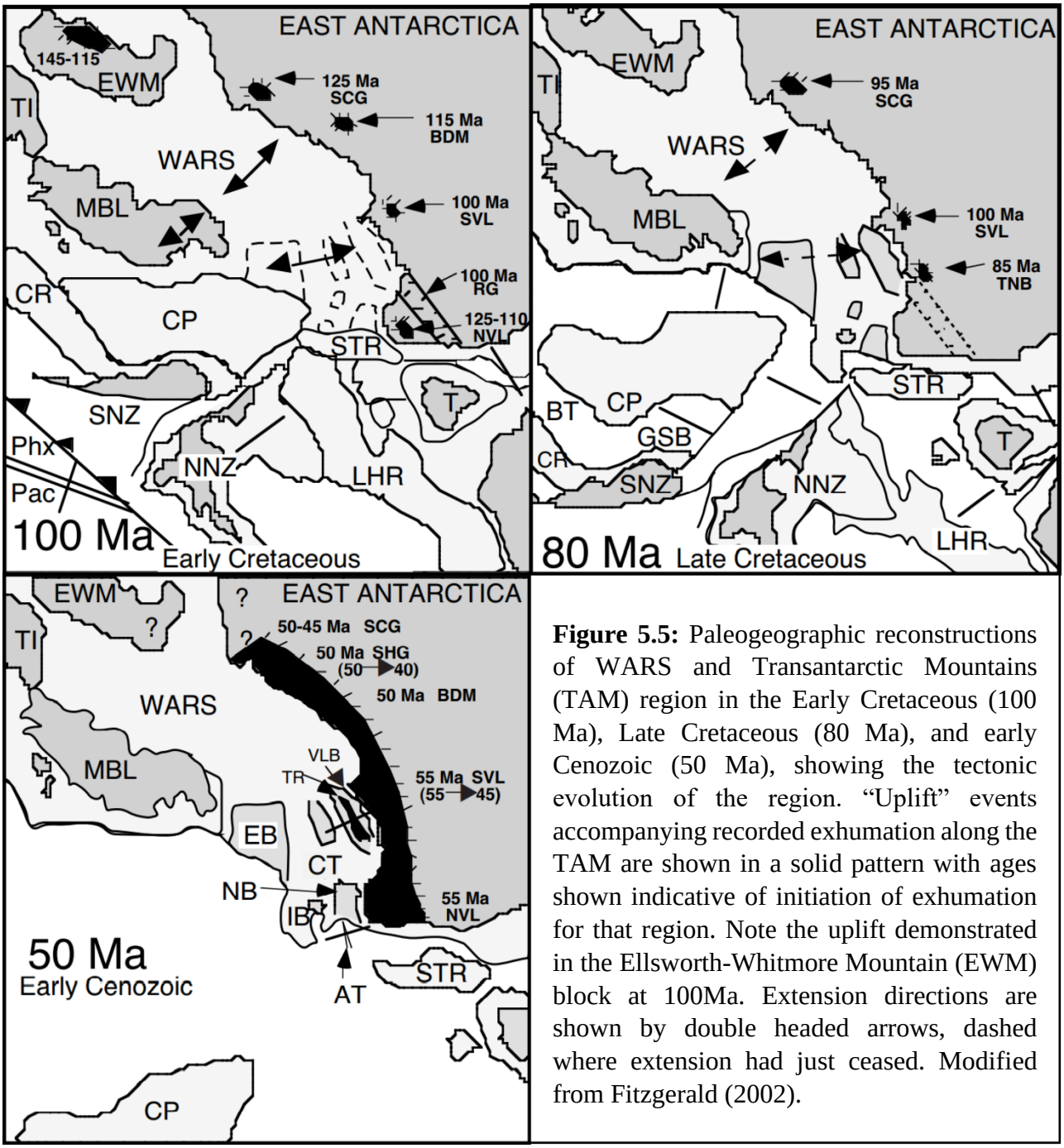

Figure 5.5: Paleogeographic reconstructions of WARS and Transantarctic Mountains (TAM) region in the Early Cretaceous (100 Ma), Late Cretaceous (80 Ma), and early Cenozoic (50 Ma), showing the tectonic evolution of the region. "Uplift" events accompanying recorded exhumation along the TAM are shown in a solid pattern with ages shown indicative of initiation of exhumation for that region. Note the uplift demonstrated in the Ellsworth-Whitmore Mountain (EWM) block at 100Ma. Extension directions are shown by double headed arrows, dashed where extension had just ceased. Modified from Fitzgerald (2002).

have potentially created enough uplift in the Evans-Rutford Region to initiate erosion of the lower surface via either marine or fluvial erosion.

Long term subsidence following rifting, or other potential mechanisms that would lead to subsidence as described in Hypothesis 1, would consequently lead to the lower elevation plateaux residing below sea level as indicated by the flexural isostatic rebounding model.

5.2.3. Hypothesis 3: Cessation of Antarctic Peninsula subduction

The third potential formational mechanism for the plateaux surfaces of the Evans-Rutford Region proposed follows the same extensive planation of the upper surface suggested in Hypothesis 2. The subsequent uplift of this surface could be explained by a different mechanism, however, which is through the cessation of subduction at the southern end of the Antarctic Peninsula. When subduction and subsidence ceased, this may have led to the uplift and formation of the second lower elevation surface and escarpment.

The collision of spreading ridge segments at the continental ocean boundary of the Antarctic Peninsula (AP) triggered the progressive northward shutdown of subduction along the Antarctic Peninsula margin (Jordan et al., 2020). The Peninsula is a largely Mesozoic magmatic arc, which prior to Middle-Jurassic disintegration and sea-floor spreading in the Weddell Sea, was founded on mid-Palaeozoic basement located on the palaeo-Pacific margin of Gondwanaland. Subduction ceased following ridge-trench collision, marking the cessation of accretion and magmatism (Storey and Nell, 1988). Prior to 90 Ma, subduction occurred along the entire margin, however after this time, subduction ceased in the southernmost part of the peninsula before 83 Ma, and the Bellingshausen Gravity Anomaly (BGA) oblique trough developed at the western margin of ocean crust that became coupled to the Antarctic Peninsula across the stalled subduction zone (Larter et al., 2002). Subduction had completely ceased on the BGA by ca. 45 Ma (Larter et al., 2002), and from ca. 20 Ma subduction ceased progressively further north (Larter and Barker, 1991). This progression is evident in Figure 5.6. Thus, the timing of initial updoming associated with the West Antarctic and New Zealand surfaces 85-75 Ma may have then been succeeded by uplift as subduction ceased between 83 and 45 Ma.

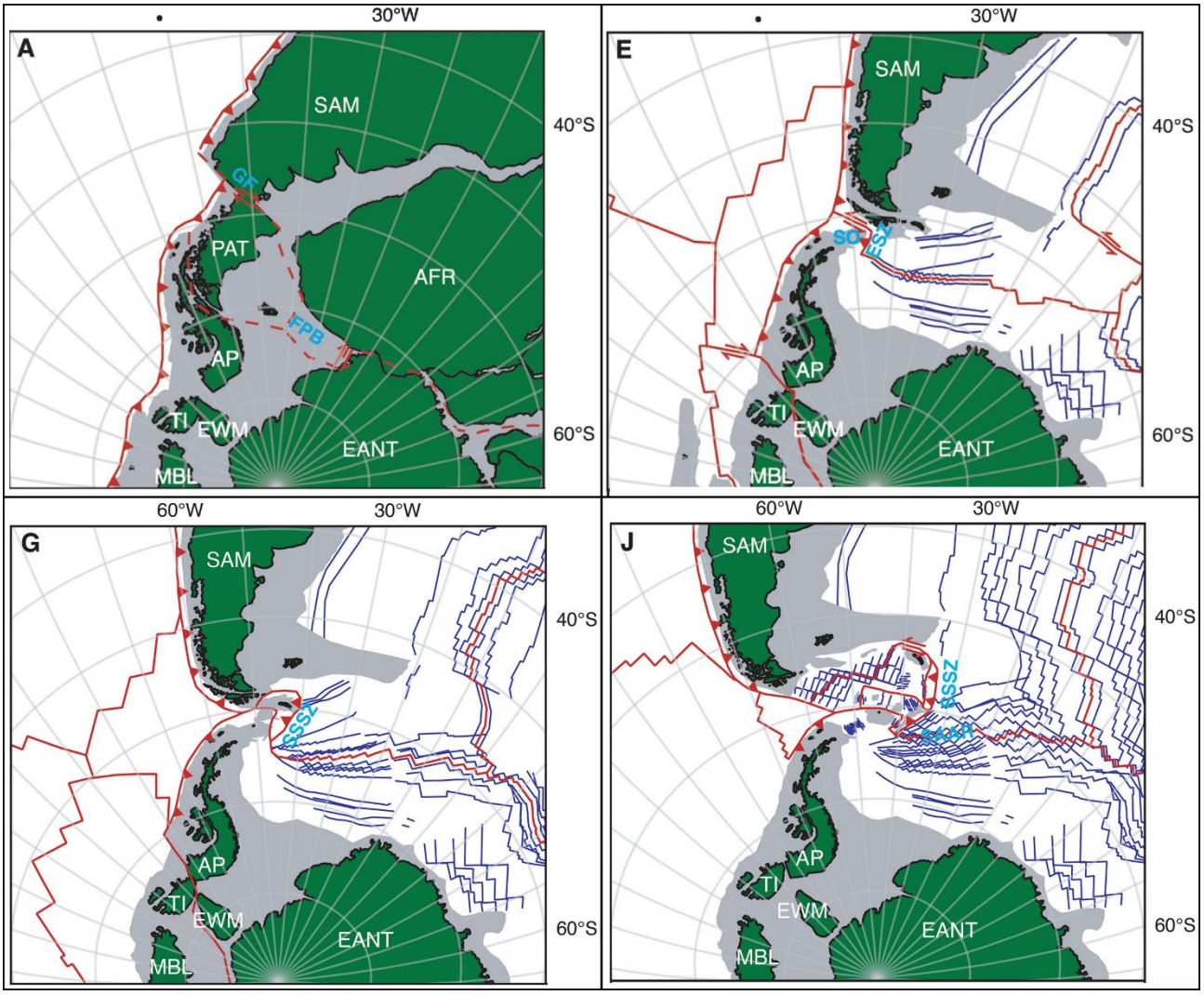

Figure 5.6: Snapshots of the kinematic reconstruction at selected time slices in an East Antarctica fixed reference frame, modified from van de Lagemaat et al. (2021). Time slices are: (A) 182 Ma, (E) 80 Ma, (G) 50 Ma, (J) 15 Ma. The active plate boundary on the western margin of the AP progressively shuts down in a northward direction after 80 Ma. Note that the relative motion of the EWM and AP is relatively little as the assembly of the microplates in this region had been completed. Dark green areas = present-day coastal boundaries of the polygons, dark gray areas = stretched and transitional continental crust, red lines = active plate boundaries, red arrows = motions on the active plate boundaries, dashed red lines = plate boundaries that are to become active soon after the reconstruction snapshot, dark blue lines = marine magnetic anomaly lineations.

The plateau surfaces formed could still be subject to processes discussed in previous hypotheses, namely dynamic topography, sediment loading in the Weddell Sea, and regional subsidence as a result of thermal relaxation, meaning that the elevations of the plateau would end up below sea level.

The three scenarios above are consistent with the geological history of the region and all imply the surfaces were likely formed prior to the onset of major Antarctic glaciation at 34 Ma (Colleoni et al, 2022). The likelihood of each scenario is difficult to constrain, as there is limited evidence to reinforce

one particular hypothesis compared to the others. The presence of erosional surfaces in the Institute and Möller catchment on the eastern side of the Evans-Rutford Region could give an indication that the surfaces were formed through passive margin evolution, as the other hypotheses involve processes of uplift due to the West Antarctic Rift System or cessation of subduction of the Antarctic Peninsula, both of which occurred on the western margin. These may not have impacted the surfaces proposed by Rose et al. (2015) as they could be too distal. However, there is currently little evidence to constrain whether these surfaces were formed via the same processes other than their similarity in terms of geomorphology. Indeed, similarities could also be drawn to the erosional surfaces found across West Antarctica by LeMasurier and Landis (1996) that are associated with the West Antarctic Rift System, so this could lend more weight to Hypothesis 2. Without direct evidence that would constrain any one of the hypotheses proposed, for example, concurring dates that provide insight into the timing of erosion of the plateaux, no one hypothesis can be preferred.

5.2.4. Timing of Alpine glacial incision

The most likely timing of local-scale glaciation which eroded an alpine topography in the Antarctic Peninsula and Ellsworth Mountains is the early stages of Antarctic glaciation, around the Eocene-Oligocene boundary, ca. 34 Ma. The Ellsworth Mountains have long been identified as a likely inception area for early ice caps that would have likely expanded to form a more expansive ice sheet, possibly over a few million years (DeConto and Pollard, 2003).

5.2.5. Glacial erosion of troughs

Erosion of the troughs lying between the plateaux is likely to have occurred after the planation of the surfaces, as the existing fault-controlled topographic depressions and structural weaknesses in the bedrock would control and reinforce ice flow into the troughs evident in the DEM (Bingham et al., 2012; Jamieson et al., 2014). In particular, the dislocation along Rutford ice stream between the Ellsworth-Whitmore Mountains and Haag microplate is an intrinsically very old and long-standing geological discontinuity, where the Ellsworth-Whitmore Mountains were thrust over the margin of the Haag Nunataks block in the Permo-Triassic, 250 Ma (Jordan et al., 2020). The horst and graben structures seen here and across the region support the idea of extensional reactivation of the tectonic structures in this region, as a result of Jurassic magmatism and extension (Curtis, 1997; Maslanyj and Storey, 1990). Therefore, these faults would act as conduits for ice during the initiation of Antarctic glaciation, providing topographic and basal boundary conditions that would have strongly influenced the structure and evolution of the ice sheet (Aitken et al., 2014).

The timing of the trough formation is likely to coincide with the inception of the West Antarctic Ice Sheet at 14 to 12 Ma, (Colleoni et al., 2022) as troughs of this magnitude would require a large ice sheet reaching extents close to the shelf edge in order to achieve the depth and magnitude of erosion shown. With a persistent continental-scale ice sheet, low-lying regions such as this are more susceptible to glacial activity, due to thicker ice and the resulting strong thermomechanical feedbacks between deformation, stress and heating (Aitken et al., 2014).

5.3. Implications for ice dynamics

The tectonic history of the Evans-Rutford Region has created a subglacial landscape that has topographically controlled the formation of the West Antarctic Ice Sheet, causing deep subglacial troughs containing ice streams to be formed where the structural weaknesses of faults have been exploited. The plateau surfaces have been preserved by slow-flowing, cold-based, non-erosive ice, creating a landscape subject to selective linear erosion. This is clearly reflected in the ice flow velocity of the region (Figure 1.2c), where the Evans and Rutford ice streams display velocities between 300-800 m yr^{-1} faster than the ice overlying the plateaux surfaces. Given that the ancient surfaces have been preserved under cold-based, slow-flowing ice, this implies that the presence of this cold-based and slow-flowing ice has been persistent on the plateaux surfaces throughout the history of the West Antarctic Ice Sheet. Therefore, the ice stream outlets seen today are also likely to be in effectively the same locations as the outlets formed during early glaciation. The alpine topography bordering the region at the base of the Antarctic Peninsula and the Ellsworth Mountains is likely to have hosted initial glaciation due to its higher elevation than the surrounding topography.

5.4. Summary

The subglacial landscape geomorphology of the Evans-Rutford Region demonstrates two populations of regionally coherent surfaces, identified as pre-glacial landscape remnants which have been preserved under cold-based, non-erosive ice. The difference in elevations and stepped surface of the Fletcher Promontory suggests the incision of the lower surface into the higher surface, creating a prominent escarpment. The plateau surfaces may also extend beyond the study region into the Institute and Möller catchment, as comparable geomorphological features have been proposed by Rose et al. (2015). Deep glacial troughs have been incised between the plateaux, some of which have been tectonically controlled, resulting in topographic steering of the ice and selective linear erosion. Alpine topography borders the region where elevations are highest, with the Ellsworth Mountains to the south and the base of the Antarctic Peninsula to the north.

Three hypotheses have been proposed in regard to the formation of these plateau surfaces. Hypothesis 1 suggests passive margin evolution, where the upper surface may have formed in association with initial updoming resulting from the breakup of the supercontinent Gondwana, with post-rifting scarp retreat then forming the lower surface. Hypothesis 2 describes extensive surface planation throughout the region, which has then been uplifted in association with the WARS to allow incision of the second surface. Uplift may also have occurred as a result of the cessation of subduction of the Antarctic Peninsula, as proposed in Hypothesis 3. Following these processes, the surfaces are likely to have subsided in order to sit below sea level where they now reside. Alpine glaciation occurred later at the Eocene-Oligocene boundary (ca. 34 Ma), followed by the coalescence of the WAIS at 14-12 Ma which would allow glacial erosion of the deep troughs.

6. Conclusions

This study assessed the subglacial topography of the Evans-Rutford Region, the formational processes recorded in its landscape, and the relationship between subglacial topography, its underlying geological structure, and ice flow. Below I outline the key findings of this work before then suggesting some potential avenues for future research.

6.1. Subglacial topography of the Evans-Rutford Region

A high-resolution DEM of the Evans-Rutford Region has been produced in order to investigate its subglacial topography in detail. We combine bed picks from the newly released GRADES-IMAGE RES survey, alongside the TORUS and Evans 1994/95 RES surveys (Frémand et al., 2022), and exposed bedrock datapoints derived from the REMA dataset to generate a 500 m resolution map of the subglacial topography. After extensive testing the bed elevation data points were interpolated using a continuous bivariate cubic spline algorithm and produced a Digital Elevation Model highly similar to BedMachine (Morlighem et al., 2020). However, in comparison to BedMachine (Morlighem et al., 2020), the new DEM resolves the sharp trough boundaries without relying on inversion techniques.

Geomorphological mapping of the subglacial DEM was undertaken to identify large-scale features in the landscape. These included plateau surfaces, defined as nearly flat surfaces separated from surrounding lower elevations by at least one steep side, and alpine topography, identified as sharp peaks and ridges interspersed with deep closely spaced troughs. Three morphological types of troughs were also defined including wide U-shaped, asymmetric V-shaped, and fault-bounded or W-shaped. Hypsometric analysis was conducted in order to characterize landscape morphology through analysing the frequency-distribution of elevations. A flexural isostatic rebounding model was also applied to the DEM to provide insight into the genesis of the landscape if it were to be assumed it was created prior to the development of the ice sheet.

Ten flat plateau surfaces were identified across the region, with an additional two potential plateau surfaces highlighted by opportunistic radar surveys. These are low relief surfaces lying at broadly similar elevations and are currently overlain by slow flowing ice. Deeply incised troughs containing fast-flowing ice are present between these plateaux, with some demonstrating abrupt linear margins. Low wavelength, rough topography with sharp peaks and troughs was identified as alpine topography at the base of the Antarctic Peninsula. The hypsometric analysis of the DEM identified three significant peaks with other minor inflection points, which highlighted two populations of plateau surfaces sitting between -50 m and 500 m (higher elevation peak) and -50 to -550 m (lower elevation peak). The other hypsometric peak

represented the floors of the troughs. In contrast, the isostatically rebounded DEM demonstrated only two major peaks in area-elevation, but this still highlighted two distinct sets of plateau surfaces, rebounded to higher elevations. The lower rebounded population sits between 0 m and -450 m below modern sea level, whereas the higher population of plateaux sits between 150 m to 600 m above modern sea level.

6.2. Formational processes

The two populations of plateau surfaces suggest two regionally coherent surfaces, which can be identified as pre-glacial landscape remnants lying at similar elevations over a large area, separated by sharp boundaries (Jamieson et al., 2014). The topography of the region suggests the incision of the lower surface into the higher surface, given the two populations lying at different elevations and the stepped topography evident on the Fletcher Promontory. This is supported by the DEM produced by the flexural isostatic rebounding model, which shows the majority of the plateaux remained within the same two hypsometric peaks. These surfaces may also be consistent with similar potential pre-glacial erosional surfaces which have been found in the Institute and Möller catchment (Rose et al., 2015) on the other side of the Ellsworth Mountains. Deep troughs have been incised between plateaux through selective linear erosion over repeated glacial cycles, potentially due to the exploitation of the bedrock weaknesses that have resulted from faulting. Their W-shaped morphology is a result of excavation at the base of the trough walls, producing features that are similar to those found in the George VI Sound (Smith et al., 2007). Asymmetric V-shaped troughs have been formed in relation to areas where we suggest faulting has been concentrated on one side of a trough in an extensional tectonic setting. Alpine topography borders the Evans-Rutford Region to the north at the base of the Antarctic Peninsula, and the south with the Ellsworth Mountains and likely records the previous existence of smaller scale valley glaciers which eroded into the landscape.

6.3. Relationship between subglacial topography, underlying geological structure, and ice flow

The overarching regional landscape suggests the evolution of two preglacial surfaces, where one was potentially cut into the other, leaving a prominent escarpment. The surrounding troughs are likely to be tectonically controlled, due to the horst and graben and half-graben structures present in the landscape, which has led to increasingly enhanced topographic steering of the overlying ice (Jamieson et al., 2014).

Three hypotheses have been proposed for the large-scale, long-term formational processes underlying the geomorphology of the Evans-Rutford Region. Firstly, the plateaux were formed as a consequence of passive margin evolution, where the upper surface has formed through initial updoming and erosion

associated with the break-up of the Gondwana supercontinent, with subsequent post-rifting scarp retreat forming the lower surface. The second hypothesis suggests the subaerial planation of an extensive surface to base level, which has then been uplifted in association with the West Antarctic Rift System to allow the subsequent incision of the lower elevation surface to base level. The third hypothesis follows the same theory of extensive surface planation, however, rather than a WARS influence, the subsequent uplift may have been as a result of the cessation of Antarctic Peninsula subduction before 83 Ma (Larter et al., 2002). There is limited evidence to constrain the likelihood of one hypothesis over another, however, the presence of other erosional surfaces in the Institute and Möller catchment could indicate formation through passive margin evolution. However, without direct evidence that the formational processes were linked, no one hypothesis can be preferred.

The fact that these surfaces now sit below sea level even if rebounded, can be explained by subsidence of the surfaces post-formation as a result of long-term thermal relaxation after the main magmatic event at 180 Ma (Jordan et al., 2020), sediment loading in Weddell Sea (Hochmuth et al., 2020), or dynamic topography (Austermann et al., 2015), or may have been as a result of a combination of these processes. Alpine glaciation likely took place at the early stages of Antarctic glaciation at the Eocene-Oligocene boundary at 34 Ma (DeConto and Pollard, 2003). Glacial erosion of the troughs occurred post-planation of the surfaces and coincided with the inception of the West Antarctic Ice Sheet at 14-12 Ma (Colleoni et al., 2022).

Overall, the tectonic history of the Evans Rutford Region has created a subglacial landscape that has topographically controlled the formation of the West Antarctic Ice Sheet through the exploitation of structural weaknesses in the bedrock, as well as allowing the preservation of pre-glacial plateau surfaces where cold-based, non-erosive ice has prevailed for much of the WAIS history.

6.4. Future research

In order to constrain the potential formational mechanisms that have produced the subglacial topography evident in the Evans-Rutford Region, further investigation into its tectonic and geological history is required. Dating constraints could be obtained from apatite fission track dating of the subglacial bedrock if bedrock samples, or even longer bedrock cores could be obtained. In other regions such an approach has allowed elucidation of the rates of denudation associated with passive margin evolution (Brown et al., 2000; Cockburn et al., 2000). This would require drilling of the bedrock to obtain samples, which could take place in a vertical transect down a trough wall in order to capture samples for fission track analysis, which might capture a longer history of exhumation. This would provide a clearer picture about

the age at which incision occurred (e.g. the age at which these samples passed through the closure isotherm). Higher resolution magnetic or seismic surveys may also allow further investigation of the tectonic history of the region, for example allowing adjacent differences in bedrock geology to be identified, or to help constrain geophysical modelling.

As well as this, the radar data collected by the GRADES-IMAGE survey could be used to assess englacial structures present within the overlying ice, which should provide insight into recent (millennial timescale) changes in ice dynamics. We can identify both sub-horizontal layers and other englacial structures that reflect ice movement or changes in ice dynamics over time. Layers could be classified into continuous or well-defined layering, compared to discontinuous or buckled layering, to identify areas of fast or slow ice flow (Winter et al., 2015). Narrow areas of particularly disturbed layers could be used to indicate past or present shear margins. Whilst initially assessing the radargrams for data quality, whirlwind englacial structures similar to those identified by Winter et al. (2015) were seen at the transitions between the cold-based plateau edges, and the fast-flowing glaciers in the troughs. Mapping of internal reflection horizons (IRHs) in this area would potentially allow them to be tied to IRHs mapped across the Pine Island Glacier catchment and West Antarctic Ice Sheet (WAIS). Where this linkage can be made, it might enable the use of previously dated horizons mapped across the WAIS (Bodart et al., 2021, Ashmore et al., 2020), but relies on IRH preservation across large areas of the ice sheet.

7. Appendix 1

The tables, alongside Figure 7.1, below give details of parameter testing of multiple interpolation methods that did not create a suitable Digital Elevation Model. A test was considered a 'fail' when the interpolation produced a model that appeared to be very different to the bed elevation point dataset or BedMachine. Testing was also carried out on a subset of the bed elevation point dataset in order to save processing time, so a region around the Rutford ice stream was selected as it contained a range of features within the landscape that would need to be resolved accurately, such as steep trough walls.

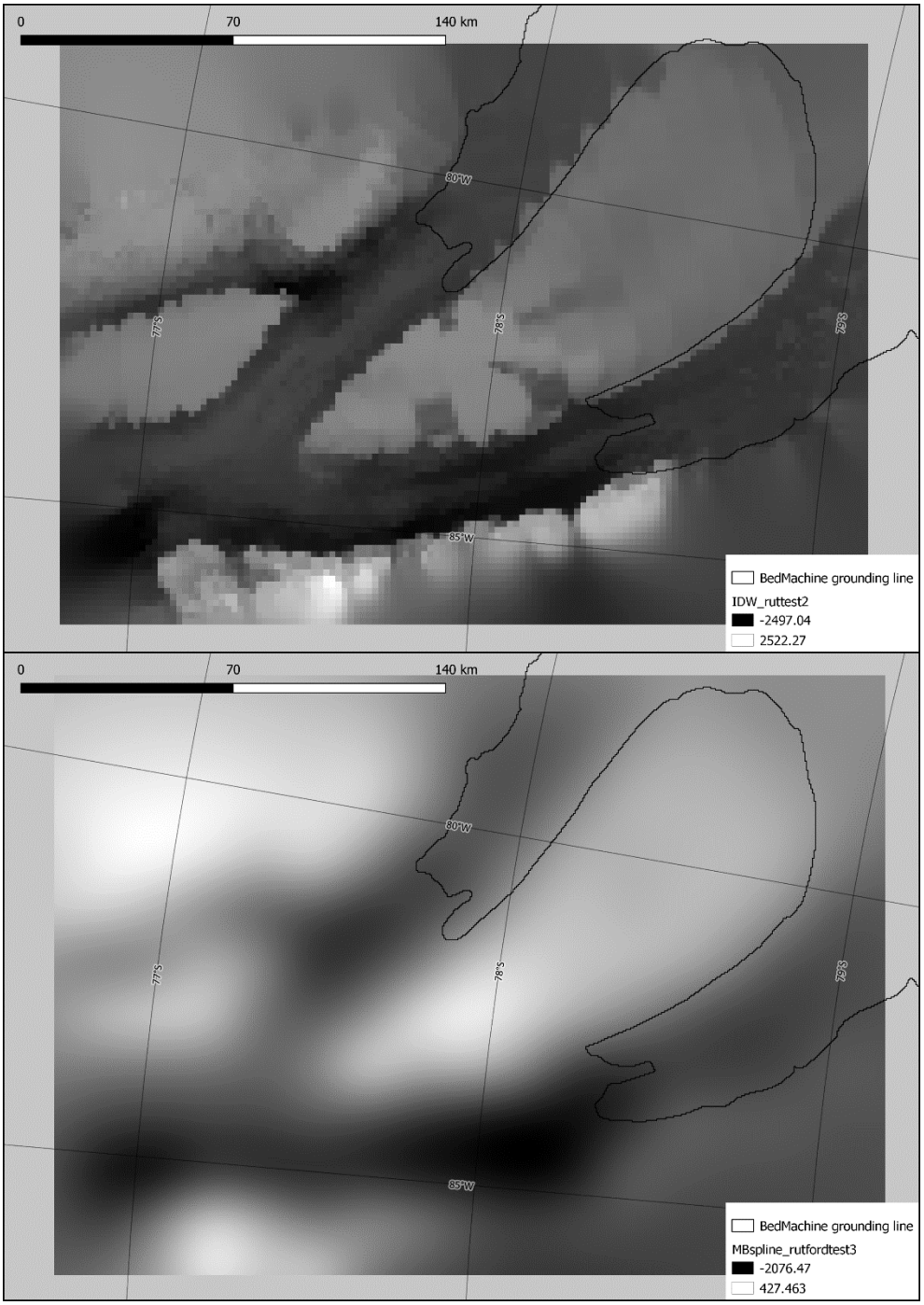

Figure 7.1: Examples of unsuccessful interpolation methods. The blocky and squared topography or extremely blurry topography is evident, showing why these methods were unsuitable for interpolating the bed elevation point dataset. Top map illustrates output IDW_ruttest2, and bottom map illustrates output MBspline_rutfordtest3.

TIN (linear)– QGIS

Output name	Data included	Cell size	Notes
rutford_test_1000px	GRADES	1000	Pixel size too large
rutford_test_500px	GRADES	500	Pixel size too large, signficant errors around edges
rutford_test_500px_rema	GRADES, REMA	500	Improvement around edges of Ellsworth
rutford_test_500px_rema_torus_evans	GRADES, REMA, TORUS, Evans	500	Improvement towards Evans, around plateau edges
rutford_test_diff	diff of rema vs rema+torus+evans	500	Difference around end of Ellsworth, edges of plateaus
rutford_test_250px_rema_torus_evans	GRADES, REMA, TORUS, Evans	250	Higher resolution, improves edges of ice streams

Multilevel B-Spline – QGIS

Output name	Cell size	Refinement	Threshold Error	Maximum Level	Notes
MBspline_rutfordtest1	500	0	0.0001	11	
MBspline_rutfordtest2	500	1	0.0001	5	Very blurry and no defined edges
MBspline_rutfordtest3	500	0	0.0001	5	Very blurry and no defined edges
MBspline_rutfordtest4	500	0	0.0001	14	

TopoToRaster – ArcMap

Output name	Cell size	Notes
topotr_rut1	500	fail - no topography produced
topotr_rut2	500	fail
topotr_rut3	500	fail

IDW – QGIS

Output name	Distance coefficient	Cell size
IDW_ruttest1	2	2000
IDW_ruttest2	10	2000
IDW_ruttest3	7	2000
IDW_ruttest4	50	2000
IDW_ruttest5	20	2000
IDW_ruttest6	10	500

Spline - ArcMap

Output name	Cell size	Spline type	Weight	No. of points	Notes
spline_rutfordtest1	500	T	0.35	12	fail - edge of Ellsworths and plateau edges
spline_rutfordtest2	500	T	0.35	12	fail - edge of Ellsworths and plateau edges
spline_test3	500	T	1	100	multiple low/high points
spline_rut4	500	T	0.35	1000	fail
spline_rut5	500	T	0.35	100	fail
spline_rut6	500	R	0.35	12	fail
spline_rut7	500	T	5	100	spiky edges, low point at TI/C
spline_rut8	500	T	10	100	spiky edges, low point at TI/C
spline_rut9	500	T	5	500	fail
spline_rut10	500	T	5	150	fail
spline_rut11	500	T	3.5	100	spiky edges and low points
spline_rut12	500	T	5	50	spiky edges and low points
spline_rut13	500	T	6	100	fail
Including firn corrected GRADES data					
spline_rut14	500	T	5	100	points included outside of text extent
spline_rut15	500	T	5	100	limited to test extent
spline_rut16	500	T	5	80	fail - low points and spiky edges
spline_rut17	2000	T	0.35	12	fail - spiky edges on plateaus
spline_rut18	2000	T	5	12	fail - spiky edges and low points
spline_rut19	500	T	5	12	fail - spiky edges of plateaus
spline_rut20	500	T	5	15	fail - spiky edges of plateaus
spline_rut21	2000	T	5	100	fail - edge of Ellsworths and plateau edges bad
spline_rut22	500	T	5	10	fail - disjointed topo, Ellsworths not realised
spline_rut23	500	T	5	150	fail - low points on FP edge, plateau edges not straight
spline_rut24	500	R	0.35	100	fail - no topo
spline_rut25	500	T	5	500	fail - huge low point on FP edge
spline_rut26	500	T	5	400	low point on FP edge and corners of plateaus
spline_rut27	500	T	5	300	low point on FP edge and corners of plateaus
spline_rut28	500	T	5	200	low point on FP edge and corners of plateaus
spline_rut29	500	T	5	25	low points on FP and Ellsworths
spline_rut30	500	T	10	100	spiky edges, low point at TI/C

spline_rut31	500	T	10	25	spiky edges, low point on FP edge
spline_rut32	500	T	10	500	big low point on FP channel
spline_rut33	500	T	10	250	big low point on FP channel
spline_rut34	500	T	7.5	100	small low point on TI corner, spiky edges
spline_rut35	500	T	7.5	250	spiky edges, high point and low point on FP
Using rasterised 100m resolution points					
spline_rut36	500	T	0.35	12	still has some obvious high/low points around FP edges and TI edges
spline_rut37	500	T	5	12	12 points creates line at mid points between flightlines on FP
spline_rut38	500	T	5	100	
spline_rut39	500	T	5	50	
spline_rut40	500	T	5	200	
Using rasterised 250m resolution points					
spline_rut41	500	T	0.35	12	Reduces high/low points but still has spiky edges
spline_rut42	500	T	0.35	100	250 points blurs out topography
spline_rut43	500	T	5	100	
spline_rut44	500	T	0.35	250	
spline_rut45	500	T	5	250	
spline_rut46	500	T	10	100	
spline_rut47	500	T	5	12	
spline_rut48	500	T	5	50	
spline_rut49	500	T	5	200	
Using rasterised 500m resolution points					
spline_rut50	500	T	0.35	12	Spiky edges and midpoint lines more obvious with 12 points
spline_rut51	500	T	0.35	50	No major difference between tensions
spline_rut52	500	T	0.35	100	
spline_rut53	500	T	5	12	
spline_rut54	500	T	5	50	
spline_rut55	500	T	5	100	
Using downsampled points - n=10 (every 10th point)					
spline_rut56	500	T	0.35	12	Obvious high points on T0.35
spline_rut57	500	T	0.35	50	Spiky edges seem reduced at T5
spline_rut58	500	T	0.35	100	
spline_rut59	500	T	5	12	
spline_rut60	500	T	5	50	
spline_rut61	500	T	5	100	

8. Bibliography

Aitken, A.R.A., Young, D.A., Ferraccioli, F., Betts, P.G., Greenbaum, J.S., Richter, T.G., Roberts, J.L., Blankenship, D.D., Siegert, M.J., 2014. The subglacial geology of Wilkes Land, East Antarctica. Geophysical Research Letters 41, 2390–2400. https://doi.org/10.1002/2014GL059405

Anderson, J.B., Shipp, S.S., 2001. Evolution of the West Antarctic Ice Sheet. The West Antarctic Ice Sheet: Behaviour and Environment. Antarctic Research Series 77, 45–57. https://doi.org/10.1029/AR077P0045

Ashmore, D.W., Bingham, R.G., Hindmarsh, R.C.A., Corr, H.F.J., Joughin, I.R., 2014. The relationship between sticky spots and radar reflectivity beneath an active West Antarctic ice stream. Annals of Glaciology 55, 29–38. https://doi.org/10.3189/2014AoG67A052

Ashmore, D.W., Bingham, R.G., Ross, N., Siegert, M.J., Jordan, T.A., Mair, D.W., 2020. Englacial Architecture and Age-Depth Constraints Across the West Antarctic Ice Sheet. Geophysical Research Letters 47, e2019GL086663. https://doi.org/10.1029/2019GL086663

Austermann, J., Mitrovica, J.X., Huybers, P., Rovere, A., 2017. Detection of a dynamic topography signal in last interglacial sea-level records. Science Advances 3.

Austermann, J., Pollard, D., Mitrovica, J.X., Moucha, R., Forte, A.M., DeConto, R.M., Rowley, D.B., Raymo, M.E., 2015. The impact of dynamic topography change on Antarctic ice sheet stability during the mid-Pliocene warm period. Geology 43, 927–930. https://doi.org/10.1130/G36988.1

Beaumont, C., Kooi, H., Willett, S., 2000. Coupled tectonic-surface process models with applications to rifted margins and collision orogens, in: Summerfield, M.A. (Ed.), Geomorphology and Global Tectonics. John Wiley and Sons , Chichester, pp. 29–55.

Bell, R.E., Seroussi, H., 2020. History, mass loss, structure, and dynamic behaviour of the Antarctic Ice Sheet. Science (1979) 367, 1321–1325. https://doi.org/10.1126/SCIENCE.AAZ5489

Bianchi, C., Cafarella, L., de Michelis, P., Forieri, A., Frezzotti, M., Tabacco, I.E., Zirizzotti, A., 2003. Radio Echo Sounding (RES) investigations at Talos Dome (East Antarctica): bedrock topography and ice thickness. Annals of Geophysics 46, 1265–1270.

Bingham, R.G., Ferraccioli, F., King, E.C., Larter, R.D., Pritchard, H.D., Smith, A.M., Vaughan, D.G., 2012. Inland thinning of West Antarctic Ice Sheet steered along subglacial rifts. Nature 487, 468–471. https://doi.org/10.1038/nature11292

Bodart, J.A., Bingham, R.G., Ashmore, D.W., Karlsson, N.B., Hein, A.S., Vaughan, D.G., 2021. Age-Depth Stratigraphy of Pine Island Glacier Inferred From Airborne Radar and Ice-Core Chronology. Journal of Geophysical Research: Earth Surface 126, e2020JF005927. https://doi.org/10.1029/2020JF005927

Brocklehurst, S.H., Whipple, K.X., 2004. Hypsometry of glaciated landscapes. Earth Surface Processes and Landforms 29, 907–926. https://doi.org/10.1002/ESP.1083

Brown, R.W., Gallagher, K., Gleadow, A.J.W., Summerfield, M.A., 2000. Morphotectonic evolution of the South Atlantic margins of Africa and South America, in: Summerfield, M.A. (Ed.), Geomorphology and Global Tectonics. John Wiley and Sons , Chichester, pp. 255–281.

Burbank, D.W., Anderson, R.S., 2001. Tectonic Geomorphology. Blackwell Science Ltd.

Burton-Johnson, A., Black, M., Fretwell, P.T., Kaluza-Gilbert, J., 2016. An automated methodology for differentiating rock from snow, clouds and sea in Antarctica from Landsat 8 imagery: a new rock outcrop map and area estimation for the entire Antarctic continent. The Cryosphere 10, 1665–1677. https://doi.org/10.5194/tc-10-1665-2016

Cavitte, M.G.P., Blankenship, D.D., Young, D.A., Schroeder, D.M., Parrenin, F., Lemeur, E., MacGregor, J.A., Siegert, M.J., 2016. Deep radiostratigraphy of the East Antarctic plateau: Connecting the Dome C and Vostok ice core sites. Journal of Glaciology 62, 323–334. https://doi.org/10.1017/jog.2016.11

Cockburn, H.A.P., Brown, R.W., Summerfield, M.A., Seidl, M.A., 2000. Quantifying passive margin denudation and landscape development using a combined fission-track thermochronology and cosmogenic isotope analysis approach. Earth and Planetary Science Letters 179, 429–435.

Colleoni, F., de Santis, L., Naish, T.R., DeConto, R.M., Escutia, C., Stocchi, P., Uenzelmann-Neben, G., van de Flierdt, T., Perez, L.F., Leitchenkov, G., Sangiorgi, F., Jamieson, S., Bentley, M.J., Wilson, D.J., and the PAIS community, 2022. Past Antarctic ice sheet dynamics (PAIS) and implications for future sea-level change, in: Florindo, F., Siegert, M., de Santis, L., Naish, T. (Eds.), Antarctic Climate Evolution. Elsevier, Oxford , pp. 689–766.

Corr, H., 2021. Processed airborne radio-echo sounding data from the GRADES-IMAGE survey covering the Evans and Rutford Ice Streams, and ice rises in the Ronne Ice Shelf, West Antarctica (2006/2007) (Version 1.0) [Data set]. NERC EDS UK Polar Data Centre.

Corr, H., 2020. Processed bed elevation picks from airborne radar depth sounding across the Evans Ice Stream, Southern Palmer Land (1994/95 season) (Version 1.0) [Data set]. . UK Polar Data Centre, Natural Environment Research Council, UK Research & Innovation. .

Corr, H., Ferraccioli, F., Frearson, N., Jordan, T., Robinson, C., Armadillo, E., Caneva, G., Bozzo, E., Tabacco, I., 2007. Airborne Radio-Echo Sounding of the Wilkes Subglacial Basin, the Transantarctic Mountains, and the Dome C Region. Terra Antarctica Reports 13, 55–63.

Corr, H., Popple, M., 1994. Airborne radio echo sounding on the Evans flowline, Ronne Ice Shelf. Bergen.

Corr, H., Smith, A., 2020. Processed bed elevation picks from airborne radar depth sounding across Ellsworth Land (2001) [Data set]. . UK Polar Data Centre, Natural Environment Research Council, UK Research & Innovation. .

Curtis, M.L., 1997. Gondwanian age dextral transpression and spatial kinematic partitioning within the Heritage Range, Ellsworth Mountains, West Antarctica. Tectonics 16, 172–181. https://doi.org/10.1029/96TC01418

Curtis, M.L., Storey, B.C., 1996. A review of geological constraints on the pre-break-up position of the Ellsworth Mountains within Gondwana: implications for Weddell Sea evolution. Weddell Sea Tectonics and Gondwana Break-up 108.

Dalziel, I.W.D., 2013. Antarctica and supercontinental evolution: Clues and puzzles. Earth and Environmental Science Transactions of the Royal Society of Edinburgh 104, 3–16. https://doi.org/10.1017/S1755691012000096

Dalziel, I.W.D., Garrett, S.W., Grunow, A.M., Pankhurst, R.J., Storey, B.C., Vennum, W.R., 1987. The Ellsworth-Whitmore Mountains Crustal Block: Its Role in the Tectonic Evolution of West Antarctica. Gondwana Six: Structure, Tectonics, and Geophysics 173–182. https://doi.org/10.1029/GM040P0173

Dalziel, I.W.D., Lawver, L.A., 2001. The Lithospheric Setting of the West Antarctic Ice Sheet. Antarctic Research Series 77, 29–44.

DeConto, R.M., Pollard, D., 2003. Rapid Cenozoic glaciation of Antarctica induced by declining atmospheric CO2. Nature 421, 245–249. https://doi.org/10.1038/nature01290

Doake, C.S.M., Crabtree, R.D., Dalziel I W D, 1983. Subglacial morphology between Ellsworth Mountains and Antarctic Peninsula: New data and tectonic significance, in: Oliver, R.L., James, P.R., Jago, J.B. (Eds.), Antarctic Earth Science: Fourth International Symposium . pp. 270–273.

Dowdeswell, J.A., Evans, S., 2004. Investigations of the form and flow of ice sheets and glaciers using radio-echo sounding. Reports on Progress in Physics 67, 1821–1861. https://doi.org/10.1088/0034-4885/67/10/R03

Escutia, C., Deconto, R.M., Dunbar, R., de Santis, L., Shevenell, A., Naish, T., 2019. Keeping an Eye on Antarctic Ice Sheet Stability. Oceanography 32, 32–46. https://doi.org/10.2307/26604948

Fitzgerald, P.G., 1992. The Transantarctic Mountains of southern Victoria Land: the application of apatite fission track analysis to a rift shoulder uplift. Tectonics 11, 634–662.

Fitzgerald, P.G., 2002. Tectonics and landscape evolution of the Antarctic plate since the breakup of Gondwana, with an emphasis on the West Antarctic Rift System and the Transantarctic Mountains. Royal Society of New Zealand Bulletin 35, 453-469.

Fitzgerald, P.G., Stump, E., 1992. Early Cretaceous Uplift of the Southern Sentinel Range, Ellsworth Mountains, West Antarctica. Recent Progress in Antarctic Earth Science 331–340.

Fitzgerald, P.G., Stump, E., 1991. Early cretaceous uplift in the Ellsworth Mountains of West Antarctica. Science (1979) 254, 92–94. https://doi.org/10.1126/science.254.5028.92

Frémand, A.C., Bodart, J.A., Jordan, T.A., Ferraccioli, F., Robinson, C., Corr, H.F.J., Bingham, R.G., Vaughan, D.G., 2022. British Antarctic Survey's aerogeophysical data: releasing 25 years of airborne gravity, magnetic, and radar datasets over Antarctica. Earth Systems Science Data 14, 3379-3410. https://doi.org/10.5194/essd-14-3379-2022

Fretwell, P., Pritchard, H.D., Vaughan, D.G., Bamber, J.L., Barrand, N.E., Bell, R., Bianchi, C., Bingham, R.G., Blankenship, D.D., Casassa, G., Catania, G., Callens, D., Conway, H., Cook, A.J., Corr, H.F.J., Damaske, D., Damm, V., Ferraccioli, F., Forsberg, R., Fujita, S., Gim, Y., Gogineni, P., Griggs, J.A., Hindmarsh, R.C.A., Holmlund, P., Holt, J.W., Jacobel, R.W., Jenkins, A., Jokat, W., Jordan, T., King, E.C., Kohler, J., Krabill, W., Riger-Kusk, M., Langley, K.A., Leitchenkov, G., Leuschen, C., Luyendyk, B.P., Matsuoka, K., Mouginot, J., Nitsche, F.O., Nogi, Y., Nost, O.A., Popov, S. v., Rignot, E., Rippin, D.M., Rivera, A., Roberts, J., Ross, N., Siegert, M.J., Smith, A.M., Steinhage, D., Studinger, M., Sun, B., Tinto, B.K., Welch, B.C., Wilson, D., Young, D.A., Xiangbin, C., Zirizzotti, A., 2013.

Bedmap2: Improved ice bed, surface and thickness datasets for Antarctica. Cryosphere 7, 375–393. https://doi.org/10.5194/tc-7-375-2013

Galeotti, S., DeConto, R., Naish, T., Stocchi, P., Florindo, F., Pagani, M., Barrett, P., Bohaty, S.M., Lanci, L., Pollard, D., Sandroni, S., Talarico, F.M., Zachos, J.C., 2016. Antarctic Ice Sheet variability across the Eocene-Oligocene boundary climate transition. Science (1979) 352, 77–80. https://doi.org/10.1126/science.aad8892

Garrett, S.W., Herrod, L.D.B., Mantripp, D.R., 1987. Crustal Structure of the Area Around Haag Nunataks, West Antarctica: New Aeromagnetic and Bedrock Elevation Data. Gondwana Six: Structure, Tectonics, and Geophysics 40, 109–115. https://doi.org/10.1029/gm040p0109

Goodfellow, B.W., 2006. Relict non-glacial surfaces in formerly glaciated landscapes. Earth Science Reviews 80, 47–73. https://doi.org/10.1016/j.earscirev.2006.08.002

Gulick, S.P.S., Shevenell, A.E., Montelli, A., Fernandez, R., Smith, C., Warny, S., Bohaty, S.M., Sjunneskog, C., Leventer, A., Frederick, B., Blankenship, D.D., 2017. Initiation and long-term instability of the East Antarctic Ice Sheet. Nature 552, 225–229. https://doi.org/10.1038/nature25026

Hélière, F., Lin, C.C., Corr, H., Vaughan, D., 2007. Radio echo sounding of Pine Island Glacier, West Antarctica: Aperture synthesis processing and analysis of feasibility from space, in: IEEE Transactions on Geoscience and Remote Sensing. pp. 2573–2582. https://doi.org/10.1109/TGRS.2007.897433

Hochmuth, K., Gohl, K., Leitchenkov, G., Sauermilch, I., Whittaker, J.M., Uenzelmann-Neben, G., Davy, B., de Santis, L., 2020. The Evolving Paleobathymetry of the Circum-Antarctic Southern Ocean Since 34 Ma: A Key to Understanding Past Cryosphere-Ocean Developments. Geochemistry, Geophysics, Geosystems 21. https://doi.org/10.1029/2020GC009122

Holtedahl, H., 1967. Notes on the Formation of Fjords and Fjord-Valleys. Source: Geografiska Annaler. Series A, Physical Geography 49, 188–203.

Howat, I.M., Porter, C., Smith, B.E., Noh, M.-J., Morin, P., 2019. The Reference Elevation Model of Antarctica. The Cryosphere 13, 665–674.

Huang, X., Gohl, K., Jokat, W., 2014. Variability in Cenozoic sedimentation and paleo-water depths of the Weddell Sea basin related to pre-glacial and glacial conditions of Antarctica. Global and Planetary Change 118, 25–41. https://doi.org/10.1016/J.GLOPLACHA.2014.03.010

Jamieson, S.S.R., Hulton, N.R.J., Sugden, D.E., Payne, A.J., Taylor, J., 2005. Cenozoic landscape evolution of the Lambert basin, East Antarctica: the relative role of rivers and ice sheets. Global and Planetary Change 45, 35–49. https://doi.org/10.1016/J.GLOPLACHA.2004.09.015

Jamieson, S.S.R., Stokes, C.R., Ross, N., Rippin, D.M., Bingham, R.G., Wilson, D.S., Margold, M., Bentley, M.J., 2014. The glacial geomorphology of the Antarctic ice sheet bed. Antarctic Science 26, 724–741. https://doi.org/10.1017/S0954102014000212

Jamieson, S.S.R., Sugden, D.E., 2008. Landscape Evolution of Antarctica, in: Cooper, A.K., Barrett, P.J., Stagg, H., Storey, B., Stump, E., Wise, W., and the 10th ISEAS editorial team (Eds.), Antarctica: A Keystone in a Changing World. Proceedings of the 10th International Symposium on Antarctic Earth Sciences. The National Academies Press, Washington, DC, pp. 39–54.

Jamieson, S.S.R., Sugden, D.E., Hulton, N.R.J., 2010. The evolution of the subglacial landscape of Antarctica. Earth and Planetary Science Letters 293, 1–27. https://doi.org/10.1016/j.epsl.2010.02.012

Jeofry, H., Ross, N., Corr, H.F.J., Li, J., Gogineni, P., Siegert, M.J., 2018a. A deep subglacial embayment adjacent to the grounding line of Institute Ice Stream, West Antarctica, in: Geological Society Special Publication. Geological Society of London, pp. 161–173. https://doi.org/10.1144/SP461.11

Jeofry, H., Ross, N., Corr, H.F.J., Li, J., Morlighem, M., Gogineni, P., Siegert, M.J., 2018b. A new bed elevation model for the Weddell Sea sector of the West Antarctic Ice Sheet. Earth System Science Data 10, 711–725. https://doi.org/10.5194/essd-10-711-2018

Jones, P.C., Johnson, A.C., von Frese, R.R.B., Corr, H., 2002. Detecting rift basins in the Evans Ice Stream region of West Antarctica using airborne gravity data. Tectonophysics 347, 25–41. https://doi.org/10.1016/S0040-1951(01)00236-0

Jordan, T.A., Ferraccioli, F., Leat, P.T., 2017. New geophysical compilations link crustal block motion to Jurassic extension and strike-slip faulting in the Weddell Sea Rift System of West Antarctica. Gondwana Research 42, 29–48. https://doi.org/10.1016/j.gr.2016.09.009

Jordan, T.A., Riley, T.R., Siddoway, C.S., 2020. The geological history and evolution of West Antarctica. Nature Reviews Earth and Environment. https://doi.org/10.1038/s43017-019-0013-6

Joughin, I., Alley, R.B., 2011. Stability of the West Antarctic ice sheet in a warming world. Nature Geoscience 4, 506–513. https://doi.org/10.1038/ngeo1194

King, E.C., 2011. Ice stream or not? Radio-echo sounding of Carlson Inlet, West Antarctica. Cryosphere 5, 907–916. https://doi.org/10.5194/tc-5-907-2011

King, E.C., Hindmarsh, R.C.A., Stokes, C.R., 2009. Formation of mega-scale glacial lineations observed beneath a West Antarctic ice stream. Nature Geoscience 2, 585–588. https://doi.org/10.1038/ngeo581

King, E.C., Woodward, J., Smith, A.M., 2007. Seismic and radar observations of subglacial bed forms beneath the onset zone of Rutford Ice Stream, Antarctica. Journal of Glaciology 53, 665–672.

König, M., Jokat, W., 2006. The Mesozoic breakup of the Weddell Sea. Journal of Geophysical Research: Solid Earth 111. https://doi.org/10.1029/2005jb004035

Larter, R.D., Barker, P.F., 1991. Effects of ridge crest-trench interaction on Antarctic-Phoenix spreading: forces on a young subducting plate. Journal of Geophysical Research 96, 19583–19607. https://doi.org/10.1029/91jb02053

Larter, R.D., Cunningham, A.P., Barker, P.F., Gohl, K., Nitsche, F.O., 2002. Tectonic evolution of the Pacific margin of Antarctica 1. Late Cretaceous tectonic reconstructions. Journal of Geophysical Research: Solid Earth 107, 2345. https://doi.org/10.1029/2000jb000052

LeMasurier, W.E., Landis, C.A., 1996. Mantle-plume activity recorded by low-relief erosion surfaces in West Antarctica and New Zealand. Geological Society of America Bulletin 108, 1450–1466.

Livermore, R., Hillenbrand, C.D., Meredith, M., Eagles, G., 2007. Drake Passage and Cenozoic climate: An open and shut case? Geochemistry, Geophysics, Geosystems 8. https://doi.org/10.1029/2005GC001224

Maslanyj, M.P., Storey, B.C., 1990. Regional aeromagnetic anomalies in Ellsworth Land: Crustal structure and Mesozoic microplate boundaries within West Antarctica. Tectonics 9, 1515–1532. https://doi.org/10.1029/TC009I006P01515

McGibbon, K.J., Smith, A.M., 1991. New geophysical results and preliminary interpretation of crustal structure between the Antarctic Peninsula and Ellsworth Land, in: Geological Evolution of Antarctica. International Symposium on Antarctic Earth , Cambridge.

Miller, K.G., Browning, J. v., John Schmelz, W., Kopp, R.E., Mountain, G.S., Wright, J.D., 2020. Cenozoic sea-level and cryospheric evolution from deep-sea geochemical and continental margin records. Science Advances 6. https://doi.org/10.1126/SCIADV.AAZ1346/SUPPL_FILE/AAZ1346_TABLE_S1.PDF

Montgomery, D.R., Balco, G., Willett, S.D., 2001. Climate, tectonics, and the morphology of the Andes. Geology.

Morlighem, M., 2020. MEaSUREs BedMachine Antarctica, Version 2. [189467428]. NASA National Snow and Ice Data Center Distributed Active Archive Center.

Morlighem, M., Rignot, E., Binder, T., Blankenship, D., Drews, R., Eagles, G., Eisen, O., Ferraccioli, F., Forsberg, R., Fretwell, P., Goel, V., Greenbaum, J.S., Gudmundsson, H., Guo, J., Helm, V., Hofstede, C., Howat, I., Humbert, A., Jokat, W., Karlsson, N.B., Lee, W.S., Matsuoka, K., Millan, R., Mouginot, J., Paden, J., Pattyn, F., Roberts, J., Rosier, S., Ruppel, A., Seroussi, H., Smith, E.C., Steinhage, D., Sun, B., Broeke, M.R. van den, Ommen, T.D. van, Wessem, M. van, Young, D.A., 2020. Deep glacial troughs and stabilizing ridges unveiled beneath the margins of the Antarctic ice sheet. Nature Geoscience 13, 132–137. https://doi.org/10.1038/S41561-019-0510-8

Naish, T., Powell, R., Levy, R., Wilson, G., Scherer, R., Talarico, F., Krissek, L., Niessen, F., Pompilio, M., Wilson, T., Carter, L., DeConto, R., Huybers, P., McKay, R., Pollard, D., Ross, J., Winter, D., Barrett, P., Browne, G., Cody, R., Cowan, E., Crampton, J., Dunbar, G., Dunbar, N., Florindo, F., Gebhardt, C., Graham, I., Hannah, M., Hansaraj, D., Harwood, D., Helling, D., Henrys, S., Hinnov, L., Kuhn, G., Kyle, P., Läufer, A., Maffioli, P., Magens, D., Mandernack, K., McIntosh, W., Millan, C., Morin, R., Ohneiser, C., Paulsen, T., Persico, D., Raine, I., Reed, J., Riesselman, C., Sagnotti, L., Schmitt, D., Sjunneskog, C., Strong, P., Taviani, M., Vogel, S., Wilch, T., Williams, T., 2009. Obliquity-paced Pliocene West Antarctic ice sheet oscillations. Nature 458, 322–328. https://doi.org/10.1038/nature07867

Napoleoni, F., Jamieson, S.S.R., Ross, N., Bentley, M.J., Rivera, A., Smith, A.M., Siegert, M.J., Paxman, G.J.G., Gacitúa, G., Uribe, J.A., Zamora, R., Brisbourne, A.M., Vaughan, D.G., 2020. Subglacial lakes and hydrology across the Ellsworth Subglacial Highlands, West Antarctica. The Cryosphere 14, 4507–4524. https://doi.org/10.5194/tc-14-4507-2020

Paxman, G., Austermann, J., Hollyday, A., 2021. Total Rebound: solid Earth isostatic response to the complete unloading of the Greenland and Antarctic Ice Sheets. Arctic Data Center.

Paxman, G.J.G., Austermann, J., Hollyday, A., 2022. Total isostatic response to the complete unloading of the Greenland and Antarctic Ice Sheets. Scientific Reports 2022 12:1 12, 1–10. https://doi.org/10.1038/s41598-022-15440-y

Paxman, G.J.G., Gasson, E.G.W., Jamieson, S.S.R., Bentley, M.J., Ferraccioli, F., 2020. Long-Term Increase in Antarctic Ice Sheet Vulnerability Driven by Bed Topography Evolution. Geophysical Research Letters 47, e2020GL090003. https://doi.org/10.1029/2020GL090003

Paxman, G.J.G., Jamieson, S.S.R., Ferraccioli, F., Bentley, M.J., Forsberg, R., Ross, N., Watts, A.B., Corr, H.F.J., Jordan, T.A., 2017. Uplift and tilting of the Shackleton Range in East Antarctica driven by glacial erosion and normal faulting. Journal of Geophysical Research: Solid Earth 122, 2390–2408. https://doi.org/10.1002/2016JB013841

Paxman, G.J.G., Jamieson, S.S.R., Ferraccioli, F., Bentley, M.J., Ross, N., Armadillo, E., Gasson, E.G.W., Leitchenkov, G., DeConto, R.M., 2018. Bedrock Erosion Surfaces Record Former East Antarctic Ice Sheet Extent. Geophysical Research Letters 45, 4114–4123. https://doi.org/10.1029/2018GL077268

Paxman, G.J.G., Jamieson, S.S.R., Ferraccioli, F., Bentley, M.J., Ross, N., Watts, A.B., Leitchenkov, G., Armadillo, E., Young, D.A., 2019a. The Role of Lithospheric Flexure in the Landscape Evolution of the Wilkes Subglacial Basin and Transantarctic Mountains, East Antarctica. Journal of Geophysical Research: Earth Surface 124, 812–829. https://doi.org/10.1029/2018JF004705

Paxman, G.J.G., Jamieson, S.S.R., Ferraccioli, F., Jordan, T.A., Bentley, M.J., Ross, N., Forsberg, R., Matsuoka, K., Steinhage, D., Eagles, G., Casal, T.G., 2019b. Subglacial Geology and Geomorphology of the Pensacola-Pole Basin, East Antarctica. Geochemistry, Geophysics, Geosystems 20, 2786–2807. https://doi.org/10.1029/2018GC008126

Paxman, G.J.G., Jamieson, S.S.R., Hochmuth, K., Gohl, K., Bentley, M.J., Leitchenkov, G., Ferraccioli, F., 2019c. Reconstructions of Antarctic topography since the Eocene–Oligocene boundary. Palaeogeography, Palaeoclimatology, Palaeoecology 535. https://doi.org/10.1016/j.palaeo.2019.109346

Pedersen, V.K., Egholm, D.L., Nielsen, S.B., 2010. Alpine glacial topography and the rate of rock column uplift: a global perspective. Geomorphology 122, 129–139. https://doi.org/10.1016/J.GEOMORPH.2010.06.005

Plewes, L.A., Hubbard, B., 2001. A review of the use of radio-echo sounding in glaciology. Progress in Physical Geography 25, 203–236.

Pollard, D., Deconto, R.M., 2009. Modelling West Antarctic ice sheet growth and collapse through the past five million years. Nature 458. https://doi.org/10.1038/nature07809

Rippin, D.M., Bamber, J.L., Siegert, M.J., Vaughan, D.G., Corr, H.F.J., 2004. The role of ice thickness and bed properties on the dynamics of the enhanced-flow tributaries of Bailey Ice Stream and Slessor Glacier, East Antarctica. Annals of Glaciology 39, 366–372. https://doi.org/10.3189/172756404781814375

Rose, K.C., Ross, N., Jordan, T.A., Bingham, R.G., Corr, H.F.J., Ferraccioli, F., le Brocq, A.M., Rippin, D.M., Siegert, M.J., 2015. Ancient pre-glacial erosion surfaces preserved beneath the West Antarctic Ice Sheet. Earth Surface Dynamics 3, 139–152. https://doi.org/10.5194/ESURF-3-139-2015

Ross, N., Bingham, R.G., Corr, H.F.J., Ferraccioli, F., Jordan, T.A., le Brocq, A., Rippin, D.M., Young, D., Blankenship, D.D., Siegert, M.J., 2012. Steep reverse bed slope at the grounding line of the Weddell Sea sector in West Antarctica. Nature Geoscience 5, 393–396. https://doi.org/10.1038/ngeo1468

Ross, N., Jordan, T.A., Bingham, R.G., Corr, H.F.J., Ferraccioli, F., Brocq, A. le, Rippin, D.M., Wright, A.P., Siegert, M.J., 2014. The Ellsworth Subglacial Highlands: Inception and retreat of the West Antarctic Ice Sheet. GSA Bulletin 126, 3–15. https://doi.org/10.1130/B30794.1

Schroeder, D.M., Bingham, R.G., Blankenship, D.D., Christianson, K., Eisen, O., Flowers, G.E., Karlsson, N.B., Koutnik, M.R., Paden, J.D., Siegert, M.J., 2020. Five decades of radioglaciology. Annals of Glaciology 61, 1–13. https://doi.org/10.1017/aog.2020.11

Siegert, M.J., 2008. Antarctic subglacial topography and ice-sheet evolution. Earth Surf. Process. Landforms 33, 646–660. https://doi.org/10.1002/esp.1670

Siegert, M.J., Florindo, F., 2009. Antarctic Climate Evolution, in: Developments in Earth and Environmental Sciences. Elsevier. https://doi.org/10.1016/S1571-9197(08)00001-3

Smith, A.M., Murray, T., 2009. Bedform topography and basal conditions beneath a fast-flowing West Antarctic ice stream. Quaternary Science Reviews 28, 584–596. https://doi.org/10.1016/J.QUASCIREV.2008.05.010

Smith, A.M., Murray, T., Nicholls, K.W., Makinson, K., Aðalgeirsdóttir, G., Behar, A.E., Vaughan, D.G., 2007. Rapid erosion, drumlin formation, and changing hydrology beneath an Antarctic ice stream. Geology 35, 127–130. https://doi.org/10.1130/G23036A.1

Smith, J.A., Bentley, M.J., Hodgson, D.A., Cook, A.J., 2007. George VI Ice Shelf: Past history, present behaviour and potential mechanisms for future collapse. Antarctic Science 19, 131–142. https://doi.org/10.1017/S0954102007000193

Storey, B.C., Nell, P.A.R., 1988. Role of strike-slip faulting in the tectonic evolution of the Antarctic Peninsula. J Geol Soc London 145, 333–337.

Strahler, A.N., 1952. Hypsometric (Area-Altitude) Analysis of Erosional Topography. Bulletin of the Geological Society of America 63, 1117–1142.

Studinger, M., Miller, H., 1999. Crustal structure of the Filchner-Ronne shelf and Coats Land, Antarctica, from gravity and magnetic data: Implications for the breakup of Gondwana. Journal of Geophysical Research: Solid Earth 104, 20379–20394. https://doi.org/10.1029/1999jb900117

Sugden, D.E., Jamieson, S.S.R., 2018. The pre-glacial landscape of Antarctica. Scottish Geographical Journal 134, 203–223. https://doi.org/10.1080/14702541.2018.1535090

Sugden, D.E., John, B.S., 1976. Glaciers and Landscape: A Geomorphological Approach. Arnold, Great Britain.

Summerfield, M.A., 1991. Global Geomorphology. Longman Scientific and Technical , New York.

Tinto, K.J., Padman, L., Siddoway, C.S., Springer, S.R., Fricker, H.A., Das, I., Caratori Tontini, F., Porter, D.F., Frearson, N.P., Howard, S.L., Siegfried, M.R., Mosbeux, C., Becker, M.K., Bertinato, C., Boghosian, A., Brady, N., Burton, B.L., Chu, W., Cordero, S.I., Dhakal, T., Dong, L., Gustafson, C.D., Keeshin, S., Locke, C., Lockett, A., O'Brien, G., Spergel, J.J., Starke, S.E., Tankersley, M., Wearing, M.G., Bell, R.E., 2019. Ross Ice Shelf response to climate driven by the tectonic imprint on seafloor bathymetry. Nature Geoscience 12, 441–449. https://doi.org/10.1038/s41561-019-0370-2

van de Lagemaat, S.H.A., Swart, M.L.A., Vaes, B., Kosters, M.E., Boschman, L.M., Burton-Johnson, A., Bijl, P.K., Spakman, W., van Hinsbergen, D.J.J., 2021. Subduction initiation in the Scotia Sea region and opening of the Drake Passage: When and why?. Earth-Science Reviews 215, 103551. https://doi.org/10.1016/j.earscirev.2021.103551

Vaughan, D.G., Corr, H.F.J., Ferraccioli, F., Frearson, N., O'Hare, A., Mach, D., Holt, J.W., Blankenship, D.D., Morse, D.L., Young, D.A., 2006. New boundary conditions for the West Antarctic ice sheet: Subglacial topography beneath Pine Island Glacier. Geophysical Research Letters 33. https://doi.org/10.1029/2005GL025588

Vaughan, D.G., Corr, H.F.J., Smith, A.M., Pritchard, H.D., Shepherd, A., 2008. Flow-switching and water piracy between Rutford Ice Stream and Carlson Inlet, West Antarctica. Journal of Glaciology 54, 41–48.

Watts, A.B., 2001. Isostasy and Flexure of the Lithosphere. Cambridge University Press, Cambridge.

Wilson, D.S., Jamieson, S.S.R., Barrett, P.J., Leitchenkov, G., Gohl, K., Larter, R.D., 2011. Antarctic topography at the Eocene-Oligocene boundary. Palaeogeography, Palaeoclimatology, Palaeoecology 335–336, 24–34. https://doi.org/10.1016/j.palaeo.2011.05.028

Wilson, D.S., Luyendyk, B.P., 2009. West Antarctic paleotopography estimated at the Eocene-Oligocene climate transition. Geophysical Research Letters 36. https://doi.org/10.1029/2009GL039297

Wilson, D.S., Luyendyk, B.P., 2006. Bedrock platforms within the Ross Embayment, West Antarctica: Hypotheses for ice sheet history, wave erosion, Cenozoic extension, and thermal subsidence. Geochemistry, Geophysics, Geosystems 7. https://doi.org/10.1029/2006GC001294

Wilson, D.S., Pollard, D., Deconto, R.M., Jamieson, S.S.R., Luyendyk, B.P., 2013. Initiation of the West Antarctic Ice Sheet and estimates of total Antarctic ice volume in the earliest Oligocene. Geophysical Research Letters 40, 4305–4309. https://doi.org/10.1002/GRL.50797

Winter, K., Woodward, J., Ross, N., Dunning, S.A., Bingham, R.G., Corr, H.F.J., Siegert, M.J., 2015. Airborne radar evidence for tributary flow switching in Institute Ice Stream, West Antarctica: Implications for ice sheet configuration and dynamics. Journal of Geophysical Research: Earth Surface 120, 1611–1625. https://doi.org/10.1002/2015JF003518

Young, D.A., Wright, A.P., Roberts, J.L., Warner, R.C., Young, N.W., Greenbaum, J.S., Schroeder, D.M., Holt, J.W., Sugden, D.E., Blankenship, D.D., van Ommen, T.D., Siegert, M.J., 2011. A dynamic early East Antarctic Ice Sheet suggested by ice-covered fjord landscapes. Nature 474, 72–75. https://doi.org/10.1038/nature10114

Zachos, J.C., Kump, L.R., 2005. Carbon cycle feedbacks and the initiation of Antarctic glaciation in the earliest Oligocene. Global and Planetary Change 47, 51–66. https://doi.org/10.1016/j.gloplacha.2005.01.001

Zundel, M., Spiegel, C., Lisker, F., Monien, P., 2019. Post Mid-Cretaceous Tectonic and Topographic Evolution of Western Marie Byrd Land, WestAntarctica: Insights from Apatite FissionTrack and (U-Th-Sm)/He Data. Geochemistry, Geophysics, Geosystems 20, 5831–5848. https://doi.org/10.1029/2019GC008667